CRANFIELD UNIVERSITY

SYED ATIF SHAFI

CIVIL AERO-PROPULSION APPLICATION: EFFECT OF THRUST RATING CHANGE ON ENGINE TIME ON-WING

SCHOOL OF AEROSPACE, TRANSPORT SYSTEMS AND MANUFACTURING

AEROSPACE PROPULSION

MSc by Research

Academic Year: 2014 - 2015

Supervisors: Panagiotis Laskaridis / Riti Singh

November 2015

CRANFIELD UNIVERSITY

SYED ATIF SHAFI

CIVIL AERO-PROPULSION APPLICATION: EFFECT OF THRUST RATING CHANGE ON ENGINE TIME ON-WING

SCHOOL OF AEROSPACE, TRANSPORT SYSTEMS AND MANUFACTURING

AEROSPACE PROPULSION

MSc by Research

Academic Year: 2014 - 2015

Supervisors: Panagiotis Laskaridis / Riti Singh

November 2015

ABSTRACT

Engine fleet management has always been one of the most challenging tasks in any airline as it requires assuring reliability and cost effectiveness of engine operation at all times. The engine maintenance expenses are quite significant and accounts for about one third of the total aircraft maintenance costs. For all airlines with “Labour & Material” type of contractual arrangement with respective OEM / MRO provider, maximizing engine’s Time On-Wing (TOW) is extremely crucial to face lower maintenance costs, while at the same time abiding by governing airworthiness standards. Engine’s TOW is generally limited due to at least one of the following reasons: performance degradation reflected by lower Exhaust Gas Temperature (EGT) margin, hot section hardware life monitored by regular borescope inspections and Life Limited parts (LLP) expiry enforced by OEM or regulatory authority.

After introducing relevant aero engine maintenance concepts and terminology, this thesis will serve to provide both qualitative and quantitative assessment of how certain operational factors of flight profile influence engine performance deterioration and maintenance costs. One such factor is the thrust rating of the engine. Higher thrust gives rise to higher internal temperatures, exposing engine hardware to greater mechanical and thermal stresses and therefore leading to faster rate of degradation and earlier engine removal.

This thesis will be of interest to airlines having at least two different types of aircraft models in their fleet with different average flight profiles but powered by the same engine model with the required thrust variant. A particular engine may spend some time first on the aircraft that requires higher thrust rating before being switched to the aircraft that requires lower thrust rating or vice versa. This thesis will look into the feasibility of such an operational strategy through different aspects and discuss its effectiveness in retaining the engine performance for a longer time, thereby affecting the operating fuel costs and restoration costs per flying hour expected at the time of shop visit.

Keywords: Gas Turbine, Turbofan, Soft Life, EGT Margin, Creep, Low Cycle Fatigue

ACKNOWLEDGEMENTS

I would like to express my sincere gratitude to Professor Laskaridis for the help and guidance he provided me throughout my research.

I am thankful to Cranfield Staff for being helpful whenever I had a query.

Very special thanks to my Line Manager Salah El Berizi for his understanding, and for allocating me leave when I needed for my research.

I am grateful to my colleague and mentor Bahgat for his valuable ideas and inspirations.

I owe respect, love and gratitude to my dear parents who have always been there for my siblings and me.

May Almighty God grant all of them health and cheerfulness.

TABLE OF CONTENTS

LIST OF FIGURES

LIST OF TABLES

LIST OF ABBREVIATIONS

BPR	Bypass Ratio
CFD	Computational Fluid Dynamics
CP	Corner Point
DMC	Direct Maintenance Cost
DP	Design Point
EGT	Exhaust Gas Temperature
EGTM	Exhaust Gas Temperature Margin
FAR	Fuel to Air Ratio
FF	Fuel Flow
FPR	Fan Pressure Ratio
GT	Gas Turbine
HP	High Pressure
ISA	International Standard Atmosphere
IT	Information Technology
LLP	Life Limited Parts
LP	Low Pressure
MDTOW	Maximum Design Takeoff Weight
MEW	Manufacturer's Empty Weight
MLW	Maximum Landing Weight
MZFW	Maximum Zero-Fuel Weight
OAT	Outside Air Temperature
OD	Off Design
OEW	Operator's Empty Weight
OPR	Overall Pressue Ratio
SFC	Specific Fuel Consumption
ST	Specific Thrust
SVR	Shop Visit Rate
SVR	Shop Visit Rate
TET	Turbine Entry Temperature
TO	Takeoff
USD/EFH	US Dollars per Engine Flight Hour

1 INTRODUCTION

1.1 Context

One of the factors that influence engine operation and performance on-wing is the thrust rating of the engine and there are thrust management options available to enhance engine's life on-wing and thereby reduce the overall maintenance costs. The project would perform the feasibility study of one such option that may be known in the airline and MRO industry but has not been yet discussed in academia to the best of the author's knowledge. This option involves splitting the engine usage between high thrust rated aircraft and low thrust rated aircraft before the engine undergoes heavy maintenance and overhaul.

Although the expertise lie with the manufacturer of the engine, with moderate awareness of physics based lifing methods combined with the capability of performing empirical studies based on readily available engine performance data through diagnostic tools, the operator is able to more closely predict engine's time on wing and prepare accurate engine removal forecast plans. In addition to the robust engine fleet management, this strategy would allow flexibility and confidence in making the operators take decisions themselves, rather than strictly following all the time, the recommendations and MRO solutions from OEMs and repair vendors, which may not serve the operator's financial interest.

1.2 Inspiration

There exist several examples in civil aviation where one engine model in the market possesses options for multiple thrusts that meet the propulsion requirements of more than one similar aircraft type. The CFM56-7BE, for instance, is the exclusive engine for the Boeing Next-Generation single-aisle aircraft family (B737-600/-700/-800/-900/-900ER/ BBJ) [1]. The CFM56-5B is a powerplant for entire Airbus A320 family [2]. Rolls Royce Trent 500 can be installed on both A340-500 and -600 aircraft with different thrust ratings. The airline operators with such mixed fleets have a distinct commonality advantage and can appreciate operational, maintenance and provisioning synergies [3].

The thesis will conduct the study by considering the practical case of an airline that operates aircraft similar to two versions of Boeing 777 aircraft. One is B777-300ER and the other is B777-200LR. Both aircraft types have the same GE90 engine installed but with different thrust ratings. B777-300ER is powered by GE90-115B, while B777-200LR is powered by GE90-110B. Some of the questions that would be explored are as follows. How long can the engines on the two B777 variants continue flying before their next shop visit? Can a study be performed to analyse and determine the best possible usage of a new or an overhauled GE90 engine between two different B777 versions? In other words, will the strategy of using the engine with a high thrust rating initially on B777-300ER and then with a lower thrust rating on B777-200LR be beneficial from the operational or maintenance cost perspective? If it exists, where exactly should be that point of switch between two thrust ratings in order to maximise the engine's time on wing?

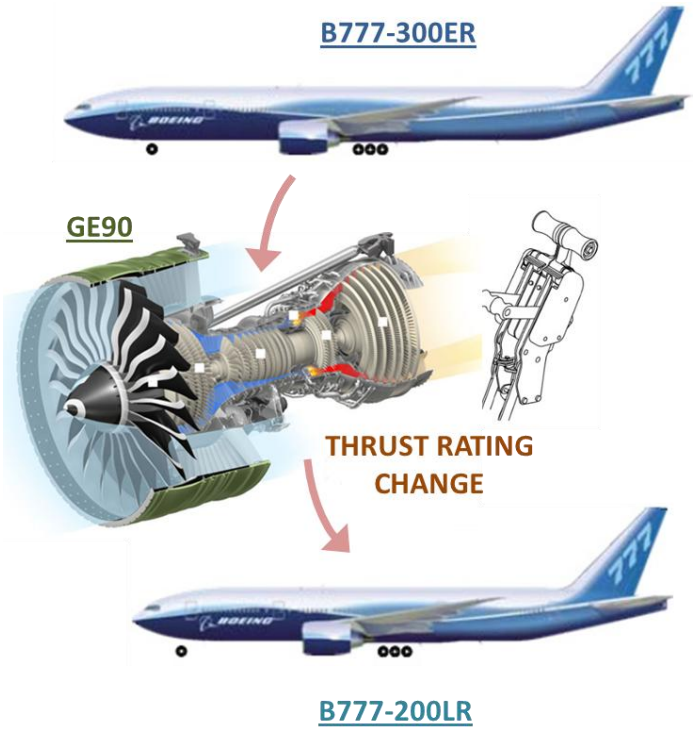

Figure 1-1 B777 Thrust Rating Change

1.3 Aims & Objectives

The main aim of this research is to examine the impact of thrust rating change on the engine's life expectancy on-wing and its effect on operating costs and refurbishment costs incurred off-wing. To commence with, two baseline flight mission profiles are set up with identical specifications but with the appointment of two different aircraft variants with slightly different engine thrust ratings. For comparison purposes following objectives were set with regards to each of the flight missions.

- To evaluate the mechanical and thermal stresses experienced by the engine's High Pressure Turbine (HPT) Stage 1 blade during different phases of the flight.
- To estimate the engine hardware life also called 'soft life' by performing physics based lifing analysis on the HPT Stage 1 blade.
- To illustrate the performance of a clean versus degraded engine and to assess the impact of degradation on engine time on-wing (TOW)
- To determine the limiting factor for engine time on-wing, Soft Life Expiry, or EGT Margin depletion.
- To demonstrate the effect of maximizing or minimizing engine Time On-wing on engine shop visit maintenance and engine operating fuel cost.

1.4 Thesis Structure

The present thesis is divided into nine main chapters where each chapter contributes towards achieving the main objectives.

Chapter 2: Background & Literature Review

This chapter provides theoretical concepts and background information relevant to this study. It discusses the factors that influence engine's life on the aircraft

and the major causes of engine removal. The chapter also entails literature review on the lifing methodologies and the dominant failure modes in aero-engines.

Chapter 3: Methodology

This chapter provides an overview of the multidisciplinary physics based approach adopted and used iteratively throughout the project to estimate engine Time On-Wing.

Chapter 4: Engine Model Creation & Simulation

This chapter demonstrates the use of Turbomatch software tool to create a baseline model for a high bypass turbofan engine similar to GE90 and select the engine thermodynamic cycle parameters for best design point performance. It also analyses the results from off-design performance simulations based on variations in mach number, altitude and outside air temperature.

Chapter 5: Aircraft and Flight Mission Model

This chapter explains the use of aircraft performance software tool, named Hermes, to create two reference flight mission profiles, one for each of the two aircraft variants with different thrust ratings. The engine operational data generated for the two missions through simulations is finally compared to understand the effect of thrust rating on severity of operation. Also, the aircraft models built in Hermes are validated by means of Payload-Range diagram.

Chapter 6: Engine HPT Blade Model

This chapter reveals the geometry and material characteristics of the high pressure turbine (HPT) stage one blade chosen as the component for analysis to determine engine's overhaul life. It mainly discusses the development and usage of stress and thermal models that actually translate the engine performance data into blade centrifugal stresses and metal temperatures, considered to be the primary ingredients of an overall lifing model.

Chapter 7: Engine Soft Life Estimation

This chapter discusses the lifing theories for the two main HPT blade damage mechanisms considered in this thesis - Creep and Low Cycle Fatigue (LCF). It elaborates and demonstrates the use of associated physics and empirical based formulations to estimate the life for the respective failure mode, and then finally an appropriate cumulative damage rule to estimate the overall life of the component, also regarded as the engine soft life. In this chapter the soft lives calculated for the engines flying the baseline missions do not take into account any effect of degradation.

Chapter 8: Engine Time On-Wing Assessment

This chapter first introduces a performance degradation profile and then re-evaluates the engine soft lives to obtain more realistic figures. The chapter also explores the options an airline operator may exercise to influence the engine Time On-wing by sharing the engine life usage between the high thrust and the low thrust rated aircraft. Furthermore, it points out the expected economic implications of such options in terms of operational and maintenance cost.

Chapter 9: Conclusions & Further Recommendations

This chapter summarizes the main achievements of the research work and also highlights some of the limitations. Furthermore, it outlines few proposals for future work which would add refinements and perhaps lead to exploration of new aspects within the same research area.

2 BACKGROUND & LITERATURE REVIEW

The purpose of this section is to offer a preliminary familiarization of the standard engine maintenance concepts and terminology used by the airlines, OEMs and MRO industry. It also provides theoretical background information and literature review performed relevant to the study.

2.1 Civil Aircraft Gas Turbine Engines

Turbofan is the most conventional gas turbine engine seen on commercial and business jet aircraft nowadays. The most distinguishing feature of a turbofan is the large fan, enclosed in the bypass duct right in front of the engine. The airflow that enters the engine splits into two air streams. The air entering the propulsor or core of the engine (core stream) is compressed along various stages of the compressor, until this highly pressurized air is mixed and burned with fuel in the combustor. Energetic hot gases produced as a result of combustion drive the turbine, which in turn rotates the compressor through a shaft, and also generate small percentage of thrust through exhaust. The airflow entering in the bypass duct (fan stream) is accelerated separately, providing majority of the thrust from the engine. Turbofan engines are fuel efficient, relatively quiet, and can provide higher thrust [4].

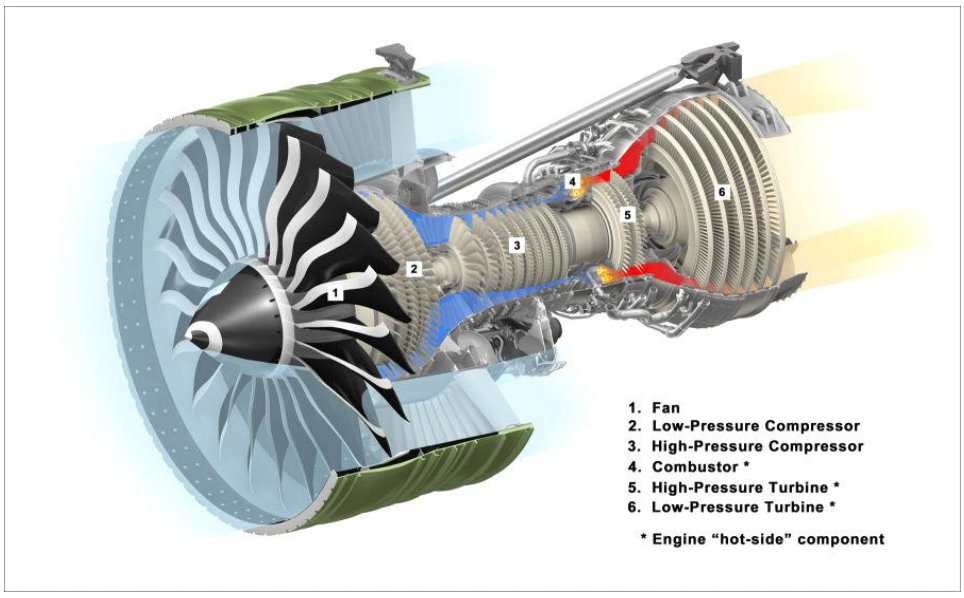

Figure 2-1 GE90 Twin Spool Turbofan Engine [5]

Turbofans with twin-spool architecture include Low Pressure Compressor (LPC) fan and High Pressure Compressor (HPC) independently driven by Low Pressure Turbine (LPT) and High Pressure Turbine (HPT) respectively. Alternatively, triple spool architecture includes an additional independent shaft, coupled with intermediate pressure compressor (IPC) and intermediate pressure turbine (IPT). Although this design involves complex construction, it provides better operational stability [4][6].

The engine's hot section, which comprises HPC, Combustor and HPT modules, is subjected to most severe conditions in terms of temperature, pressure and rotational speed and therefore experiences fast deterioration. The temperature is maximum at the face of the HPT, post combustor. With turbine entry temperatures (TET) as high as above 1500^{o}C [4], measurement of such high temperatures, even using the most sophisticated instrumentation, becomes impossible. The temperature at the engine exhaust (EGT), though relatively lower than TET, is a good reflection of the temperatures upstream. This is why EGT is one of the key operating parameters used for engine health monitoring [7].

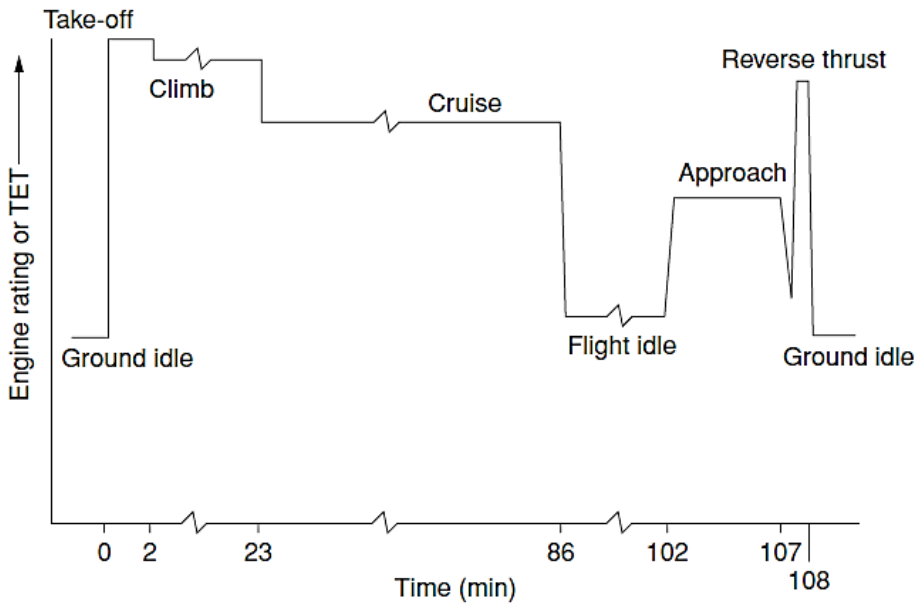

Figure 2-2 Variation of the TET during a typical flight cycle of a civilian aircraft [8]

2.2 Major causes of Engine Removals

Engine Condition Monitoring (ECM) and regular borescope inspections of the gas path help engineers predict the appropriate time for engine removal for shop visit. Generally there are three major causes that lead to engine removal: EGT margin deterioration, hardware degradation, and LLP expiry. It has been observed that the causes of engine removals depend heavily on the type of aircraft operation. Short haul sector removals tend to be due to EGT margin deterioration and LLP expiry, while medium to long-haul sectors removals are rather caused by hardware degradation and EGTM deterioration [4] [7].

EGT Margin Degradation

Among the many reasons for the fall in EGTM is the rubbing wear that occurs in both engine components: compressors and turbines. Rubbing wear refers to the loss of material due to the contact between blade tips and static knife edge seals or shrouds around the casing [9]. This increases seal or tip clearances with time, which results in the leakage of working fluid, decreasing the efficiency of the respective component and consequently affecting the overall engine performance [7]. In order to maintain the same desired thrust level there is a rise in fuel burn and hence EGT. Ultimately, the engine will be planned for a shop visit when there is little or no EGT margin left.

Some of the other important degradation mechanisms that lead to loss of EGT margin are as follows. Fouling is caused by airborne contaminants deposited on the airfoils and gas path annulus surfaces. Erosion involves wearing away of material from the airfoils and surfaces by small solid particles in the atmosphere. Corrosion also causes material loss and surface roughness due to the chemical reaction between flow path components and ingested contaminants through air, water and fuel. All the above mentioned mechanisms manage to change the airfoil shape profile, thereby affecting the flow capacity and efficiency of the respective engine component [9].

Hardware Deterioration

This relates to the general wear and tear of the engine gas path components, particularly the physical deterioration of the hot section modules (HPC, Combustor and HPT) which experience the highest mechanical and/or thermal stresses during engine operation. An HPT blade, for example, gets exposed to harshest conditions as it is subjected to extreme rotational speeds and high TETs, and therefore suffers from the following principal damage mechanisms: Creep, Fatigue and Oxidation. These mechanisms are responsible for the depletion of the hardware life and in worst case have the potential to cause catastrophic engine failures if not detected at earlier stages.

Engine hardware failures due to such phenomena cannot be precisely predicted [7]. However, engine manufacturers, from their experience or after carefully studying the engine utilization and operational details, do recommend 'soft life', beyond which the operators are advised to remove the engine from the aircraft for overhaul. In addition, borescope inspections carried out at regular intervals, as part of a conservative maintenance program, provide a good reflection of the engine's health by spotting any signs of anomalies in the gas path such as cracks and/or missing material exposing the internal cavities of the blade. If the inspection results fall outside the limits of the manufacturer's engine manual guidelines, the engine is soon called for removal.

Creep

Creep refers to the tendency of a material to undergo progressive deformation with time under the effect of high temperature and constant mechanical stress. Creep is said to be a time-dependent deformation. Under the influence of relatively high temperature, plastic deformation of a material is bound to take place even if the stress is smaller than the yield stress. This deformation is time-dependent and is known as creep. Gas turbine engine on a civilian aircraft spends majority of its flight time in steady state cruise conditions and therefore sets an opportunity for creep to act on the HPT blade during that time period. Creep is highly sensitive to temperature and shows its significance when metal temperature reaches about 40% to 50% of the melting temperature [10]. The

cooling technology used in the HPT is always carefully and precisely designed. In the absence of appropriate cooling, the creep deformation may become large enough to cause a turbine blade to touch the casing, resulting in blade tip failure.

The creep process can be represented by the following strain versus time curve.

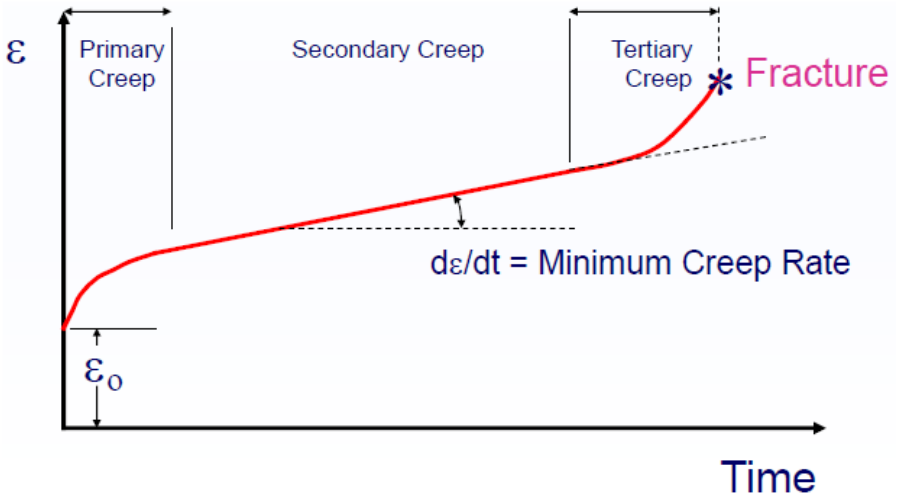

Figure 2-3 Strain vs Time Creep Curve [11]

The slope of the curve is called strain rate or creep rate. Initially, there is always some instantaneous elastic strain ε_o immediately upon application of load. Then, in the primary stage, the high creep rate tends to drop with time as the material faces an increase in strain hardening due to the build-up of a large number of dislocations. Deformation then becomes relatively difficult as the material is strained. In the secondary stage the creep attains constancy while maintaining a balance between the two metallurgical processes of strain hardening and thermal recovery. It is this stage where the material spends most part of its creep life [10]. Lastly, in the tertiary stage the strain rate accelerates rapidly leading to ultimate failure known as rupture. This failure could be the result of reduction in cross sectional area often termed as necking, caused by micro structural changes such as coalescence of voids or cavities, formation of internal micro cracks, sliding of grain boundaries [12].

Fatigue

Fatigue refers to the tendency of a material to undergo progressive deterioration when subjected to conditions involving cycles of fluctuating stresses or strains. It is the repeated application of load that leads to localized plastic deformation and potential failure even though the maximum stress may still be less than the yield stress [11]. The applied stress could be in the form of axial tension/compression, flexural bending, or torsional twisting [13].

The evolution of fatigue failure normally takes place in three main phases: crack initiation, crack propagation and final fracture. It starts with a minuscule crack that develops on the material surface at some local stress concentration caused by microscopic dislocation movement or slip. The effect of stress concentration increases after crack initiation, causing the crack to slightly grow and deepen first along the plane of high shear stresses and then elongate and propagate further across the grains and/or grain boundaries along the plane normal to high tensile stresses [10] [14]. The cross sectional area bearing the cyclic loading keeps on decreasing, until eventually it is no longer able to sustain the increasing load. At this instance there is a sudden failure which occurs without any prior warning.

Gas turbine engine is susceptible to three main types of fatigue namely Low Cycle fatigue (LCF) High cycle fatigue (HCF) and thermo mechanical fatigue (TMF). LCF is mechanical fatigue characterized by relatively high stress cycles that make plastic deformation dominant compared to elastic deformation. Consequently the material has shorter life and survives less than 10^4 to 10^5 cycles to failure. In aero gas turbine engines, LCF is caused by recurrent loading cycles of transient operation including conditions during engine start, takeoff or shutdown. In contrast, HCF is mechanical fatigue characterized by relatively high number of low stress cycles which solely produce elastic deformation. The material therefore has longer life and is expected to experience stress cycles above 10^4 or 10^5 before failure. The following are few reasons of HCF in turbomachinery operation:
- mechanical vibration due to rotor imbalance, wake excitation in downstream blades and upstream stator vanes, and aeromechanical instability due to aerofoil vibration or flutter [11].

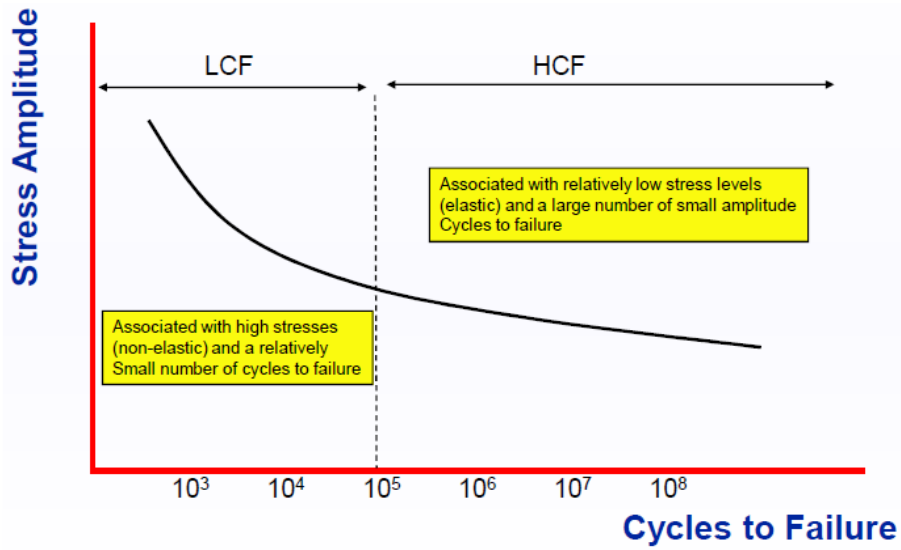

Figure 2-4 Cycles to Failure for LCF and HCF [11]

TMF is a form of fatigue which involves recurring thermal stresses in addition to the cyclic mechanical loading. TMF normally occurs during transient segments of engine operation when there are dramatic variations in temperature and load profiles, for example during engine start-up, takeoff acceleration or shutdown etc. The HPT blades for instance, with sophisticated and effective internal cooling system within their cavities, are able to face increasingly hot gas temperatures. Adversely, the resultant strong thermal gradients produced in the thickness of the blade surface, together with high mechanical stresses, induce localized transient strains which eventually cause TMF crack formation. Hence, 'as greater performance is demanded of gas turbines, operating temperatures increase, rotational speeds increase, thermal transients intensify, and durability suffers [15].

Oxidation

Oxidation is another time dependant complex damage mechanism, traces of which are widely seen in the hot components of the gas turbine engine where temperatures are above 500^{o}C [16]. Turbine blades, in particular, made up of nickel based superalloys, experience surface deterioration due to the formation

of thin layer of nickel oxide, leading to erosion and spallation of blade material, thus affecting the mechanical integrity.

LLP Replacement

Life-Limited Parts (LLPs) designate specific rotating and static structural parts of an aero engine, of which the failure can be hazardous to the safety of the aircraft. These parts are declared to be life-limited by the manufacturer and regulatory authorities in relation to their time in service, i.e. they must be removed after a specified amount of time or cycles, even if they appear new. Rotational LLPs generally include disks, spools and shafts whereas static LLPs include high pressure cases [17]

During flight, rotating LLPs in particular hold an amount of energy higher than what can be absorbed by the surrounding engine structure. Therefore, it is important to establish a time limit for such parts in a bid to prevent fatigue damage from initiating crack and/or from developing into uncontained failure [17].

The life limit is normally specified by the number of flight cycles a LLP is allowed to be in service for. The operator is required to maintain an accurate history of the total flight cycles of operation for all LLPs and must ensure not to exceed their respective cyclic life limits. ‘Stub-Life’ is the terminology often used by operators to denote shortest life remaining of all LLPs installed on an engine. Once the engine has accumulated as many flight cycles as the stub-life, the engine has to be sent to the workshop or overhaul agency for replacement of the expired LLPs [4].

Unscheduled Events

Engines may have to be removed due to unscheduled events, which can include engine system failures, engine vibration or foreign object damage (FOD).

Engine system failures can be caused for instance by lubrication system problems, such as oil leaks or oil pump malfunctions [7]. High oil consumption by

the engine can indicate an internal deterioration of the lubricated mechanical parts or even of the whole engine.

Vibrations caused by imbalance or misalignment can occur within the principle rotating system components of the gas turbine engine, such as the rotors, blades, discs, bearings or gears. Undetected, these vibrations can progressively increase and result in catastrophic failures.

Foreign objects that can result in engine FOD include birds, ice or ash as well as runway debris [4]. The ingestion of larger objects like birds can lead to significantly damage the fan- and the LPC blades, although it usually does not put a flight in danger [13]. The ingestion of foreign objects often has unobvious effects such as like minor cracks, which can however propagate by progressive engine wear.

2.3 Relation between Time on-Wing and Maintenance Cost

The amount of time an engine can stay on the aircraft before being removed for shop visit, commonly referred to as Time on Wing (TOW), directly influences the cost of a single shop visit, as well as the engine Direct Maintenance Cost (DMC) expressed in cost per flying hour (USD/EFH).

In general, an increase of the TOW results in an increased deterioration of the engine, and thus in an increase of the required maintenance work performed at one shop visit.

However, due to the extended intervals between two shop visits, this cost is compensated, which results in a decrease of the overall maintenance cost per flight hour, or Direct Maintenance Cost.

In the long-term, however, when the TOW reaches a certain point, the engine deterioration accelerates, which results in a severe increase of shop visit cost and consequently an increase of the overall DMC per flight hour [7].

The task of the shop visit management is to find the optimal TOW that corresponds to the lowest DMC. The following figure illustrates the relationship

between the engine's TOW and the DMC per flight hour, as well as the "target TOW".

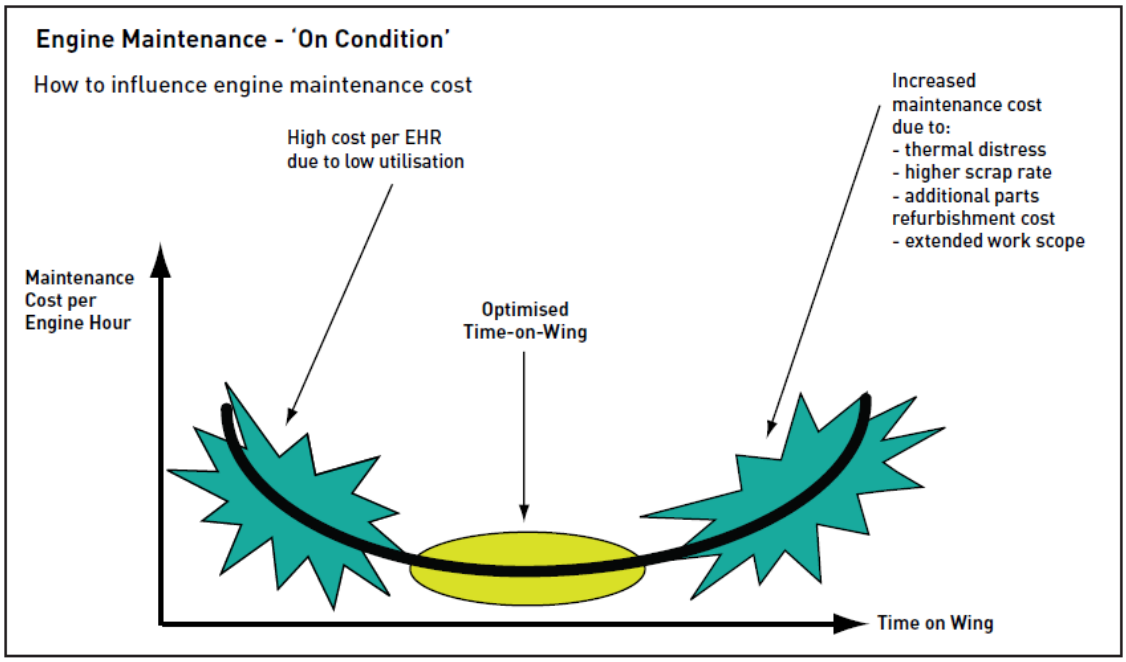

Figure 2-5 TOW vs Maintenance Cost per Engine Hour[18] [2]

2.4 Factors influencing Time on Wing

"An engine's TOW is heavily influenced by the severity of the operating environment it is exposed to" [4]. Key factors influencing the TOW, briefly discussed below, include thrust rating, flight length, take–off derate, ambient temperatures and environment.

Thrust Rating

A given engine can be operated at different thrust levels, in compliance with its variable power control setting. When operated at a higher thrust, the engine faces faster deterioration due to the increased thermal stress on the hardware, which leads to a lower EGT margin [7]. Reducing the engine's thrust rating is therefore a way to slow down its hardware deterioration, and consequently to increase its TOW. Figure 2-6 illustrates the relationship between an engine's thrust rating and its EGT Margin deterioration.

Large EGT margin combined with low EGT margin deterioration rate translates into longer time on-wing.

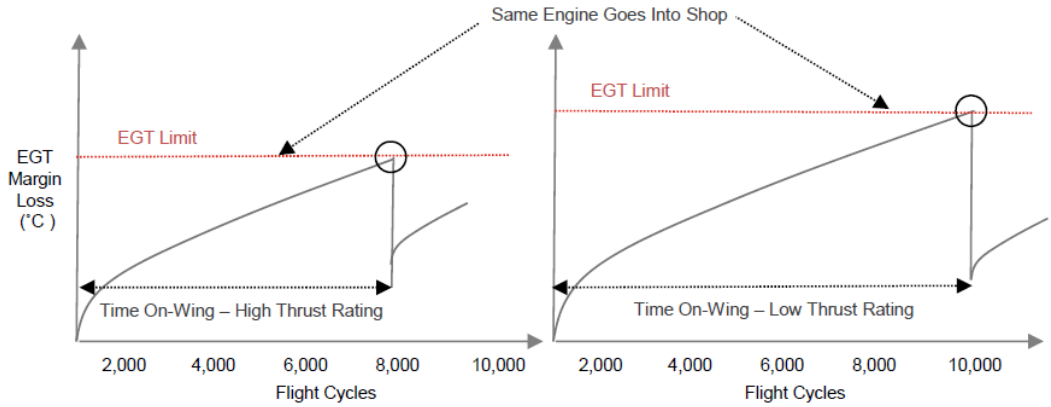

Figure 2-6 Engine Thrust Rating vs TOW [4]

Average Flight Length

The average flight length of an aircraft is an important factor influencing the engine's need for maintenance.

For short cycle flights, the engine spends most time using take-off and climb settings, and these are the phases in which an engine faces most stress and wear, and therefore more deterioration. This is why the TOW of engines operated on short cycle flights are measured in Engine Flight Cycles (EFC) rather than Engine Flight Hours (EFH). For medium to long-cycle flights, the TOW is usually calculated in EFH.

Another way to measure TOW considering the flight length is by using the flight leg length, which is the ratio flight hour to flight cycle (FH:FC).

As Figure 2-7 shows, a decrease in the average flight leg leads to shorter TOW and higher maintenance costs because the engine deteriorates faster. Shop Visit Rate, which is the number of shop visits per 1000 EFH (SV/EFH) behaves in a similar way [7].

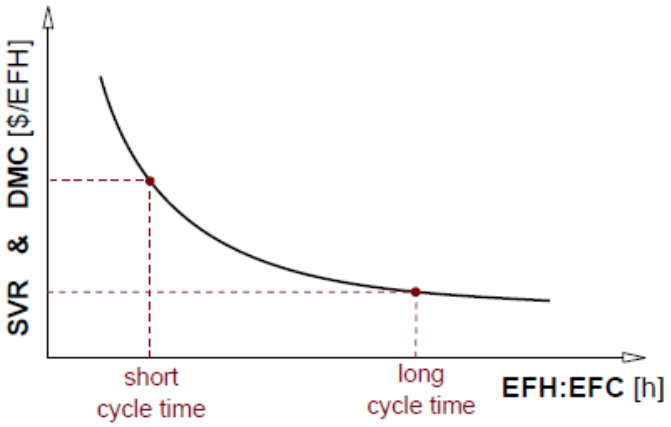

Figure 2-7 Effect of Engine flight length on SVR & DMC [7]

Take-off Derate

Take-off derate refers to setting the engine to a thrust below to its maximum level at the time of take-off. This can be done if the aircraft weight is below its maximum, in the case of lengthy runway, or in the case of relatively low ambient temperatures [7]. Usually the thrust derate falls 10-15% [7]. Take-off derate results in lowering take-off EGT, and consequently in lowering the engine deterioration, which results in lower maintenance costs. It is generally the first 5% of thrust derate that is most significant for the operational severity than the following levels [7] .

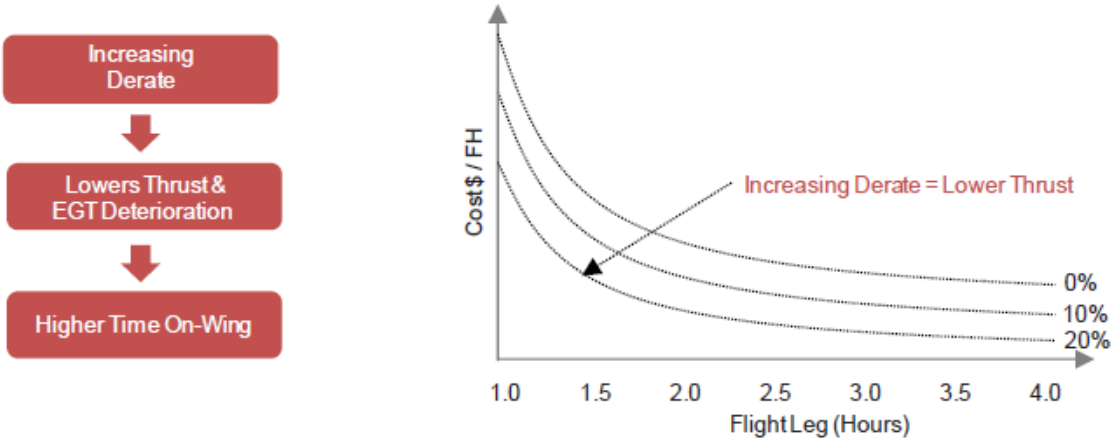

Figure 2-8 Effects of Engine Derate [4]

Ambient Temperatures

As demonstrated in Figure [] the EGT during take-off is directly influenced by the ambient air temperatures. In order to prevent the engine from operating at EGTs that could result in severe damage, the digital engine control keeps the EGT and EGT margin constant at all OATs above the corner point temperature, by reducing the engine's thrust. However, at OATs below the corner point, the thrust is kept constant and the available EGT margin increases as the OAT decreases [25]. In other words, low ambient air temperature result in low gas path temperatures, which reduces the thermal loads on the engine's hardware and thus prolongs engine time on-wing.

Turbofan engines are normally flat rated to ambient air temperatures around International Standard Atmosphere (ISA) + 15°C, or sea level conditions. The turbine entry temperature at max take-off and max climb rating increase as ambient air temperature increases, up to their limit value. Therefore, an engine exposed to high ambient temperatures will experience greater performance degradation [4].

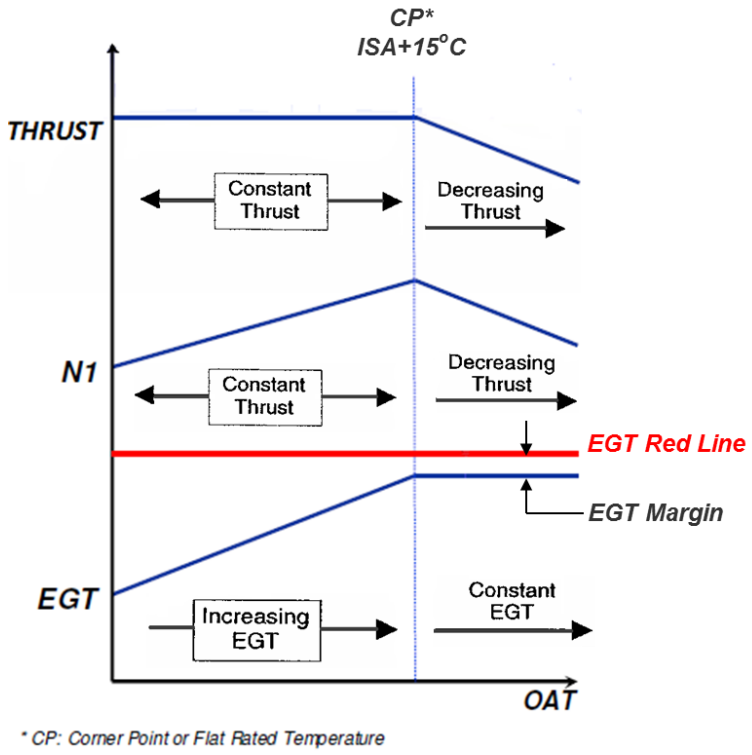

Figure 2-9 Relationship between Thrust, N1, EGT against OAT [19]

Environment

There are some environmental factors that can contribute to engine deterioration and thus influence engines' TOW. Air polluted with dust, sand, industry emission or volcanic ash can erode compressor and turbine blades, and block cooling holes. Salty air near the coast can accelerate corrosion and oxidation of engine parts [4].

Engine Age

First-run engines usually last considerably longer on wing than mature-run engines, sometimes up to 20-30 % longer [4]. This is because mature-run engines face more hardware deterioration and higher scrap rates. However, once an engine reaches maturity, which it can as early as after its first shop visit, the TOW and DMC stabilize to a relatively steady state [7].

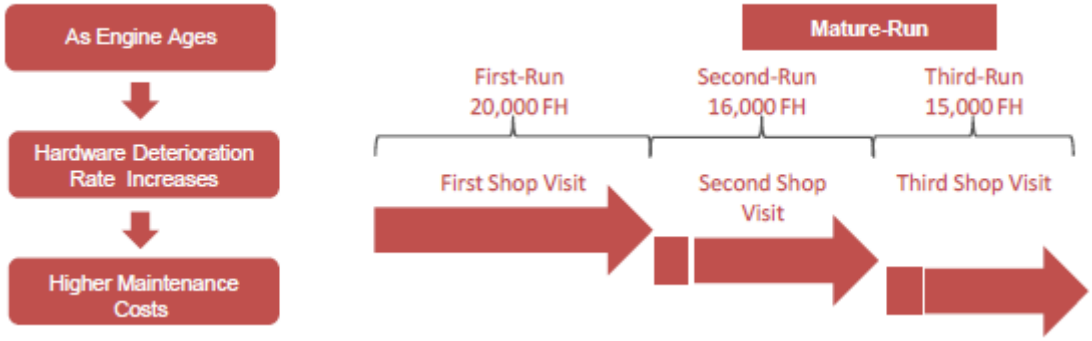

Figure 2-10 Effects of Engine Age [4]

2.5 Significance of Thrust Rating on TOW

From the earlier discussion it was noted that the operating conditions an engine experiences throughout a flight mission have a direct bearing on the shop visit rate, engine maintenance cost and engine operating cost. If all other conditions are kept constant, then higher ambient temperatures will result in higher SVR, operating from higher altitude airports will cause higher SVR, operating within

shorter flight sectors will cause higher SVR than longer flight sectors, flying in a highly erosive environment will also cause higher SVR than a low erosion environment.

All these flight conditions, whether adverse or beneficial, are to be found in airline's pre planned route structure, and hence cannot be controlled. Thrust rating, however, is a factor that airlines have power over, to some extent. Therefore, managing the engine thrust rating is an option airline operators have the privilege to avail. In fact, thrust management can be deemed as the dominant strategy to sustain engine performance.

Reducing the thrust of an engine, where applicable, implies a reduction of its peak rotational speed and TET, and hence a slower deterioration of the engine's hot section components. Therefore, thrust rate reduction can increase not just an engine's life, but also its TOW, and thereby result in reduced engine maintenance costs.

Management of thrust rating can be categorized into three types. The first one is take-off derate, a common practice among pilots during take-off under favorable flight conditions. The second one, still under research, is variable rating control, where the thrust rate of the engine is being kept at its minimum required level, which varies throughout the flight cycle. The third one, the central idea of this thesis, is thrust rating change. Here the objective is to switch an engine from an aircraft requiring higher thrust to an aircraft requiring lower thrust. Each type will be briefly elaborated on as follows.

2.5.1 Application of Derated Thrust

Derating is recognized in the aviation industry as being considerate to engine life, although its utilization is at the discretion of the pilot. Both engine manufacturers, GE and RR in their respective papers [20] and [21] have discussed in detail the potential benefits and limitations of adopting different derating philosophies during takeoff and climb in combination. Derating is possible in situations when the take-off weight is below the maximum take-off weight MTOW of the aircraft, there is availability of a long runway or the ambient temperature during take-off

is relatively low [7]. The derate ranges between 0-20%, and typically falls between 10-15% [7]. It results in a lower EGT at take-off, as well as lower turbine inlet temperature and shaft speed of the mission profile, and thus a reduced rate of engine deterioration and prolonged time on-wing [7]. This strategy can be applied not only during the takeoff phase, but also during the climb phase of the flight mission.

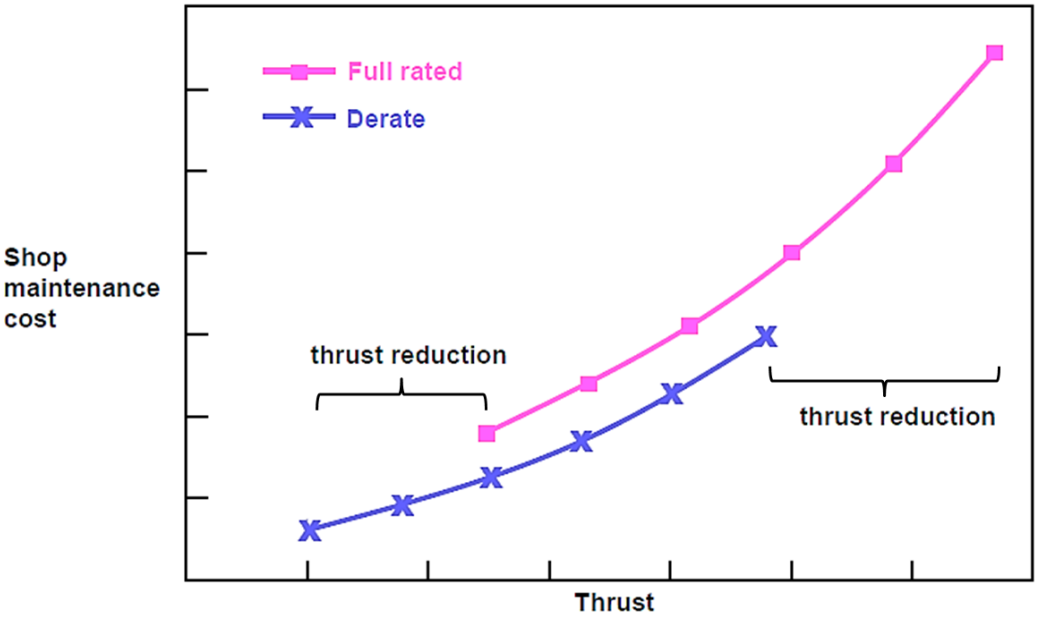

Figure 2-11 Effect of Derate on Shop Maintenance Cost [22]

2.5.2 Introduction of Variable Rating Control

Another option being considered, and still under research, is Variable Rating Control. The idea is to incorporate an automatic control system [23] that would continuously throughout the flight adjust the thrust rate and “limit the engine performance to its baseline requirement”, which varies according to the flight conditions. This means that where the flight condition allows, excess thrust will be reduced.

Flight conditions that may allow for reduction of thrust rating include low payload, long runway, low OAT and low take-off altitude. Jiannan has investigated how these conditions affect the engine performance, and concluded that runway

length, TET and Take-off altitude can significantly lower the baseline required thrust. Reduced payload, on the contrary, “does not have significant effect on engine life” [24].

If implemented, such a system is expected to result in an increase of an engine’s life as high as 4 times [25], and also in prolonging the engine’s TOW. This is mainly because by reducing the engine thrust where possible, we reduce temperatures and pressure within the turbine’s gas cycle, which itself results in a slower deterioration of the engine parts [25].

However, the option of variable rating control is far from being implemented in reality, as it involves sensitive safety issues, especially in case of emergencies, that need to be cleared first by civil aviation regulatory authorities.

2.5.3 Thrust Rating Change Strategy

In this thesis we are extending the concept of variable rating control to thrust rating change between two aircrafts. Airlines that have the advantage of possessing two different aircraft models with same engine type but different thrust ratings may adopt the strategy of replacing the engine from a higher thrust rated aircraft to a lower thrust aircraft with the following benefits: EGT Margin falls gradually, SFC is kept at low rate, better Engine performance retention, longer engine life on wing and lower Shop Visit rate.

Figure 2-12 below, illustrates this concept: an engine first operates at a higher thrust rated aircraft for a number of flight cycles The EGT margin degradation evolves at a speed that is relative to the thrust rating. Once a given margin is reached, the engine can be transferred to a lower thrust rated aircraft. Here the EGT margin suddenly becomes higher, and, as the engine operates with the new thrust rating, the EGT margin drops at a relatively lower rate.

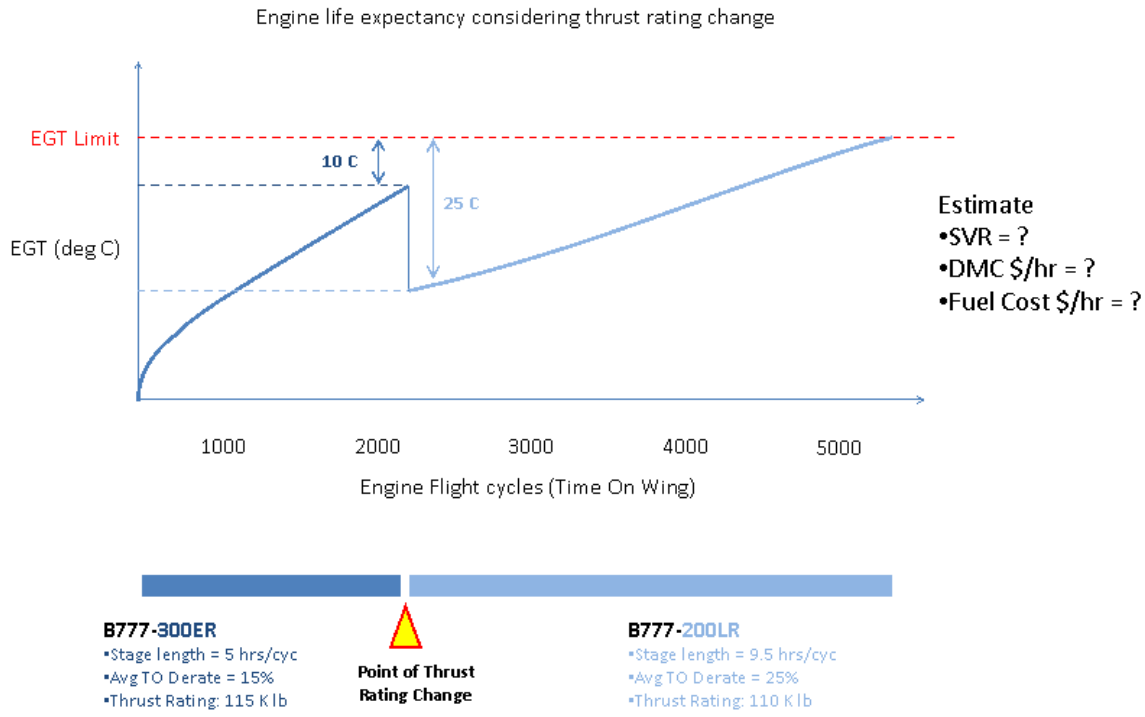

Figure 2-12 Engine Life Expectancy considering thrust rating change.

Note: The above figure is for illustration purpose only. It by no means reflects the actual values.

There are a few steps to be considered before switching the engine between two different aircraft type models: First, the engine nameplate has to be re-identified. Then, the corresponding rating plug has to be installed on the Electronic Engine Control or FADEC hardware [11]. The EEC is an engine computer that uses data from engine sensors and aircraft systems to control the engine operation. The engine rating plug selects the software in the EEC that corresponds to the thrust rating of the engine.

2.6 Lifing

2.6.1 Significance of Lifing

Lifing refers to predicting the life ahead of each gas turbine component. It is an integral concept for airlines adopting a condition-based maintenance policy as it

constitutes an important tool for their well management both from an economic perspective as well a safety perspective.

From an economic point of view, an adequate lifing programme may help extend the lives of gas-turbines, and reduce the frequency of major capital expenditures. Also, because costs spent on replacement parts have escalated, there is a growing tendency of airlines to independently assess their components' lives, rather than follow manufacturers' recommendations for soft life which, sometimes, may either be too conservative or may not be "machine-specific" [14].

From a safety perspective, airlines are and would always be interested in an engine life-assessment model to prepare engine removal forecast and avoid operational disruptions.

Additionally, whereas some types of damage in engine components may be detected by visual borescope inspections, or through the EGT margin deterioration or high engine vibration, damages due to factors such as creep or fatigue usually cannot be detected in such ways. Therefore airlines need to carry out lifing for components to forecast engine removals.

Turbine blades are the most crucial engine components that require lifing because they usually get exhausted first. Also, a failure in the blade can lead to "consequential damage of other components downstream and to catastrophic failure of the turbine" [14]. LLP parts, on the other hand, have a hard life fixed by the manufacturer; their lifing is therefore not carried out by airlines.

2.6.2 Dominant Failure Modes for Aero-Engines

The life of an aero gas turbine usually ends when a damage mechanism occurs, and the type of failure that ends an engine's life strongly depends on the flight conditions:

One factor is the average flight length. Engines operated in the short sector, i.e. may go through as many as 10 flight cycles a day, undergo the stretch between start up thrust and maximum thrust so often, and hence are most prone to low cycle fatigue [26].

Another factor is the temperature. Figure 2-13 below shows how the dominant failure mechanism varies according to the temperature range the engine is exposed to. At temperatures below approximately 800 ^{o}C, mechanical fatigue is the dominant risk. When exposed to temperatures between 800 and 1000^{o}C, failure can be caused by any of creep, oxidation or thermal fatigue. At more than 1000^{o}C creep becomes the major threat. The figure also shows how the number of engine life hours decreases for different damage mechanisms as the metal temperature increases [21].

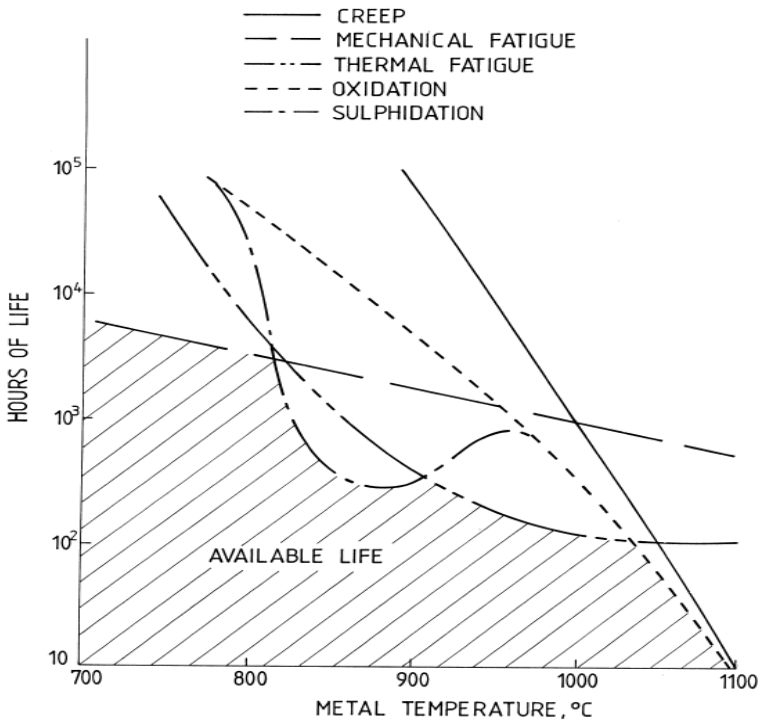

Figure 2-13 Dominant failure mechanisms according to engine temperature range [21]

2.6.3 LIFING Methodologies

The challenge of life management is to find a reasonable compromise between “safe life” and maximum usage of engine parts to reduce costs [27]. To investigate the effect of two different thrust ratings engine time on-wing there was a need of appropriate lifing method that would be able to provide the remaining life of the hot section of the engine based on the chosen damage mechanism.

NDT Methods

Non-Destructive Inspection NDI methods are very common in airline maintenance and MRO industry. These methods follow damage tolerance approach which assumes possible existence of defect in the component material. Hence, the engineer firstly declares a cyclic lifetime for each component, and after the declared life has been reached, the component may be cleared for further service after undergoing a programme of meticulous inspection. During this inspection, non-destructive tests (NDT) such as magnetic, dye penetrant eddy current, X-ray tomography and ultrasonic probe inspections are performed on the component to evaluate the presence of cracks [28]. The mentioned techniques are normally performed during engine overhaul when the engine is disassembled into piece parts. Borescope inspection, also an NDI method, is part of the engine's on-condition maintenance program generally performed on-wing. The purpose of the scheduled inspection on-wing is to inspect the hot section; combustor and HPT for defects at regular time intervals and, if required, monitor them next under a reduced repeat inspection interval, repair them or remove the engine before the expected failure of the component. If no defects are found, the engine is considered serviceable. If defects are found, the maintenance manual has to be referred, to assess if the engine is serviceable, with or without cycle limitations. Destructive Test (DT) methods are also seldom employed to study the metallography but will not be discussed.

Statistical Methods

A few researchers have looked into the application of probabilistic/statistical theories in their empirical life studies while others have demonstrated component life estimation through soft computing methods such as fuzzy logic and neural networks [28]. Philip et al [27] have developed a neural networks engine model, combined with Monte Carlo simulation to predict Thermo mechanical fatigue TMF damage in a NASA aircraft engine simulator. Fahmi [28] has proposed and analysed three artificial neural network architectures to estimate creep life for gas turbines.

Physics Based Analytical Methods

These methods mainly employ numerical and/or analytical relationships to estimate the component life. One of the contributors and users of physics based method is Tinga et al [29]. His life estimation tool for the military engine turbine blade incorporates many software tools along with physical and mathematical models used at National Aerospace Laboratory, The Netherlands. Firstly, flight conditions and crucial engine parameters monitored during the flight are downlinked directly from the aircraft through data acquisition system. Engine performance is then evaluated by a simulation program that calculates the thermodynamic properties of the fluid at relevant engine stations. A CFD model is used to determine the heat transfer from the hot gas stream to the film cooled turbine blade, based on which temperature distribution in the blade is evaluated with the help of a thermal FE model. A mechanical FE model is used to calculate the centrifugal and thermal stresses experienced by the blade. Finally, the temperature and stress distributions become the two key inputs to the life prediction model developed based on creep and fatigue damage mechanisms. Tinga uses Robinson's rule for creep damage evaluation and Miner's rule for fatigue damage evaluation and then adds the contributions from both to estimate the total/remaining life of the blade.

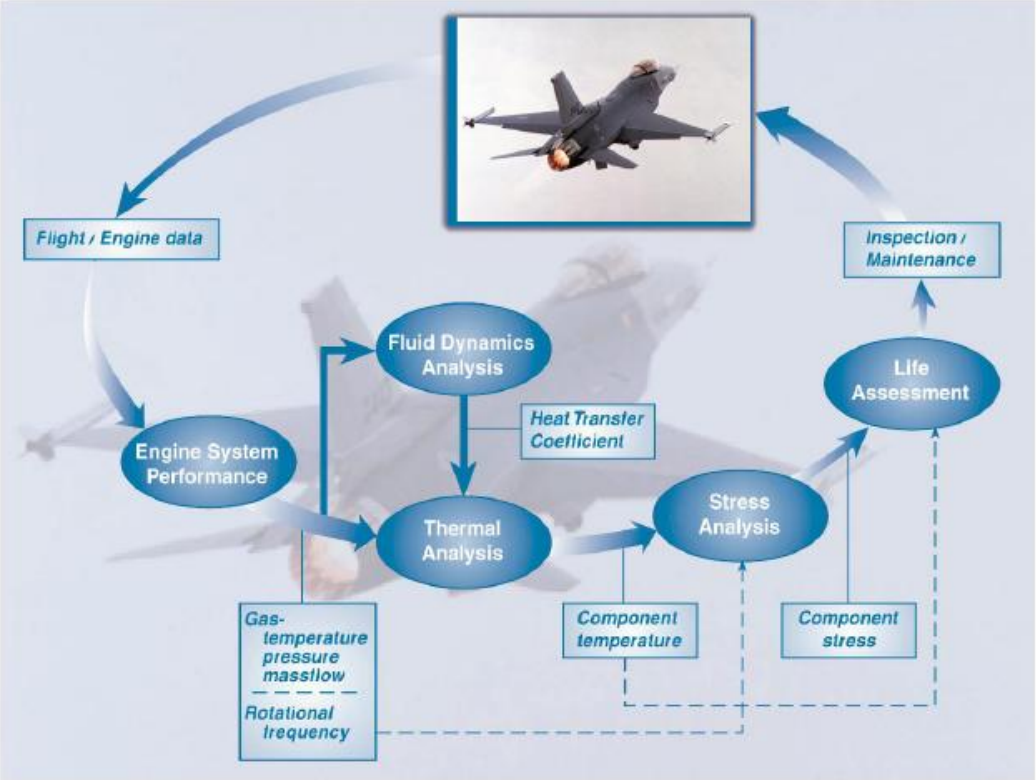

Figure 2-14 Tinga et al. Lifing Model [30]

Hanumanthan et al., in their work of establishing a method to estimate engine severity, “a measure of relative damage” [20], adopt a similar lifing procedure like that of Tinga et al. The main difference is that while Tinga et al. use real flight operation data directly from the aircraft, Hanumanthan et al. develop a generic tool for generating the required data from aircraft-engine system using two indigenous university software tools – Hermes and Turbomatch. Some of the aspects and elements of physics based lifing methodology which will be adopted in this project will be discussed in the next main section, section 3.

3 METHODOLOGY

3.1 Overview

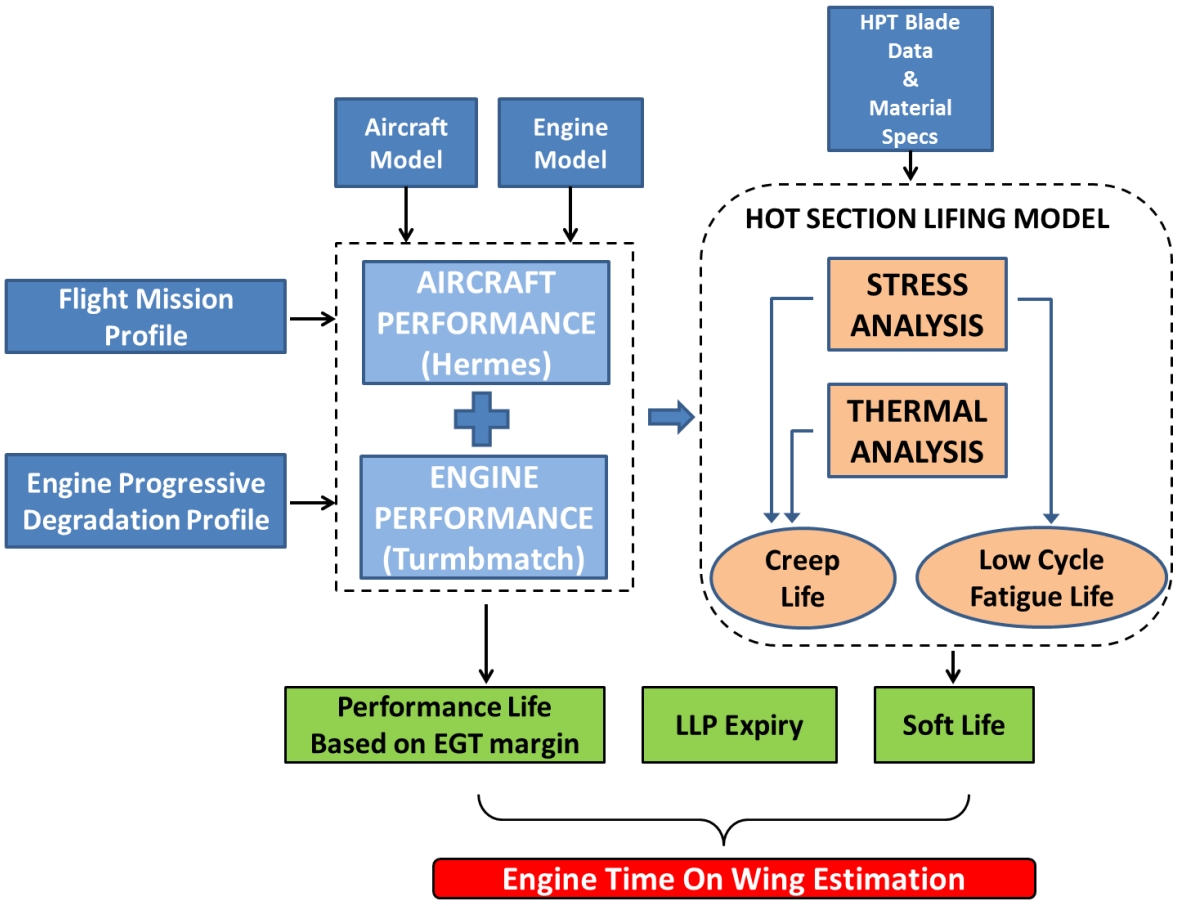

Figure 3-1 Methodology

The diagram above presents a top level multidisciplinary physics based approach which will be used iteratively throughout the following project subtasks.

- Estimation of engine TOW when operated with high thrust rated engine.
- Estimation of engine TOW when operated with lower thrust rated engine.
- Estimation of engine TOW when first operated with higher thrust rating for certain number of flight cycles and then with lower thrust rating until the shop visit.

- Parametric analysis to study the effect of shifting the point of thrust rating change on engine TOW and the effect of TOW on engine operating and maintenance costs.

Comparing the results from these subtasks will make the reader observe the expected benefits of transferring the engine from a high thrust rated aircraft to a lower thrust rated aircraft at least once prior to its shop visit. It should be noted that such a strategy can be adopted only by those operators which operate two or more aircraft models with same engine type but different thrust ratings.

In general, the methodology commences with the generation of engine operational data based on certain flight mission profile accompanied with arbitrary engine degradation characteristics. The data is then used in the estimation of mechanical and thermal loads the HPT blade is subjected to during engine operation. After the calculation of creep and LCF lives of the blade with the aid of well-established empirical relationships the engine soft life is computed. This soft life is solely considered to represent engine hardware life to failure as opposed to LLPs which have fixed hard lives. Concurrently, engine performance curve will be generated showing the decreasing trend of EGT Margin with time. The curve (EGTM vs flight cycles) is extrapolated to predict the number of flight cycles the degrading performance can be retained until the minimum allowable EGT margin is reached. This would provide the performance life of the engine. Thirdly, the lives of LLPs are considered to be fixed by the manufacturer. Since they generally expire at least after the first two shop visits they will not be considered for the purpose of this project. Any one of the three that expires first; soft life, performance life or LLP life, is considered engine TOW and the principal cause of engine removal. Engine Operating Fuel cost and Shop visit direct maintenance cost are then calculated. Some elements of the methodology are discussed in further detail in the sections ahead.

4 ENGINE MODEL CREATION & SIMULATION

This chapter demonstrates the use of Turbomatch software tool to create a baseline model for a high bypass turbofan engine similar to GE90 and select the engine thermodynamic cycle parameters for best design point performance. It also analyses the results from off-design performance simulations.

4.1 Introduction to Model Engine

GE90, manufactured by General Electric, is a dual rotor, separate exhaust, high bypass, civil turbofan engine installed on the wide body Boeing 777 aircraft [31]. It is the largest thrust producing engine thus far and enjoys a credible standing in terms of both performance and reliability, which is why it is found to be operated by many major air transport carriers around the world. Like many other turbofan engine designs GE90 has a twin spool modular architecture where 1-stage Fan and 4-stage LP Compressor (booster) are driven via 6-stage LP Turbine, while 9-stage HP Compressor is driven via 2-stage HP Turbine. Since the focus of the project is on the lifing analysis of primarily a large commercial jet engine, the baseline engine model is rationally chosen to be based on GE90 technical characteristics. The model engine will be addressed by the name TF90 in the thesis.

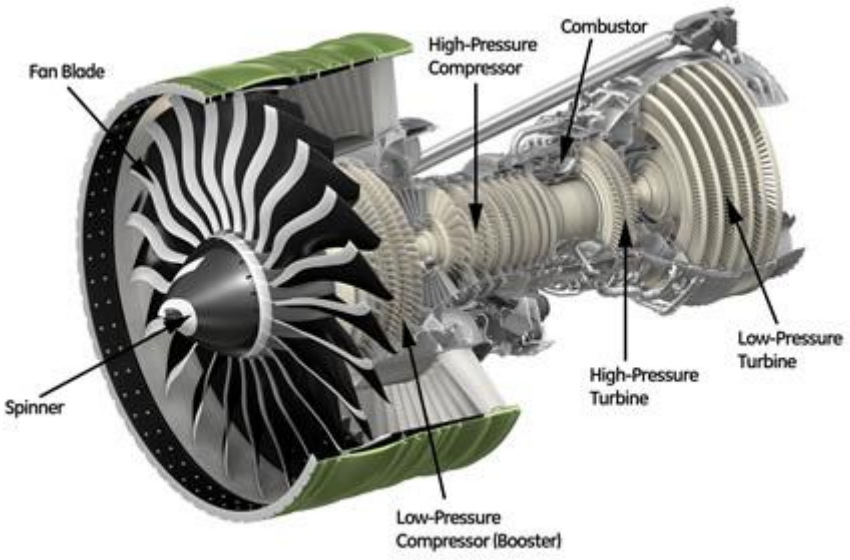

Figure 4-1 GE90 Engine Cutout [31]

Table 4-1 GE90 Engine Data[31][32]

TWO THRUST RATINGS	
GE90-115B Max TO Thrust	115540 lbf / 514 kN (@ISA + 15C)
GE90-110B1 Max TO Thrust	110760 lbf / 493 kN (@ISA + 18C)
SIZE	
Engine Weight (Dry)	8761.1 kg
Length	7.3 m
Fan Blade Tip Diameter	3.25 m
Mass Flow	1641 kg/s

STAGE COUNT	1-F/4-LPC/9-HPC 2-HPT/6-LPT
CYCLE DATA	
BPR OPR	7.1 42.2
RED LIMITS	
EGT (Max at TO)	1090 C (for 5 min)
N1 Speed (Max 110.5%)	2602 rpm
N2 Speed (Max 121.0%)	11292 rpm

4.2 Engine Model Development in Turbomatch

Turbomatch, indigenously developed by Cranfield University, is a gas turbine simulation software used for design point and off design performance analysis. The tool allows to build any GT engine model in a modular structure where different engine components represented as ‘bricks’, specified by their inherent set of features termed as ‘brick data’, are linked together by ‘station vectors’ that describe the gas state at each inlet and outlet station through a set of thermodynamic quantities. Outlet station vector from one brick is the input station vector of the following brick in series. In addition, a brick may take direct input from another brick which may not necessarily be the one just upstream in the program: such input and output data is grouped as ‘Engine Vector Data’ and ‘Engine Vector Results’ respectively. In Turbomatch there also exists a library of built-in predefined component performance maps which are then scaled according to the component specifications used in the model.

Once the model engine is assembled in the input data file, running the Turbomatch code returns values of the gas properties at all engine stations and computes the overall engine performance in terms of thrust, specific thrust, fuel flow and SFC etc., and finds the right operating point based on mass and energy

balances and rotational speed continuity between the interconnected components.

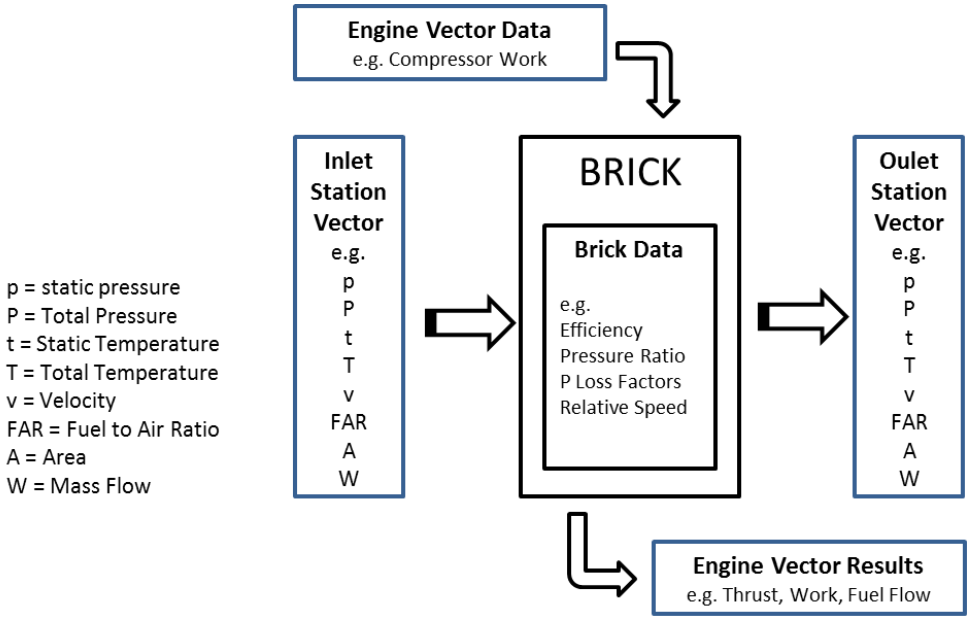

Figure 4-2 Turbomatch GT Module Terminology

Turbomatch was used to build the TF90 engine model and replicate aero thermodynamic behaviour of GE90 through performance simulation. Figure 4-3 shows representation of the model with 20 designated stations while the brick data details of individual components can be referred in the Turbomatch input data file included in Appendix A.

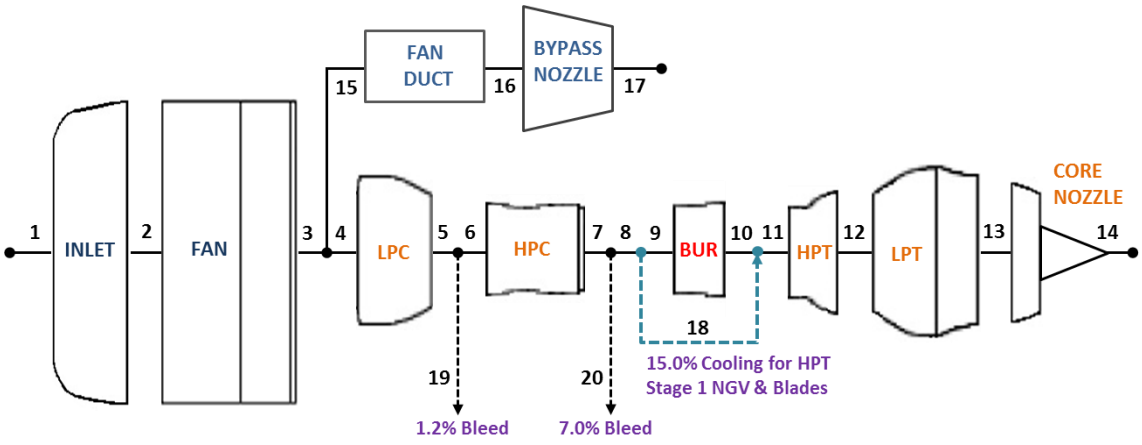

Figure 4-3 Layout of the TF90 engine model with Station designation

There were several considerations and assumptions taken into account with regards to the different model parameters especially those for which no data was available in open publications.

Isentropic efficiencies for fan, LPC (booster), HPC, HPT and LPT were all selected close to the typical values known for technologically advanced components. Combustion efficiency was selected to be 0.999.

Table 4-2 Component efficiencies chosen for the model

Fan	$\eta_{LPC(F)}$	0.90
Booster	$\eta_{LPC(B)}$	0.88
HP Compressor	η_{HPC}	0.88
HP Turbine	η_{HPT}	0.90
LP Turbine	η_{LPT}	0.90
Combustion Eff.	η_{BUR}	0.999

The overall pressure ratio of 42.2 was carefully and rationally divided between the fan, the booster and the HP Compressor. Pressure ratio across the booster was arbitrarily chosen to be 1.54 while the pressure ratio across HPC was fixed at 16.6. The split was based on the fact that the HP compressor tends to have higher number of stages and is connected to HP turbine via HP shaft running at relatively higher rotational speed. The LP shaft on the other hand is connected to the fan, the booster and the LP turbine, and its rotational speed is limited by the fan blade tip speed, 443 m/s in the case of GE90 [32]. This in turn limits the compression capability of the booster resulting in lower pressure rise.

Air bleed extraction does affect the overall engine performance and therefore was also accounted for in the model within allowable limits [11]. 1.2% bleed extraction was assumed at LPC exit. 7.0% bleed extraction was assumed from HPC for aircraft cabin pressurization, nacelle anti-icing and cooling of other hot section

areas other than HPT stage 1 NGVs and rotor blades. Additional 15.0% of the HPC discharge flow was explicitly reserved for the cooling of HPT Stage 1 NGVs and rotor blades, which is known to be a moderate figure for many modern gas turbine engines that run at high turbine entry temperatures.

Another important aspect of the model development was the selection and settlement of engine thermodynamic cycle parameters at the design point. This is discussed in the next section.

4.3 Selection of Engine Cycle Parameters

The design point of a civil aero gas turbine engine is traditionally taken as the operating point during the stable cruise phase of the flight where the engine spends most of its operating time. However, achieving the required thrust during takeoff is also extremely important. And because whatever limited GE90 data available in the public domain is mainly for takeoff condition, the design point of the model engine in this project was chosen to be the static takeoff condition at sea level, ISA + 15C, attaining maximum thrust of 514 kN. To meet this requirement, a series of iterative simulations were performed whereby the values of few model parameters, initially unknown in public domain and therefore assumed, were repeatedly altered until the performance output parameters such as thrust, specific thrust and SFC converged close to the actual published engine data.

In addition to the component level parameters discussed already in the last section, the engine thermodynamic cycle parameters were also investigated. Out of the four turbofan cycle parameters the overall pressure ratio (OPR) and the bypass ratio (BPR) were obtained directly from the GE90 published data and hence were held fixed. For the turbine entry temperature (TET) and the fan pressure ratio (FPR), iterative simulations were performed in Turbomatch. To

start with, parametric study with arbitrary high TET values was considered with the objective of meeting the takeoff thrust. At each constant TET (i.e. fixed energy input), variations in specific thrust and SFC with respect to FPR were observed as shown in Figure 4-4. These trends can be explained as follows. At low FPR the fan bypass thrust is small as there is little energy extraction from the core (LPT) to drive the fan, leaving excessive core jet velocity to result in energy wastage, lower propulsive efficiency and therefore higher SFC. At higher FPR more energy is extracted to drive the fan than required resulting in lower core thrust but this time it is the rise in bypass jet velocity which is the cause for energy wastage and therefore higher SFC. It is evident in the figure that for any value of TET there is an optimum value of FPR at which the overall energy conversion to thrust is maximized and this is indicated by the point of minimum SFC and maximum specific thrust. Furthermore, increasing the TET at fixed OPR and BPR increases the optimum FPR which can be explained due to the greater ability of the core (LPT) to drive the fan while maintaining the same core nozzle expansion.

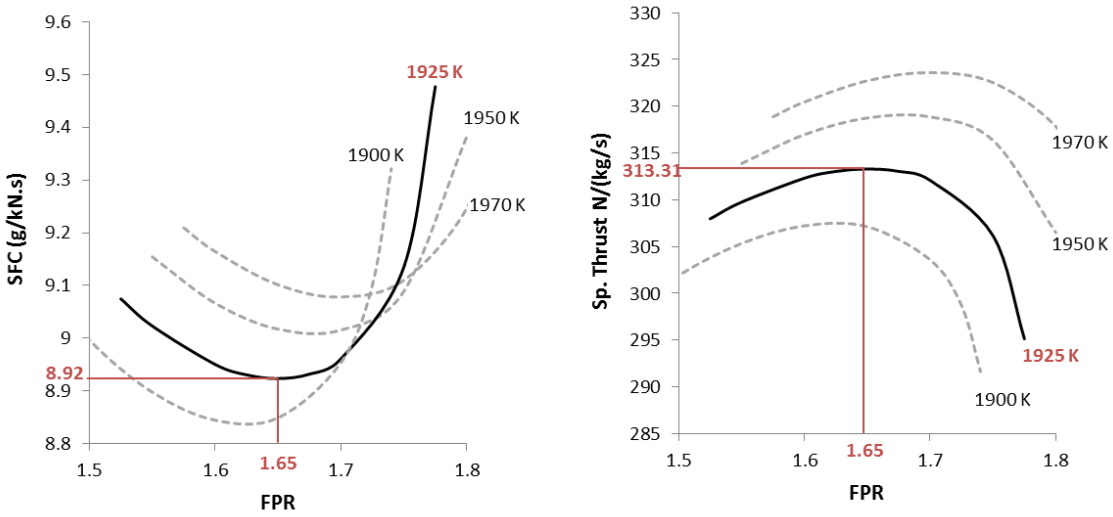

Figure 4-4 Variation of Specific Thrust and SFC vs FPR

Minimum TET of 1925 K and optimum FPR of 1.65 that provided the certified takeoff thrust of 514 kN (at sea level static condition, ISA + 15C) at minimum SFC

were finally selected. At optimum FPR SFC = 8.92 g/kN.s and Specific thrust = 313.31 N/(kg/s) respectively.

4.4 Design Point Performance Validation

The final set of selected cycle parameters (TET=1925K, OPR =42.2, BPR=7.1, FPR=1.65) ensures the best design point performance. This can be verified with the following relation (4-1) derived in [34], in which the ratio of bypass jet velocity to core jet velocity equals the energy transfer efficiency only at optimum FPR.

$$\frac{V_{j\,(Bypass)}}{V_{j\,(Core)}} = \eta_{trans} \cong \eta_{LPC(F)} \times \eta_{LPT} \qquad \textbf{(4-1)}$$

$$\frac{305.8\ m/s}{386.8\ m/s} \cong 0.9 \times 0.9 \qquad \textbf{(4-2)}$$

$$V_{j\,(Core)} = 1.265 \times V_{j\,(Bypass)} \qquad \textbf{(4-3)}$$

Since the efficiency of the energy transfer between the core and the bypass streams is mainly the product of the individual fan and LP turbine efficiencies, where both of these are always less than 100%, the optimum core jet velocity is always higher than the optimum bypass jet velocity, by a factor of nearly 1.2 [35]. This is the condition met above in equation (4-3) where Vj(core) was found to be 1.265 times Vj(bypass), indicative of optimum design point performance. The output of simulation can be viewed in Appendix A which includes the snapshot of the gas properties at each of the model stations.

To validate the baseline engine model TF90 for the selected design point, the estimated performance data from Turbomatch was finally compared with the limited published GE90 data from reliable public sources. The results obtained were found to be in harmony as shown in Table 4-3 and typical of large modern civilian high bypass turbofan engines like GE90 with high specific thrust and low SFC.

Table 4-3 Comparison of Turbomatch results with actual GE90 data

	Units	TF90 Model	GE90 Engine	% Deviation
Net Thrust	[kN]	513.83	514.00	0.03
Specific Thrust	[N/(kg/s)]	313.31	313.22	0.03
SFC	[g/kN.s]	8.92	9.21	3.06
Fuel Flow	[kg/s]	4.59	4.73	3.10
Mass flow	[kg/s]	1640	1641	0.06
TET	[deg K]	1925	-	-
OPR		42.2	42.2	0.00
BPR		7.1	7.1	0.00
FPR		1.65	-	-

4.5 Off Design performance

Once the design point is established for an aero engine, it is required to demonstrate overall satisfactory performance for the rest of the operating points encompassed within the flight envelope and over a wide range of ambient conditions. This off-design analysis is vital from both economic and safety perspectives. For instance, the effect of ambient conditions can alter the runway length required and the payload accepted by the same aircraft taking off from different geographical locations around the world.

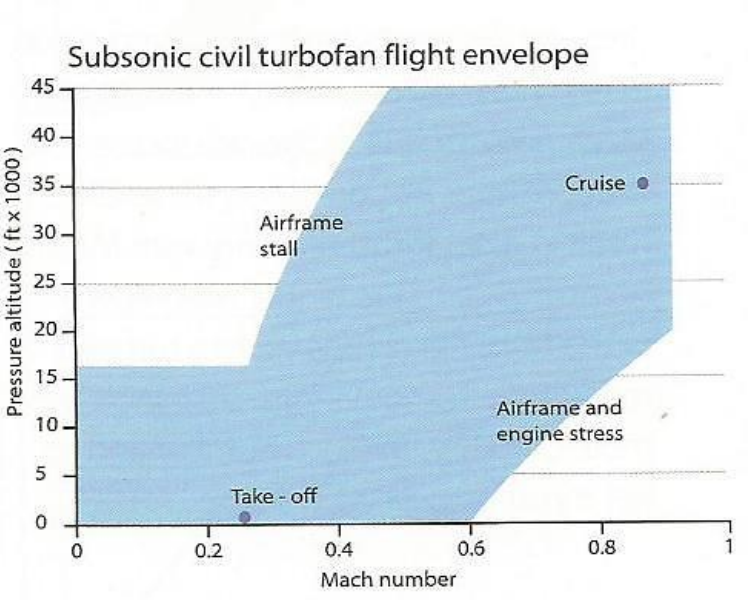

Figure 4-5 Subsonic Civil Turbofan Flight Envelope[36]

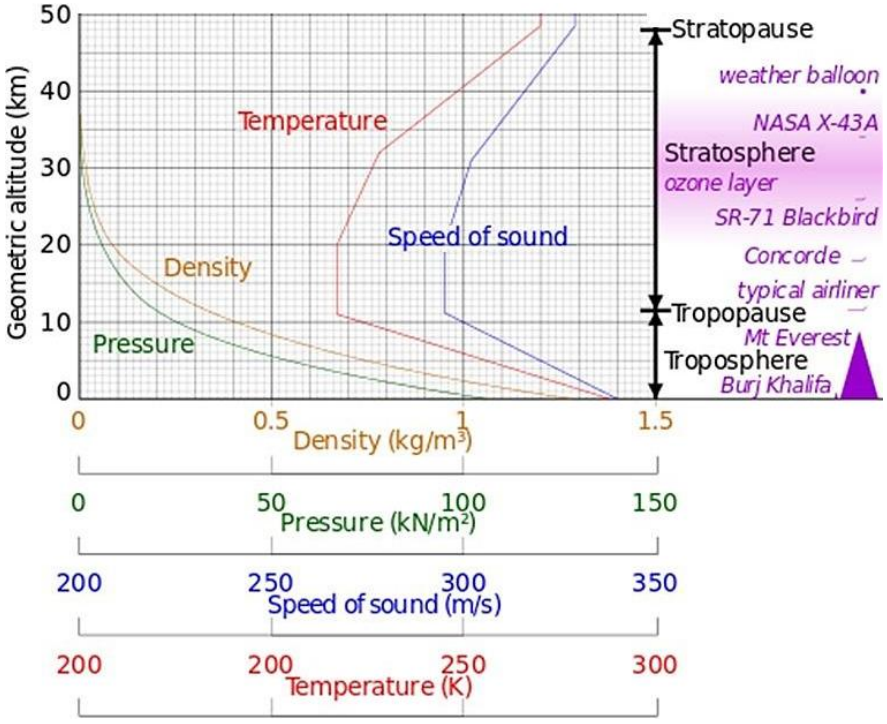

Figure 4-6 Atmosphere conditions [37]

In this project off-design simulations were performed to study the effect of varying flight speed, altitude and ambient temperature on the behaviour of the engine. The results and trends obtained were found to be in concurrence with physical explanation and typical of civilian turbofan engines, which further validated the accuracy of TF90 model built in Turbomatch.

4.5.1 Effect of Mach No and Altitude

Generally, as the flight speed varies, there are three key factors which influence the engine performance profile: momentum drag, ram compression and ram temperature rise [38]. The momentum drag (product of mass flow and flight velocity) increases with the flight velocity and hence reduces the net thrust. The momentum imparted to the flow in the gas path falls as the difference between the jet velocity and flight velocity continues to decrease with increase in flight

velocity. This effect increases propulsive efficiency. Ram compression effect on the other hand increases the pressure in the intake which raises the flow density and thereby increases the mass flow. In addition, it increases the nozzle pressure ratio, which increases the jet velocity and hence the gross thrust. This effect decreases the propulsive efficiency. The effect of ram temperature rise in the inlet due to increase in flight velocity is similar to the effect of increase in ambient temperature already discussed in previous section.

To study the effect of flight speed and altitude on the model engine performance, off design analysis was performed for subsonic Mach number range 0 to 1.0 at constant TET of 1650 K and standard ISA conditions. Same was repeated for four different altitudes 0m, 4000m, 8000m and 12000m. These sets of operating points were carefully chosen to create similar conditions that cover the climb phase of the flight. The simulation results shown in Figure 4-7, Figure 4-8 and Figure 4-9 demonstrate the cumulative effect of all three factors (momentum drag, ram compression and ram temperature) on engine thrust, mass flow and SFC respectively.

The overall effect of variation in flight speed can be explained as follows. Since the engine is a turbofan the momentum drag effect is most dominant due to lower jet velocity and thus results in continuous reduction in net thrust. However, at low speeds there is larger reduction in net thrust than at high speeds. This is because the subsonic airflow below Mach 0.3 is almost incompressible and the ram compression effect starts to be felt after Mach 0.3, increasing the mass flow and the nozzle pressure ratio, and opposing the effect of momentum drag. This counter effect gradually lessens the reduction of net thrust with Mach number. The effect of ram temperature rise is minimal and less obvious compared to the primary drivers; momentum drag and ram compression.

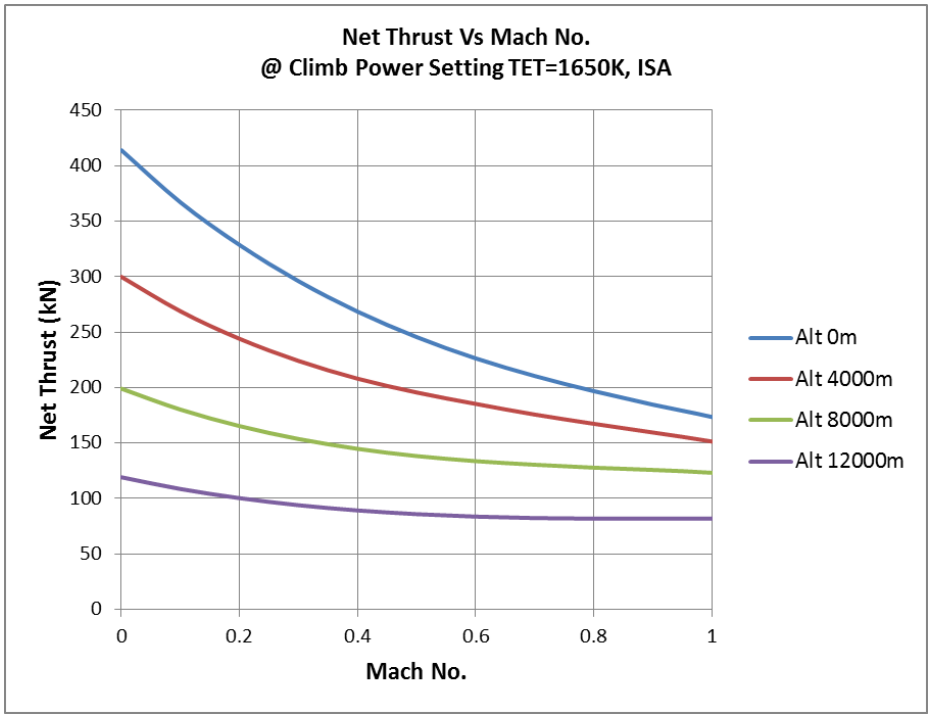

Figure 4-7 Net Thrust vs Mach No at climb Power Setting TET=1650K, ISA .

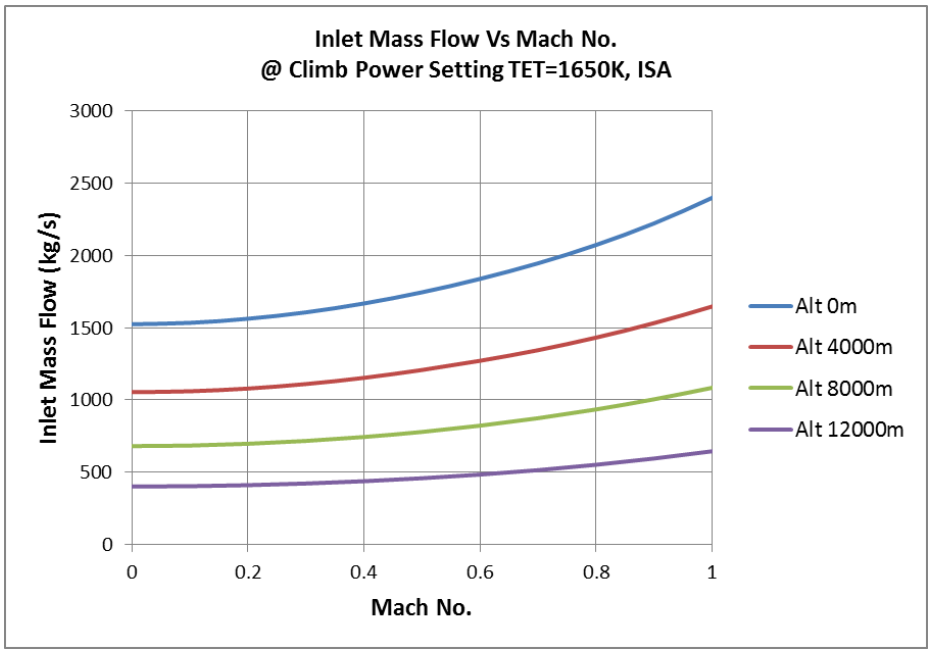

Figure 4-8 Inlet Mass Flow Vs Mach No. at Climb Power Setting TET=1650K, ISA

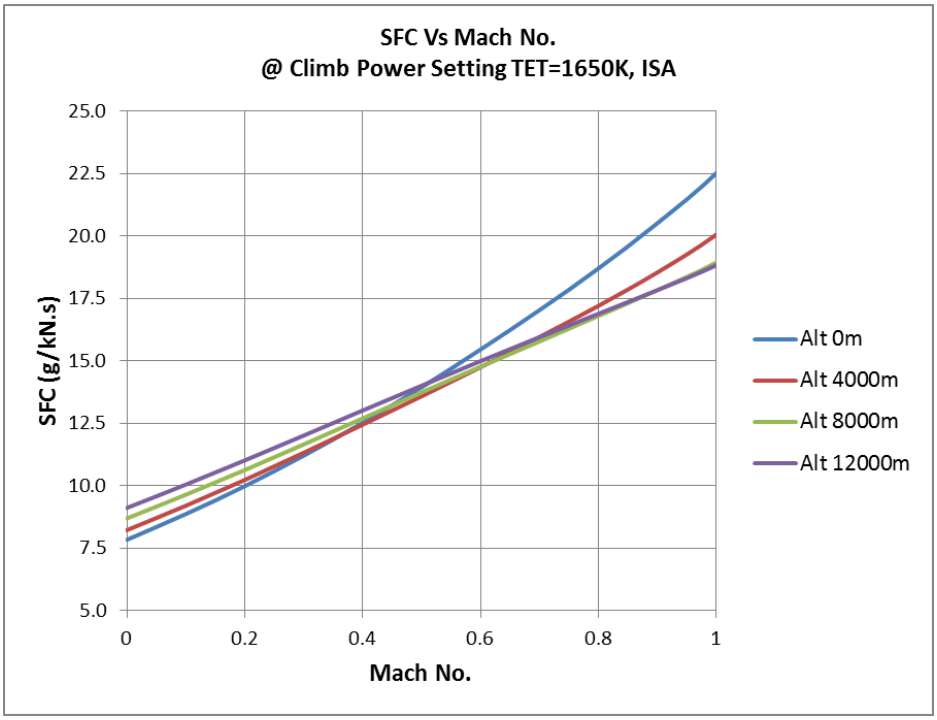

Figure 4-9 SFC Vs Mach No. at Climb Power Setting TET=1650K, ISA

Same plots in Figure 4-7, Figure 4-8 and Figure 4-9 also allow to observe the effect of increasing altitude at constant Mach number. With an increase in altitude, the static ambient pressure and the air density fall. At constant shaft speed this causes the air mass flow to drop and reduce the thrust. On the contrary, the ambient temperature which also decreases with increase in altitude tends to increase the mass flow and the thrust, partly offsetting the pressure effect. The net effect is that the engine actually generates less thrust as the altitude increases appreciating the dominant pressure effect. A decrease in thrust with an increase in flight velocity is more significant at lower altitudes. As the altitude increases the thrust variation due to airspeed tends to flatten.

SFC is directly linked to the Mach number. The density experiences a rise just as the Mach number increases. The link between the SFC and the Flight velocity can explain this; as observed from the formula documented above, a rise in flight velocity, in concurrent to a dip in thermal efficiency causing the SFC to go higher. Subsequently, an increase in altitude helps improve the SFC due to the rise in thermal efficiency. Moreover, the compressor diagram can be used to analyse

this. As studied earlier, the temperature decreases and thus the non-dimensional constant shaft speed increases due to a rise in altitude. Hence the pressure ratio also experiences a rise due to an increase in the non-dimensional speed results. While the mass flow dips against an increasing altitude (directly relative to thrust), within the lower atmosphere, the increasing pressure ratio prevails (troposphere up to 11 km. The discussed rise in pressure ratio causes an increase in thermal efficiency and subsequently resulting in a dip in SFC.

4.5.2 Effect of Outside Air Temperature

Variation in ambient air temperature greatly influences the engine behaviour based on geographical location of engine operation, season of the year and time of the day. The off design performance was studied for an outside temperature range of -30 C to 50 C, at constant altitude of 50 meters, Mach number 0.15, and repeated for four different constant TET values 1300K, 1500K, 1700K and 1900K. These operating conditions were carefully chosen to create and simulate scenarios close to the takeoff and landing phases of the flight. The results of the simulation are shown in Figure 4-10, Figure 4-11 and Figure 4-12, demonstrating the effect of ambient temperature variation on engine thrust, mass flow and SFC respectively.

On a relatively hot day, with an increase in ambient temperature the density of the air decreases, reducing the air mass flow entering the compressor(s) downstream. Since less power is now required for compression, the fuel flow is reduced to maintain constant engine rotational speed and/or TET. As a result the engine is subjected to operate at lower pressure and temperature ratio which reduces the overall engine thrust and the thermal efficiency. At an outside temperature of 45 C, average thrust loss of up to 17 % was observed with respect to ISA condition.

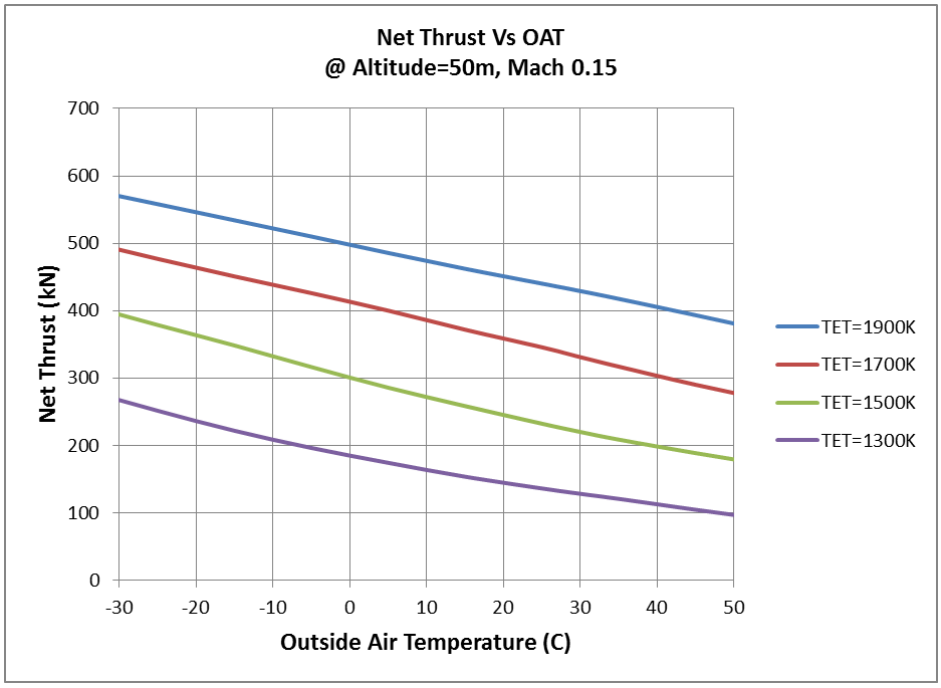

Figure 4-10 Net Thrust vs OAT at Altitude=50m, Mach 0.15

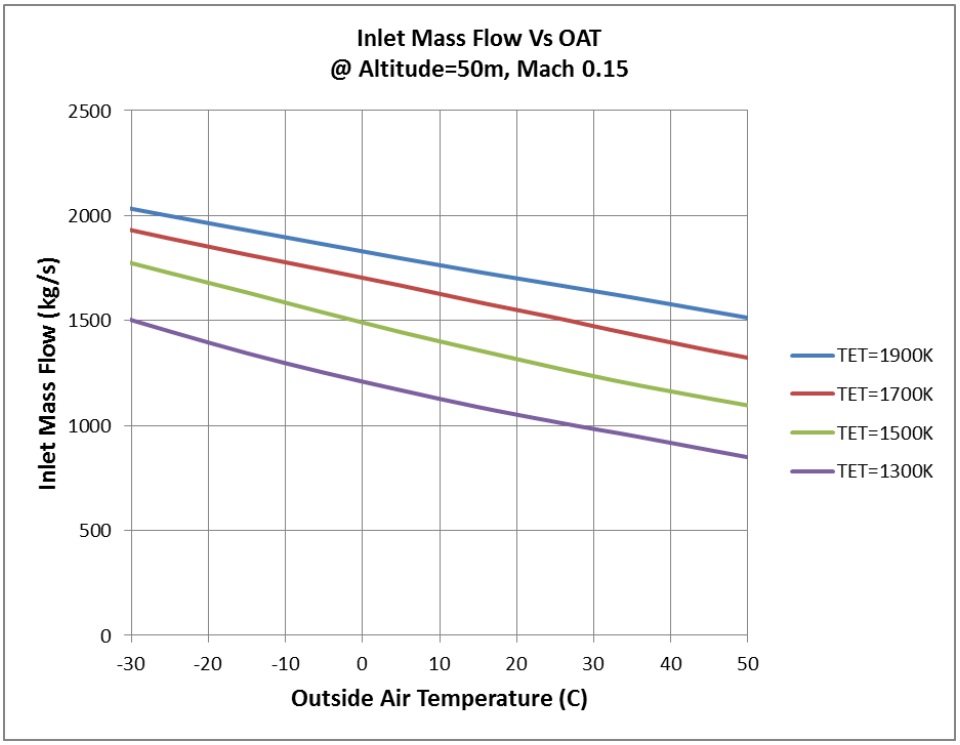

Figure 4-11 Intel Mass Flow vs OAT at Altitude=50m, Mach 0.15

Unlike the thrust and the mass flow, the relation between SFC and OAT as found in Figure 4-12 appeared to be less obvious. The trends are found to be dependent on the TET at which the engine operates. At lower constant TET the variation in

SFC with increase in ambient temperature is more sensitive than at higher TET. One way this can be understood is by looking further into the variation in thermal and propulsive efficiencies with respect to ambient temperature. Given the fact that thermal efficiency is directly proportional to the temperature ratio (TET/T1), this ratio is smaller at lower constant TET and it further drops with increase in outside temperature. Hence the reducing thermal efficiency, instead of increasing propulsive efficiency, becomes the dominant factor responsible for the rise in SFC. At lower constant TET there is greater reduction in the thrust than in fuel flow which gives rise in SFC with increase in ambient temperature. However, at higher constant TET, there is greater rise in fuel flow than in thrust which gives rise in SFC with decrease in ambient temperature.

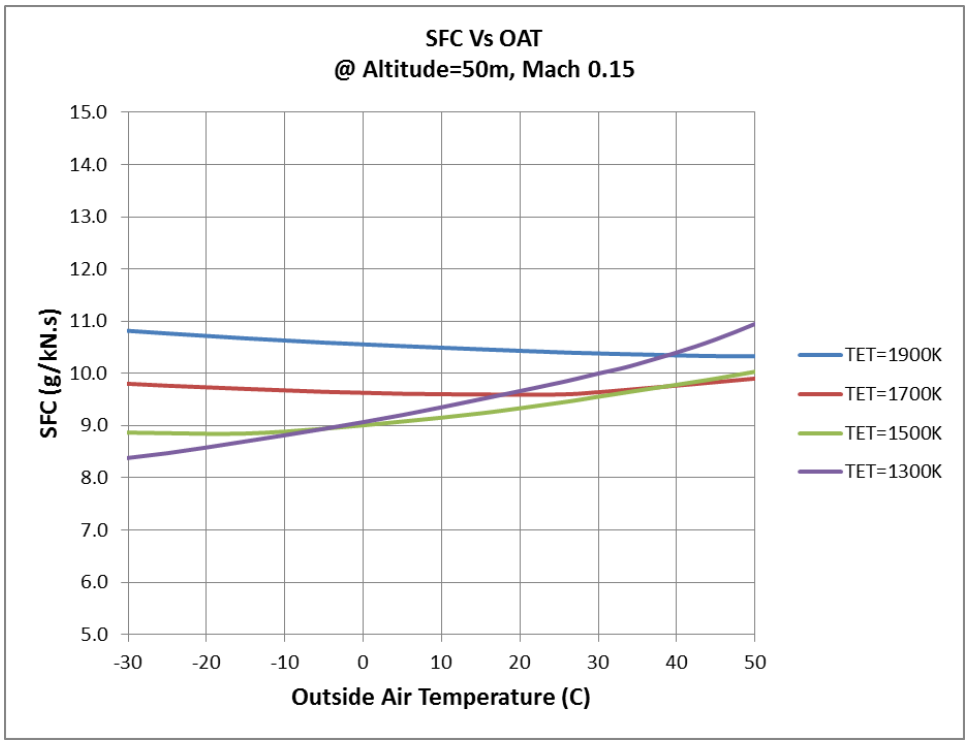

Figure 4-12 SFC vs OAT at Altitude=50m, Mach 0.15

5 AIRCRAFT & FLIGHT MISSION MODEL

5.1 Introduction to Aircraft Performance

A typical flight mission is divided into several phases: Takeoff, Climb, Cruise, Descent and Landing etc. Each phase can be analyzed in two ways: Point performance provides a snapshot of instantaneous aircraft performance at a particular moment in time (e.g. velocity, drag, fuel consumption etc.), while the path performance is the integral between two instances, evaluating performance over the flight segment (e.g. range and endurance etc.).

The general 2D translational motion of an aircraft in accelerated flight is described by the following equations of motion in terms of four physical forces acting on the aircraft; lift, weight, drag and thrust.

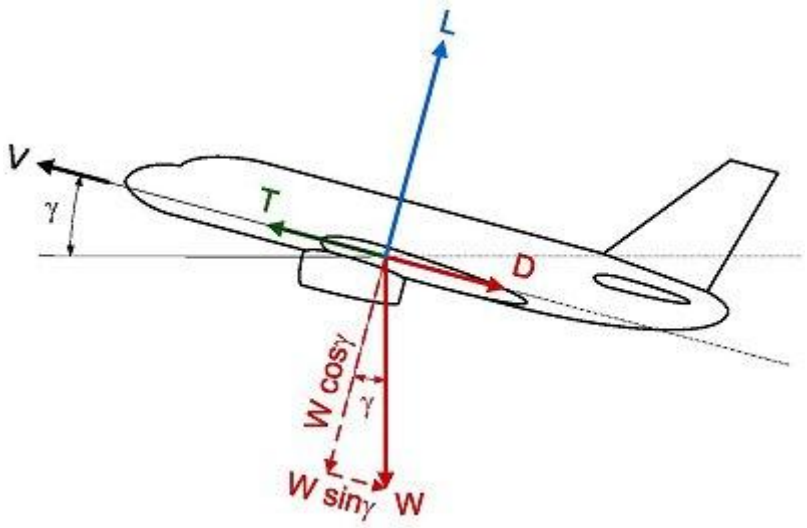

Figure 5-1 Aircraft Free Body Diagram[39]

$$T - D - W\sin\gamma = m\frac{dv}{dt} \qquad \textbf{(5-1)}$$

$$L - W\cos\gamma = m\frac{v^2}{r_c} \qquad \textbf{(5-2)}$$

Where;

Lift L, perpendicular to the flight path direction.

Drag D, parallel to the flight path direction

Thrust T, in line with engine centreline parallel to the flight path

Weight W, vertical down towards the centre of the earth

γ, flight path inclination angle with respect to horizontal

Velocity v, along the flight path

Radius of curvature r_c for the centrifugal acceleration v^2/ r_c acting normal to the curved path.

These four forces as well as the flight path inclination angle change during different flight phases. At the take-off phase the aircraft requires excess thrust to accelerate and then lift off. Same is true during climb. While descending the engine thrust is reduced to decrease the lift force in order to lower the aircraft altitude for landing.

For steady, level flight in cruise condition the equations (5-1) and (5-2) are simplified to (5-3) and (5-4).

$$T = D \quad \textbf{(5-3)}$$

$$L = W \quad \textbf{(5-4)}$$

To maintain certain flight condition at specific speed and altitude, enough thrust must be produced by the engines to overcome the aerodynamic drag and to keep the aircraft flying with enough lift against the weight. This thrust required, T_R, is an airframe associated feature [38] which depends not only on velocity and altitude but also on aerodynamic size, shape and weight of the aircraft.

The parabolic drag polar encompasses the entire aerodynamics of an aircraft. It contains almost all the necessary aerodynamics for an airplane performance analysis.

Parasite drag is that portion of the total drag associated with skin friction and pressure drag due to flow separation, integrated over the complete surface of the aircraft. It also includes the interference drag caused due to the mutual interaction of the flow fields around each component of the aircraft.

Induced drag is the pressure drag due to the pressure imbalance in the drag direction caused by the induced flow (downwash) associated with the vortices created at the tips of the wings.

Zero Lift drag is the parasite drag that exists when the airplane is at its zero-lift angle of attack i.e. when the lift of the airplane is zero. Drag due to lift is that portion of the total aircraft drag measured above the zero-lift drag. It consists of the change in parasite drag when the aircraft is at an angle of attack different from the zero-lift angle, plus the induced drag from the wings and other lifting components of the aircraft.

Equation (5-10) $C_D = C_{D,0} + KC_L^2$ is the drag polar of the aircraft where C_D is the total drag coefficient, $C_{D,0}$ is the zero-lift parasite drag coefficient and KC_L^2 term is the drag due to lift. K is the induced drag coefficient and an aerodynemic quantity which carries inherent characteristics of particular aircraft design.

$$T_R = D = \frac{1}{2}\rho v^2 S C_D \qquad \textbf{(5-5)}$$

$$L = W = \frac{1}{2}\rho v^2 S C_L \qquad \textbf{(5-6)}$$

Where C_L is lift coefficient and C_D is drag coefficient.

S is the wetted surface area of the aircraft.

Dividing equation (5-5) by equation (5-6) gives

$$\frac{T_R}{W} = \frac{C_D}{C_L} \quad \textbf{(5-7)}$$

$$T_R = \frac{W}{C_L/C_D} = \frac{W}{L/D} \quad \textbf{(5-8)}$$

$$C_L = \frac{W}{\frac{1}{2}\rho v^2 S} \quad \textbf{(5-9)}$$

$$C_D = C_{D,0} + KC_L^2 \quad \textbf{(5-10)}$$

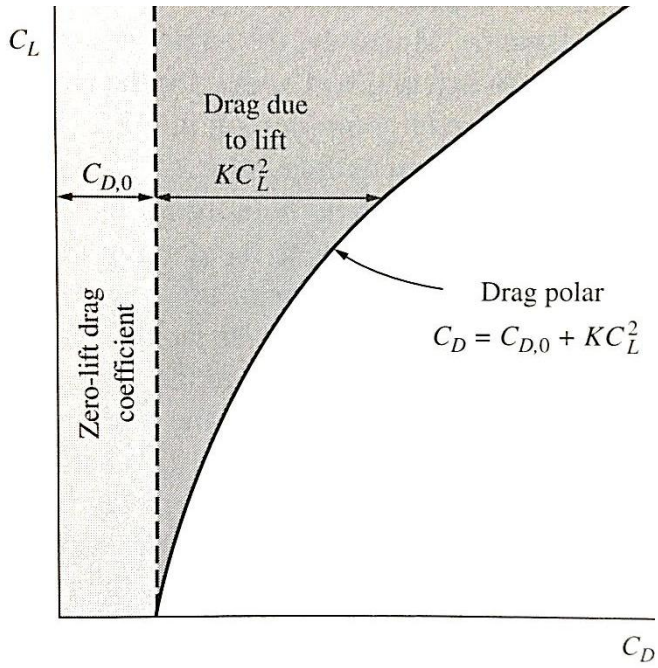

Figure 5-2 Schematic of the components of the Drag Polar – Page 131 in [38]

The T_R obtained is the thrust required to fly at the specific velocity.T_R is inversely proportional to L/D. Hence, minimum thrust required will be obtained when the airplane is flying at a velocity where L/D is maximum. The lift-to-drag ratio L/D is a measure of the overall aerodynamic efficiency of an airplane; it only makes

sense that maximum aerodynamic efficiency should lead to minimum thrust required [40].

Range and Endurance

Few of the other important elements of aircraft performance are the aircraft range and endurance. Range R is the total distance travelled by the aircraft with certain quantity of fuel in the tank. Similarly, endurance E is the total time an aircraft remains airborne with certain quantity of fuel in the tank. To maximize range there are different parameters from those which maximize endurance Following are the respective equations in simplified form; derivation details of which can be referred in [40].

$$R = \int_{W_1}^{W_0} \sqrt{\frac{2}{\rho S}} \frac{1}{(SFC)} \frac{C_L^{1/2}}{C_D} \frac{dW}{W^{1/2}} = 2\sqrt{\frac{2}{\rho S}} \frac{1}{(SFC)} \frac{C_L^{1/2}}{C_D} \left(W_0^{1/2} - W_1^{1/2}\right) \quad \textbf{(5-11)}$$

$$E = \int_{W_1}^{W_0} \frac{1}{(SFC)} \frac{L}{D} \frac{dW}{W} = \frac{1}{(SFC)} \frac{C_L}{C_D} \ln \frac{W_0}{W_1} \quad \textbf{(5-12)}$$

Where,

dW is the incremental change in aircraft weight due to fuel consumption

W_0 is the initial weight at distance = 0 or time = 0.

W_1 is the final weight at distance = R or time = E

Conditions to obtain maximum endurance as follows:

- Minimum specific fuel consumption
- Maximum fuel weight W_f
- Maximum L/D or C_L/C_D
- Maximum endurance is achieved when the aircraft flies at minimum thrust required which corresponds to flying at a velocity such that C_L/C_D is maximum.

Conditions to obtain maximum range are as follows:

- Minimum specific fuel consumption
- Maximum fuel weight W_f
- Maximum $C_L^{(1/2)}/C_D$. For maximum range, aircraft must fly at a velocity such that $C_L^{(1/2)}/C_D$ is maximum.
- Maximum range is achieved when the aircraft flies at a velocity such that $C_L^{(1/2)}/ C_D$ is maximum.

5.2 Aircraft Model Development for Hermes

Hermes is another tool developed by Cranfield University which is used in conjunction with Turbomatch for overall aircraft performance simulation. It employs principles of aerodynamics and aircraft performance to generate flight data for the entire flight mission defined. One of the key inputs required is the aircraft configuration data which includes the shape and geometry of the major aircraft components, such as fuselage, wings, tail, engine nacelle etc, as well as the general weight breakdown.

Two aircraft models were created for the purpose of this study based on two different configurations of Boeing 777 series aircraft - B777-300ER and B777-200LR. Both are wide body, twin-engine aircraft, quite well known in the aviation business for long range applications. Both of them are equipped with latest GE90 powerplant, but with different thrust ratings. Engine, when operated on B777-300ER at a higher thrust rating is considered as GE90-115B, and when operated on B777-200LR at a relatively lower thrust rating is considered as GE90-110B1. Throughout the study the aircraft models are named as A773ER and A772LR while their corresponding engine models are named as TF115 and TF110 respectively. The technical characteristics of the two aircraft models are summarized below in Table 5-1.

.

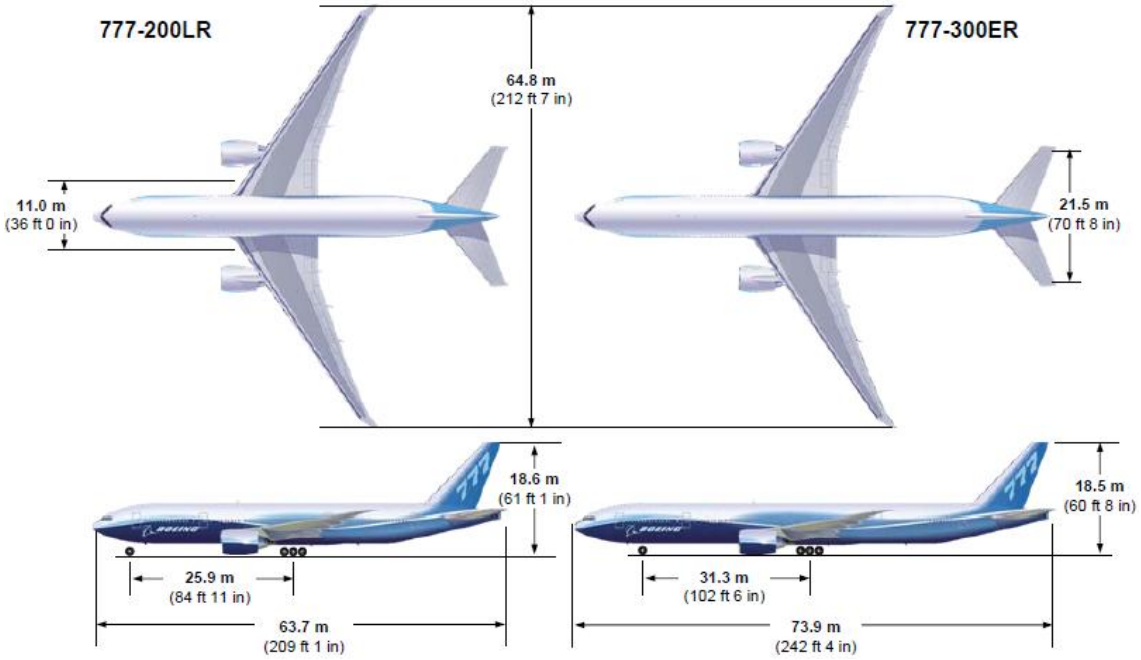

Figure 5-3 Boeing 777 dimensions [19]

Table 5-1 Aircraft Technical Data [11] [31][19]

	Units	B777-300ER	B777-200LR
Aircraft Geometry			
Fuselage Length	m	72.87	62.94
Fuselage Width	m	6.2	6.2
Wing Area	m2	436.8	436.8
Wing Aspect Ratio	-	9.69	9.69
Tailplane Area	m2	84.4	84.4
Tailplane Aspect Ratio	-	4.5	4.5
Vertical Fin	m2	44.4	44.4
Vertical Fin Span	m	9.8	9.8
Typical Cabin Seating	-	360	270
Weight Breakdown			
Operating Empty Weight	kg	167,829	145,150
Max Payload	kg	69,853	63,957
Max Design Takeoff Weight	kg	351,535	347,452
Max Landing Weight	kg	251,290	223,168
Max Zero Fuel Weight	kg	237,683	209,106
Max Fuel Weight	kg	145,538	145,538
Powerplant		GE90-115B	GE90-110B
No. of Engines	-	2	2
Engine Weight	kg	8,936	8,936
Engine Thrust (Max)	kN	514	493
or	lbf	115,540	110,760
Engine Nacelle Length	m	6.3	6.3
Engine Nacelle Diameter	m	4.1	4.1

Both the configurations share the same basic aircraft design, from wing and tail geometry to high lift systems and landing gears. Only the fuselage differs in length. Each model, according to its fuselage length, has a different passenger and cargo capacity and thus a different aircraft MTOW, OEW, and maximum payload limitation. In both the models the average weight of a passenger was assumed to be 75 kg with a 30 kg baggage allowance.

5.3 Hermes-Turbomatch Integrated Operation

The joint utilization of Hermes and Turbomatch software tools allows computation of both aircraft and engine related operational parameters for all segments of the

flight mission profile and thus provides complete performance data for analysis. Figure 5-4 shows the basic data flow diagram for the Hermes-Turbomatch Integrated Operation.

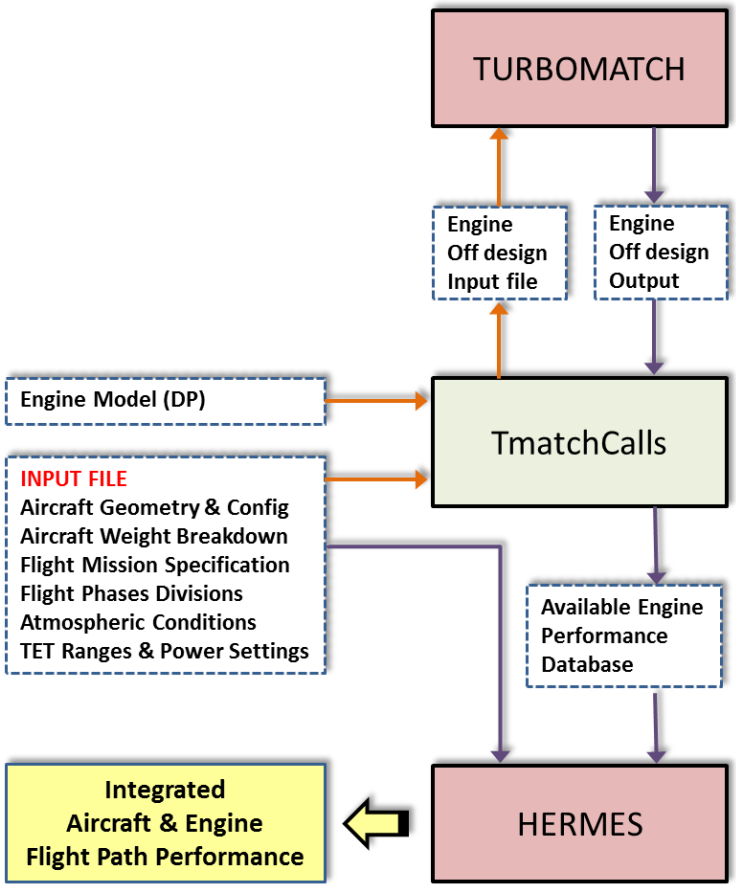

Figure 5-4 Basic Data Flow in Hermes – Turbomatch Integrated Operation

The main input file required is divided into different parts. The first part covers the geometry and configuration of the aircraft. The second part contains information regarding the flight mission and aircraft weight breakdown. The following parts in the file exist to describe the flight phases, namely Takeoff, Climb, Cruise, Descent and Flight Idle etc and divide some of them into segments with atmospheric conditions and power settings specified. The structure of the two input files prepared for the purpose of this project can be viewed in Appendix B as examples.

TmatchCalls is an interface which when executed reads the input file containing the mission profile, different TET ranges, power settings and atmospheric conditions during the different segments of the flight phases, and prepares another input file for Turbomatch to run the engine model simulation at those off design conditions. TmatchCalls formats the output results from Turbomatch into a specific structure and builds a database encompassing the entire engine performance data required for the flight mission. This data is independent of correlations with the aircraft.

Given the aircraft geometry and flight conditions as inputs, Hermes evaluates the aerodynamic characteristics of the complete aircraft in the form of zero-lift and lift-induced drag coefficients, the two terms of the parabolic drag polar. This information is used along with the engine performance database produced by Turbomatch and TmatchCalls to determine the overall performance of the aircraft at various segments of the mission profile. Typical output parameters include total fuel consumption, range and endurance of an entire flight mission, while lift to drag ratio (aerodynamic efficiency), engine SFC and rate of climb etc. are calculated for each mission segment.

5.4 Payload-Range Diagram – Aircraft Model verification

The purpose of the payload-range diagram is to reveal the maximum distance an aircraft can fly with a given payload under the authorized operational weight limitations, and also to illustrate the tradeoff relationships between the fuel weight, payload and range to allow for quantitative assessment of any deviation from the optimum operation of the aircraft. The unique shape of the aircraft's payload-range diagram is governed by its aerodynamic characteristics, structural design and engine technology etc [41] and that is why every aircraft type has its own corresponding payload-range diagram. To understand its dynamics it is first important to appreciate the terminology used for the conceptual breakdown of aircraft weights as mentioned in the chart shown in Figure 5-5.

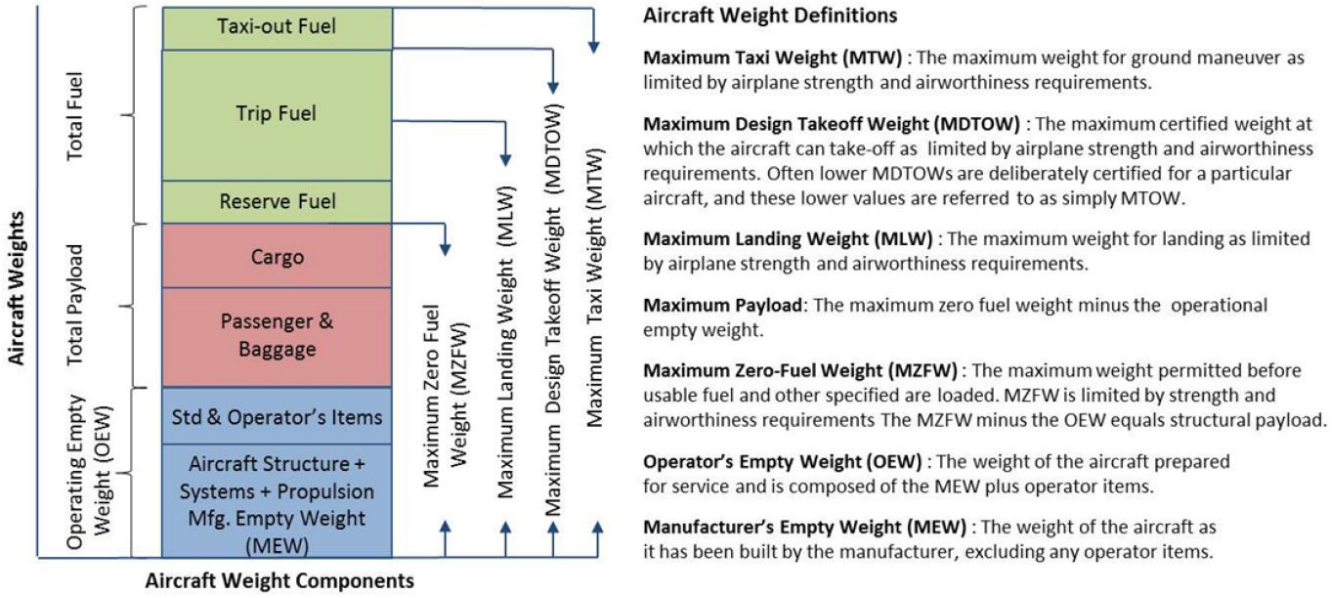

Figure 5-5 Aircraft Weight Definitions[41]

Figure 5-6 shows the construction of a payload-range diagram with Operator's Empty Weight (OEW) being the datum. There are 4 crucial points in the diagram corresponding to the following respective conditions.

A. Max. Payload + no Fuel wt. (such that TO weight < MDTOW)

B. Max. Payload + partial Fuel wt. (such that TO weight = MDTOW)

C. Max. Fuel wt. + partial Payload (such that TO weight = MDTOW)

D. Max. Fuel wt. + no Payload (such that TO weight < MDTOW)

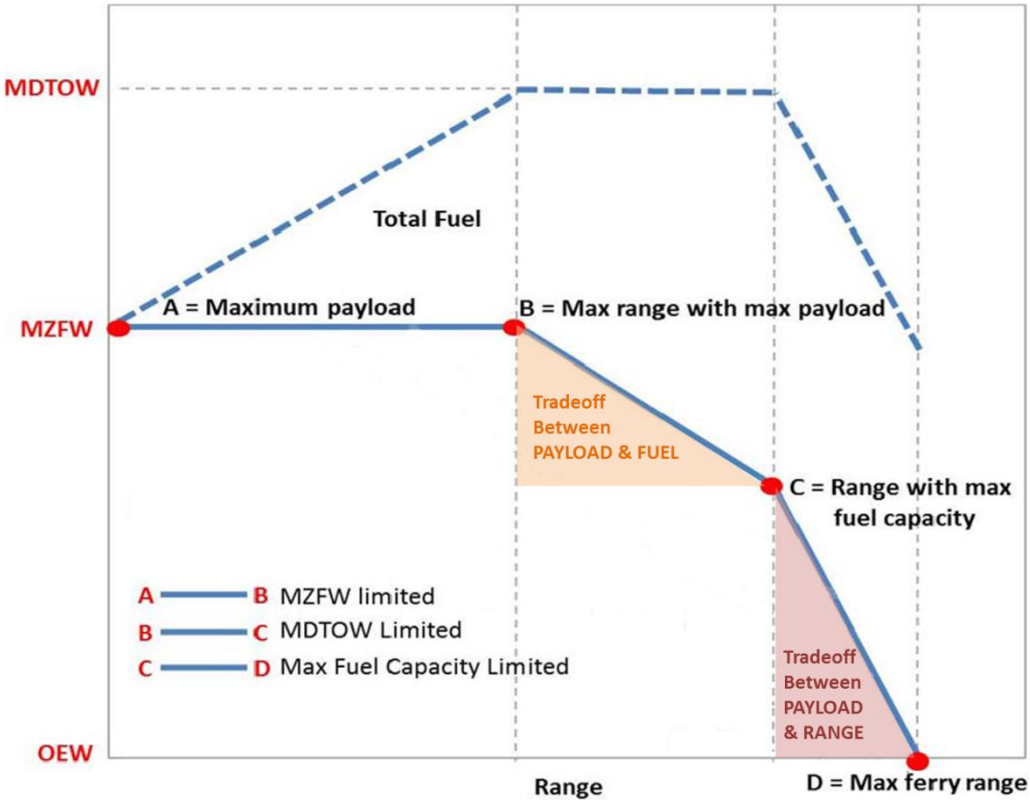

Figure 5-6 Payload-Range Diagram explained [41]

In the first part of the payload-range diagram (A-B) the payload is maximum which is limited by aircraft Maximum Zero Fuel Weight (MFZW). The range of the flight mission increases upon increasing the fuel weight until point B where the Maximum Design Takeoff Weight (MDTOW) is achieved. In the second segment (B-C) the MDTOW is maintained, but to further increase the range the payload is reduced while the fuel weight is increased. This tradeoff between payload and fuel can only continue until point C which offers maximum operational range with full fuel tanks. The maximum fuel weight remains constant beyond point C and the only way to achieve the extra bit of range is by compromising the payload and thereby reducing the overall takeoff weight. The payload weight becomes zero at point D. Flying with such condition is economically unfeasible. This option is only used when the aircraft is newly delivered to the airline operator or when a non-critical fault sanctions a one-off ferry flight without the passengers to return to home base for defect rectification.

The Payload-Range analysis was used as a means to validate the two aircraft model variants created in Hermes against the actual performance data of B777-300ER and B777-200LR found in the public domain [42]. Flight mission simulations were performed with Hermes specifically at those four crucial points A, B, C and D that define the boundary of the payload-range diagram, determining the maximum operational limits in terms of range and payload. There are two ways of analyzing a mission in Hermes. The first method involves specifying the range of the mission as input and the code automatically calculates the total fuel consumption during the flight, while the second method lets the user fix the total fuel weight carried by the aircraft and the code determines the total flight range the aircraft can fly with that given amount of fuel. In order to obtain the required data for the construction of payload-range diagram, the second method was adopted. Maximum mission ranges were calculated based on selected payloads and fuel weight allowance. Figure 5-7 shows the payload-range plots for the model airplanes and their respective counterparts all in one chart for comparison purposes.

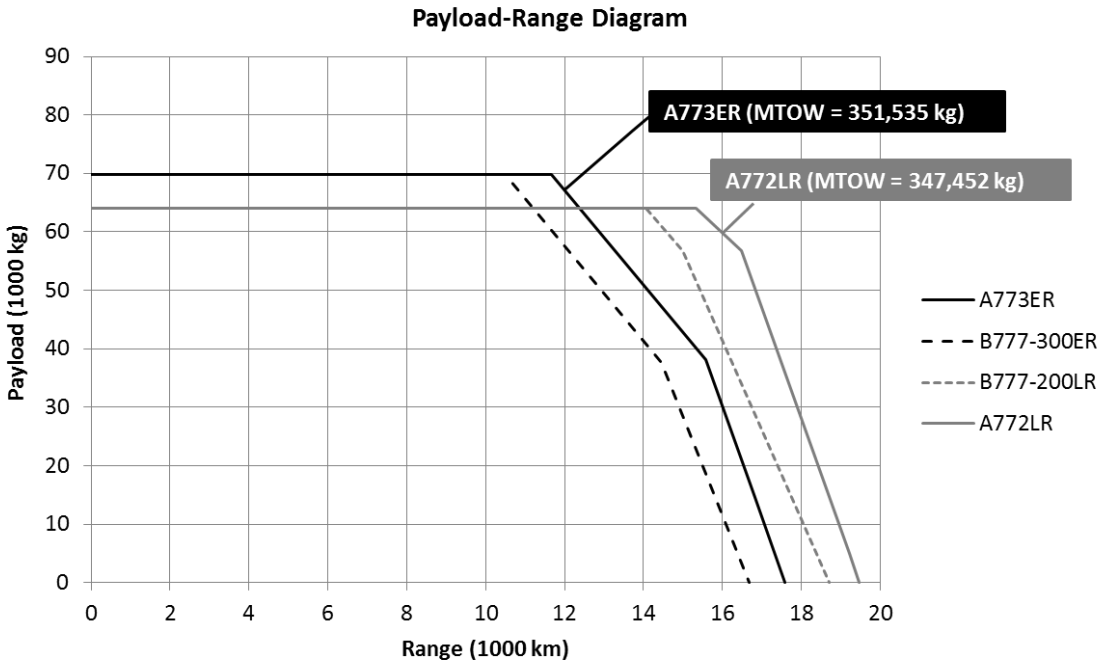

Figure 5-7 Payload-Range Diagram for A7773ER and A7772LR

Comparing the results obtained for the two models with respect to the actual aircraft in Table 5-2 and Table 5-3, there were slight deviations observed in maximum ranges calculated at boundary conditions B, C and D for the same payload. For A773ER, the largest deviation of 11.0% was found to be for the case when the aircraft takes off with MDTOW while carrying maximum payload. On the other hand, for A772LR, the largest deviation of 9.9% was found to appear when the aircraft takes off with MDTOW utilizing the full fuel capacity.

Table 5-2 A773ER Range Deviations

		A773ER	B777-300ER	
Point	Condition	Range (km)	Range (km)	Deviation (%)
A	Max Payload & MZFW	0	0	-
B	Max Payload & MDTOW	11,659	10,500	11.0
C	Max Fuel & MDTOW	15,578	14,446	7.8
D	Max Fuel & No Payload	17,588	16,668	5.5

Table 5-3 A772LR Range Deviations

		A772LR	B777-200LR	
Point	Condition	Range (km)	Range (km)	Deviation (%)
A	Max Payload & MZFW	0	0	-
B	Max Payload & MDTOW	15,330	14,075	8.9
C	Max Fuel & MDTOW	16,493	15,001	9.9
D	Max Fuel & No Payload	19,475	18,705	4.1

These differences in the depicted payload-range plots can possibly be attributed to one or combination of the following factors.

- Variation in flight mission specifications due to intricate details known only to the manufacturer, for instance step climb rate, the power extraction requirement, and the air conditioning bleed configuration etc.
- Engine model used in the study is similar to actual engine but not exactly the same, for instance, due to different design point or different component efficiencies.
- Computing code limitations of the Hermes and Turbomatch software versus the flight test experimental data from the manufacturer.

Nevertheless, considering the fact that there were no major deviations in maximum ranges and both models had similar trends when compared to actual aircraft, the models were deemed acceptable for further study work in this project.

5.5 Baseline Flight Missions and Analysis

After obtaining adequate familiarization of the integrated Hermes-Turbomatch performance tool the next step was to generate engine operational data through flight simulation and compare the severity of operation based on engine when operated with two different power setting schedules on two different versions of the same aircraft series. For this reason two reference flight mission profiles were selected, details of which were entered in two independent input files which can be referred in Appendix B. Mission 1 employs bigger version aircraft A773ER certified with higher engine thrust rating and mission 2 employs smaller version aircraft A772LR with lower engine thrust rating.

The mission specifications are listed in Table 5-4. The overall range and endurance of the trips remain unchanged. The climb and descent segments are flown with adjusted engine power settings to ensure the respective climb and descent phase intervals last the same in both missions [43]. The cruise phase in both missions is split into two segments in which the aircraft flies at two different altitudes and Mach number. Apart from the aircraft size and the actual takeoff weight all the rest of the mission specifications were carefully chosen to be the same. This precisely allowed studying the impact of available thrust utilization on engine time-on-wing (TOW) without the influence of any other factor. A reasonable average range for the missions was selected considering the payload-range limitations of both the aircraft variants. Takeoff derate was set as 10% of the original thrust ratings.

Table 5-4 Flight Mission Specifications

Flight Mission Specifications	Mission 1	Mission 2
Aircraft	A773ER (Similar to B777-300ER)	A772LR (Similar to B777-200LR)
2 x Engine (Max Thrust)	TF115 - Similar to GE90-115B (514 kN)	TF110 - Similar to GE90-110B (493 kN)
Avg TO Derate	10% (Thrust = 463 kN)	10% (Thrust = 443 kN)
Max TO Weight	351,530 kg	347,450 kg
Actual TO Weight	284,519 kg	250,263 kg
Avgerage Stage Length	6.75 hrs/flight cycle	6.75 hrs/flight cycle
OAT at Sea level	ISA + 15C	ISA + 15C
Altitude @ TO	0 m	0 m
Cruise Altitude 1	10,058 m	10,058 m
Cruise Speed @ Altitude 1	0.83 M	0.83 M
Cruise Altitude 2	11,583 m	11,583 m
Cruise Speed @ Altitude 2	0.85 M	0.85 M
Range	5750 km	5750 km

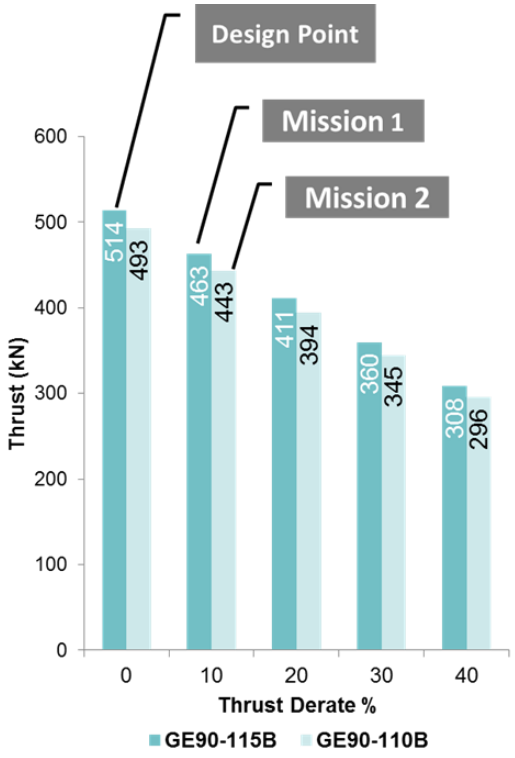

Figure 5-8 Takeoff Derates

Flight simulation data obtained for the two reference missions include the variation of altitude, net thrust and many other aircraft-engine operational parameters against time. Simulation also facilitated calculation of time spent, distance travelled, and fuel consumed during each of the flight segments.

The plot in Figure 5-9 illustrates the variation in altitude and net thrust during the entire flight mission while Table 5-5 reveals the time duration of each of the flight phases. These time intervals are the same for both missions.

Flight Phase	Time (min)
TAXI OUT	5.0
TAKEOFF	1.2
CLIMB 1	16.8
CRUISE 1	168.6
CLIMB 2	4.4
CRUISE 2	162.6
DESCENT	31.3
APPROACH	9.1
REVERSE THRUST	1.0
TAXI IN	5.0
Total	**405.0**

Table 5-5 Flight Phase duration

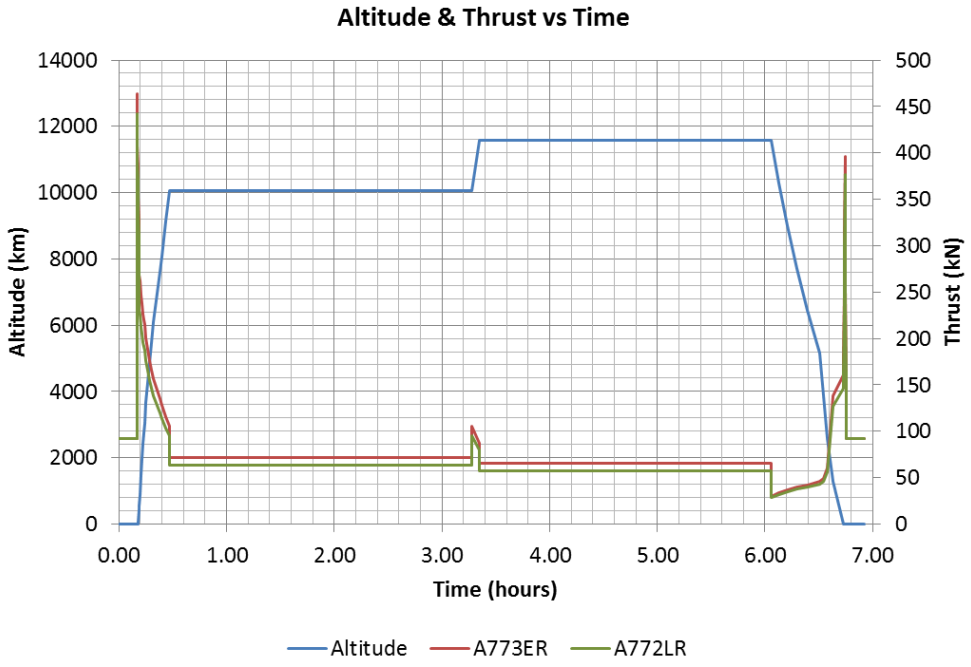

Figure 5-9 Plot of Altitude & Thrust vs Time

Out of the many outputs the most essential parameters from the perspective of engine lifing study are the non-dimensional HP shaft rotational speed, the HPC discharge cooling air temperature and the turbine entry temperature (TET). Knowing the trends of these parameters is a prerequisite to the computation of mechanical and thermal stresses acting on the HPT Stage 1 blades during the flight. These stresses and their iterative patterns of occurrence eventually lead to engine soft life estimation.

The plots in Figure 5-10, Figure 5-11 and Figure 5-12 compare the trends of TET, HP rotational speed, fuel flow and SFC obtained for the two reference missions. It is evident from the plots that the aircraft of greater size has a higher demand of thrust and fuel flow and therefore correspondingly higher TET and HP shaft rotational speed. SFC variation with time can be appreciated by revisiting the discussion on the effect of Mach No. and altitude on the SFC in the previous chapter.

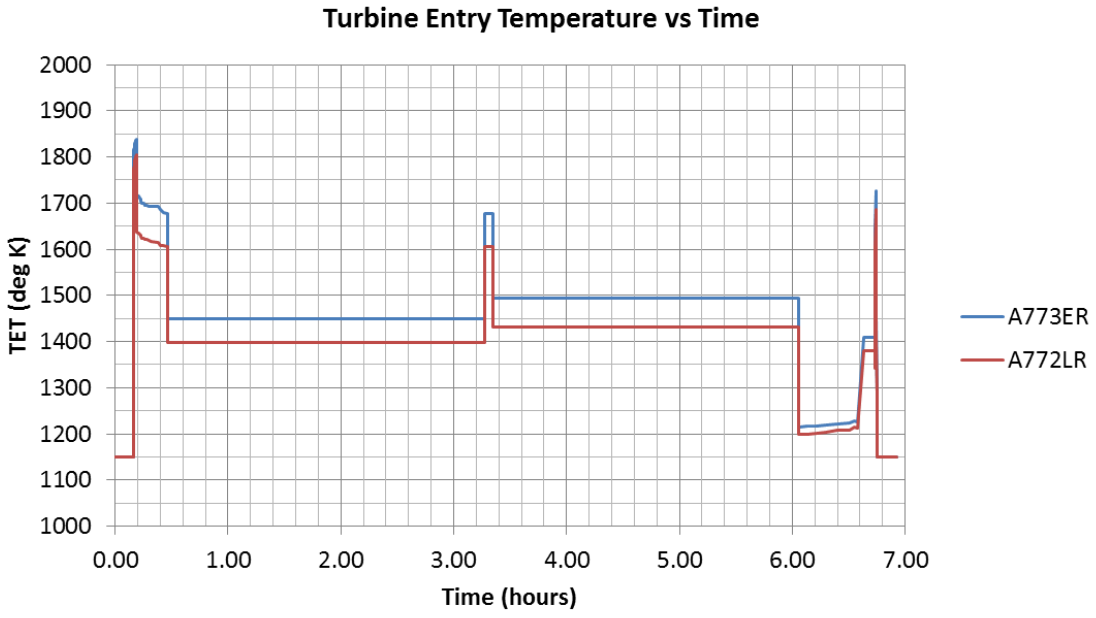

Figure 5-10 Turbine Entry Temperature vs Time

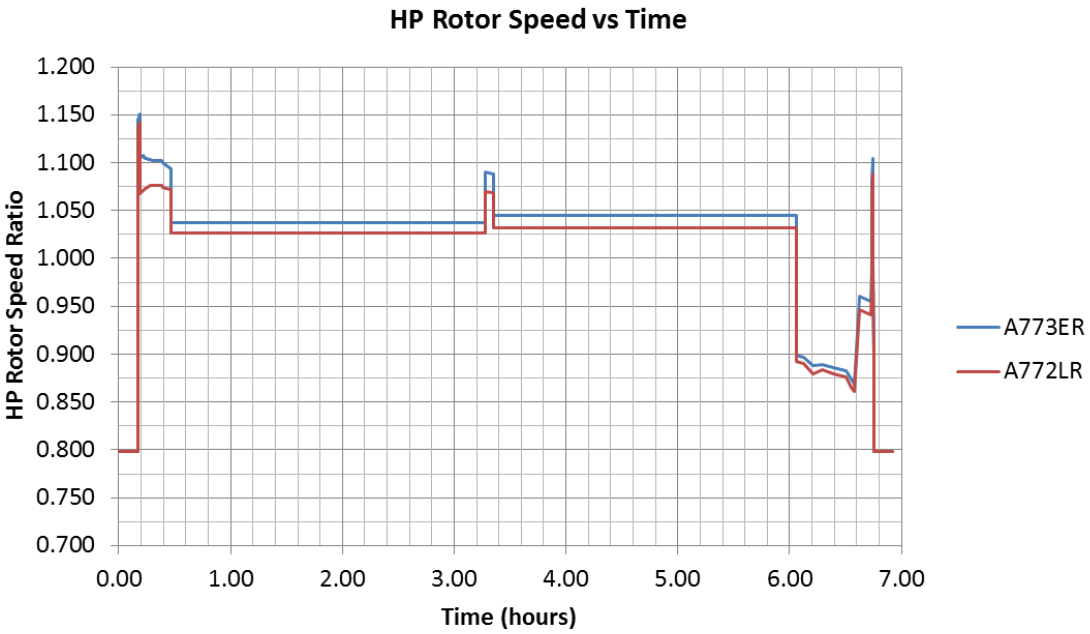

Figure 5-11 HP Rotor Speed vs Time

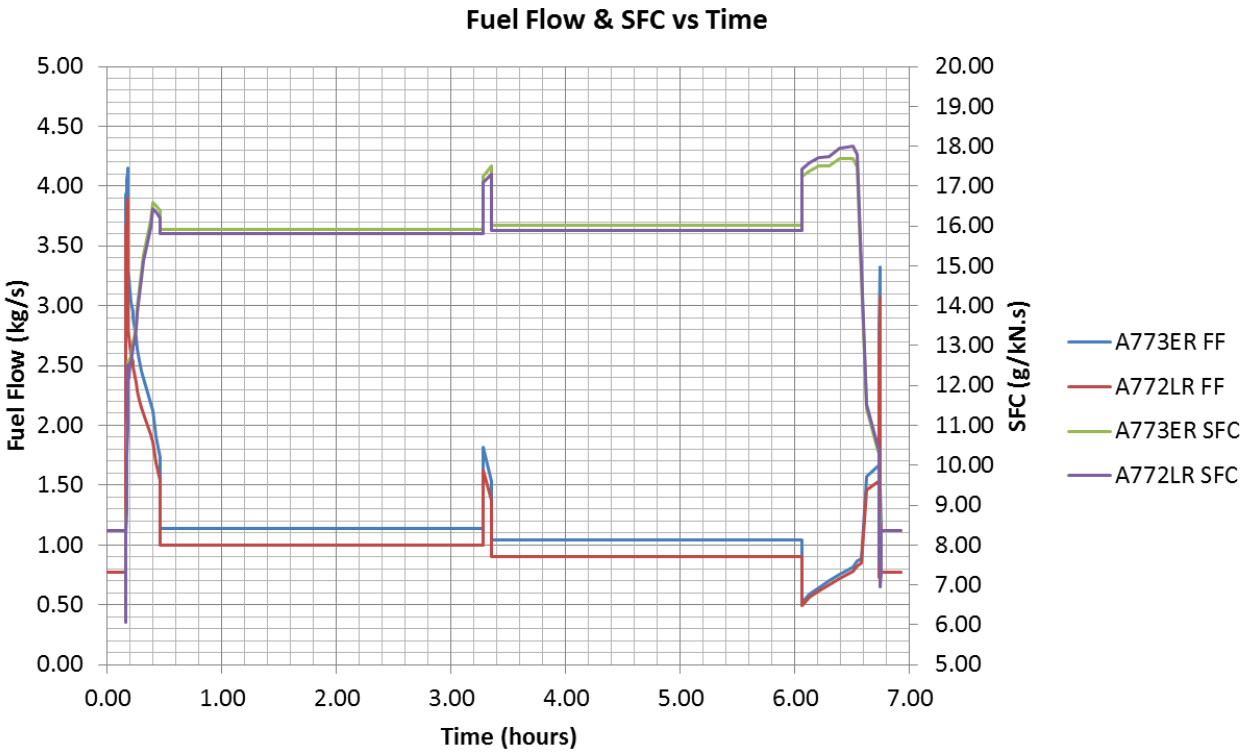

Figure 5-12 Fuel Flow & SFC vs Time

6 ENGINE HPT BLADE MODEL

Generally, an aircraft engine would last as long as its hot section would last. In a two spool engine, the hot section basically comprises of HPC, Combustor and HPT modules. These modules are subjected to extreme conditions and therefore have the tendency to show most failures and relatively earlier than others. In order to evaluate the engine soft life for overhaul, high pressure turbine stage one blade was chosen as the hot section part for analysis as it experiences the harshest environment inside the engine in terms of stresses and temperatures. We can therefore assume the engine time-on wing to be limited by HPT stage one blade life.

For HPT blade life assessment, an integrated physics based lifing tool was utilized, suitable for the analysis of low cycle fatigue (LCF) and creep damage mechanisms. The tool had been previously adopted by many other researchers in their studies in different forms. What follows ahead is a brief discussion on each of the different components of this tool. To meet the conflicting requirements.

6.1 HPT Blade Geometry

An HPT blade has a very sophisticated and optimized design which necessitates compromise between different conflicting requirements from the perspective of aerodynamics, mechanical design, cooling technology and material selection. In this project the traditional analytical methods for turbine sizing were not pursued to acquire the gas path annulus and the blade details. Instead, a real scrapped GE90 HPT stage 1 blade, acquired from an airline operator, was used to estimate some of the relevant geometrical data. In addition, the sizing of the HPT annulus with a constant mean diameter was carefully approximated by scaling of the 2D engine cross sectional view published in Jane's Aeroengines [32].

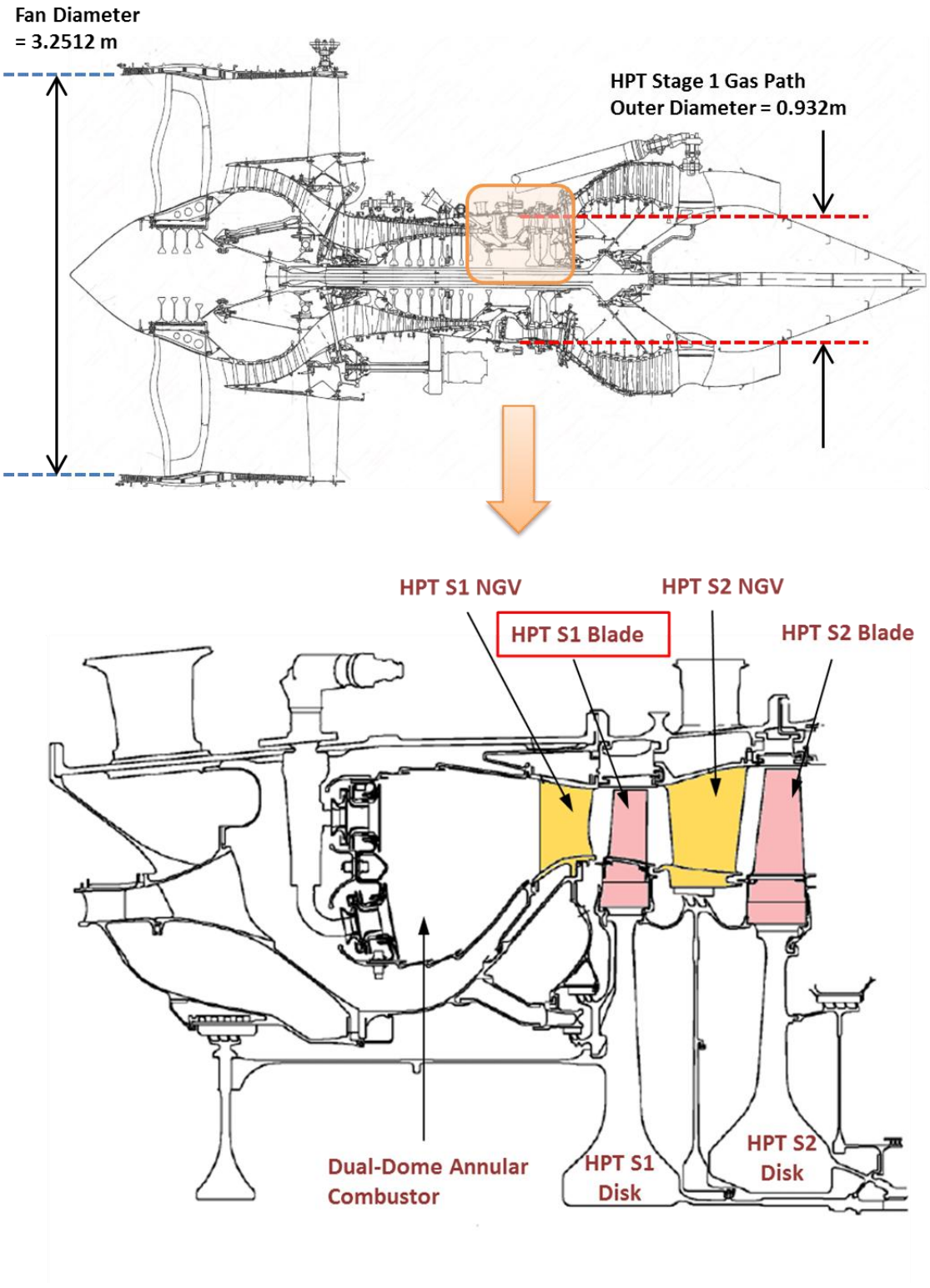

Figure 6-1 Cross section of GE 90 hot section [44] [32]

Knowing the actual fan case diameter (3.2512 m) from public literature and using the appropriate scale factor of the engine cross sectional drawing the radial

distance from engine centreline to the Tip Datum Station (TDS) of the unshrouded blade was estimated to be 0.465m and the rest 0.001m was left as tip clearance between the blade tip and the stationary shroud. The part of the blade exposed to the gas path measured 0.065m radially while the total height of the blade is 0.11 m.

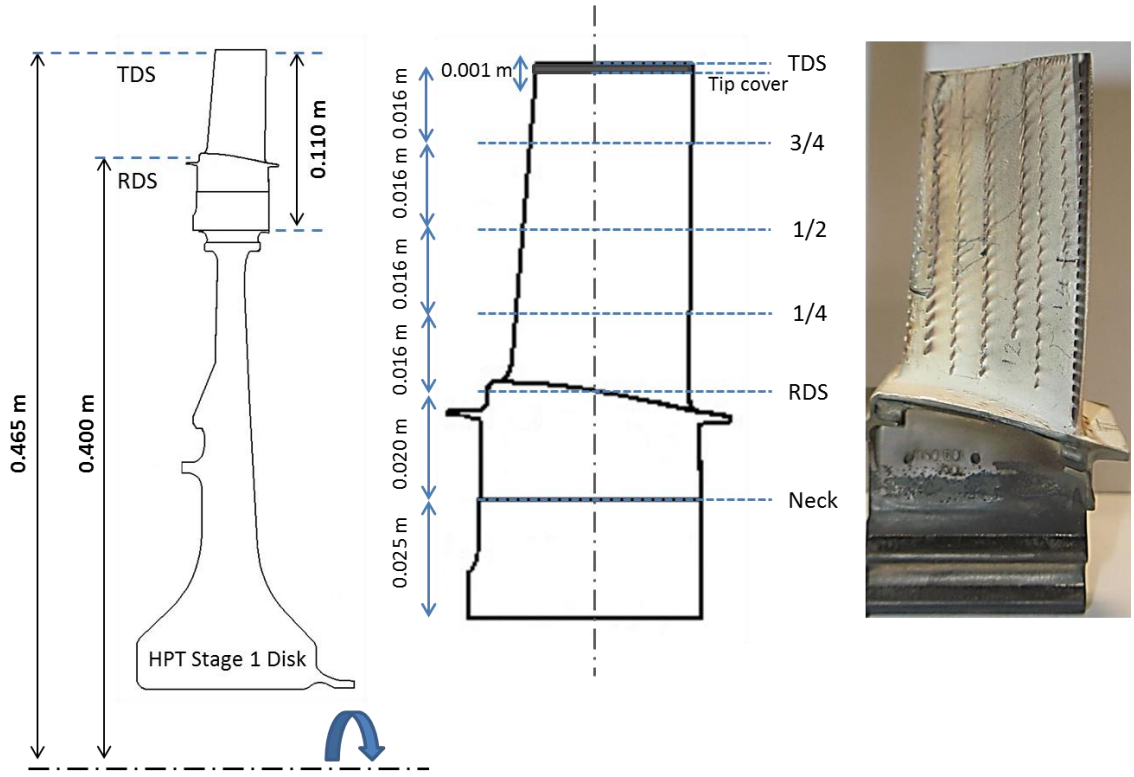

Figure 6-2 GE90 HPT Stage 1 Blade Dimensions

The blade was to be divided into 5 sections to find the trend of centrifugal stresses spanwise. The important information required in this regard was the aerofoil cross-sectional area of each of the sections, which in turn was to be used to calculate volume and mass of the respective blade section. Estimation of the cross sectional area of the HPT Stage 1 blade airfoil was possible due to the availability of another actual GE90 HPT Stage 1 blade cut at half span, exposing the internal construction of the blade as shown in Figure 6-3.

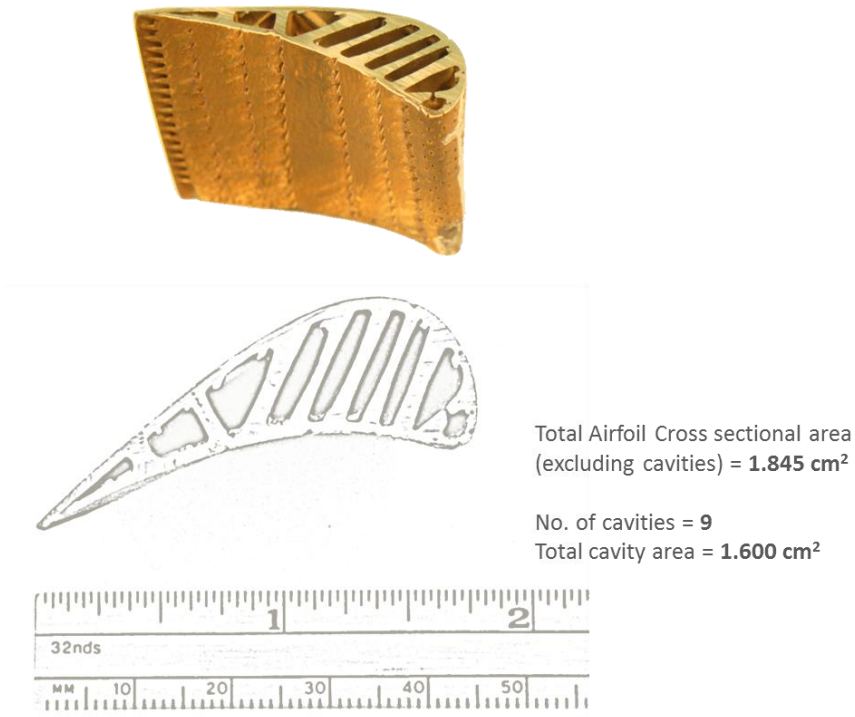

Figure 6-3 Internal cross section of HPT Stage 1 Blade

Great care was given to measuring dimensions that include the airfoil perimeter, the blade wall thickness, rib dimensions and coolant passage cavity dimensions at various points on the airfoil cross section. The airfoil was assumed to be divided into many smaller individual rectangles, triangles and circle. The areas of these simple shapes were finally added to arrive at an approximate value for the whole airfoil cross section. Since by visual examination the blade seemed to be rectangular with no considerable taper, the cross section was assumed to be uniform throughout the blade span from TDS to RDS. Table 6-1 provides a summary of the geometrical data important for the blade stress and thermal models.

Table 6-1 Dimensions of HPT Stage 1 Blade

Section	Avg Cross section Area (m2)	Section Height (m)	Section Volume (m3)	Section Mass (kg)	Distance: CG to Rotation axis (m)
Tip Cover to TDS	3.446E-04	0.0010	3.446E-07	0.0030	0.4645
3/4 height to TDS	1.845E-04	0.0160	2.952E-06	0.0255	0.4560
1/2 to 3/4 height	1.845E-04	0.0160	2.952E-06	0.0255	0.4400
1/4 to 1/2 height	1.845E-04	0.0160	2.952E-06	0.0255	0.4240
RDS to 1/4 height	1.845E-04	0.0160	2.952E-06	0.0255	0.4080
Shank Neck to RDS	-	0.0200	1.234E-05	0.1065	0.3900
Shank Root to Neck	-	0.0250	1.516E-05	0.1308	0.3675
Total	-	**0.1100**	**3.965E-05**	**0.3422**	-

6.2 Material Properties & Selection

Thermal efficiency of gas turbine engines depends significantly on the operating temperatures. Higher the TETs the engines are designed for higher the efficiencies achieved. Materials have always imposed great restraint to the maximum usable TET in a gas turbine since high TETs are often beyond the melting points of the materials themselves. The turbine blades work under very harsh environments with collective conditions of high temperature, stress, and corrosion. The materials for turbine blades are therefore required to possess the following principle properties:

- Outstanding mechanical strength
- High temperature strength
- Microstructure stability at high temperature
- Good oxidation/corrosion resistance
- High melting point
- Low density
- High stiffness
- Ease of manufacture

In pursuit of achieving the best combination of such characteristics, Nickel based alloys have evolved over the years since the advent of gas turbine engines as the appropriate metallic materials for hot section components. More modern heat resistant super alloys used in the manufacture of turbine blades and vanes along with intricate cooling technologies adopted for internal convection cooling, external boundary layer film cooling and thermal barrier coating, have led the engines to operate at high temperatures with greater efficiencies and at the same time extend the immunity to failure modes such as creep, thermal fatigue and environmental attack.

Table 6-2 shows some of the different types of nickel based alloys that that have been commonly in use in the manufacture of turbine parts.

Table 6-2 Compositions of commercial Ni-based superalloys[45]

Alloy	Cr	Co	Mo	W	Ta	Re	Nb	Al	Ti	Hf	C	B	Y	Zr	Other
Conventionally Cast Alloys															
Mar-M246	8.3	10.0	0.7	10.0	3.0	—	—	5.5	1.0	1.50	0.14	0.02	—	0.05	—
Rene′ 80	14.0	9.5	4.0	4.0	—	—	—	3.0	5.0	—	0.17	0.02	—	0.03	—
IN-713LC	12.0	—	4.5	—	—	—	2.0	5.9	0.6	—	0.05	0.01	—	0.10	—
C1023	15.5	10.0	8.5	—	—	—	—	4.2	3.6	—	0.16	0.01	—	—	—
Directionally Solidified Alloys															
IN792	12.6	9.0	1.9	4.3	4.3	—	—	3.4	4.0	1.00	0.09	0.02	—	0.06	—
GTD111	14.0	9.5	1.5	3.8	2.8	—	—	3.0	4.9	—	0.10	0.01	—	—	—
First-Generation Single-Crystal Alloys															
PWA 1480	10.0	5.0	—	4.0	12.0	—	—	5.0	1.5	—	—	—	—	—	—
Rene′ N4	9.8	7.5	1.5	6.0	4.8	—	0.5	4.2	3.5	0.15	0.05	0.00	—	—	—
CMSX-3	8.0	5.0	0.6	8.0	6.0	—	—	5.6	1.0	0.10	—	—	—	—	—
Second-Generation Single-Crystal Alloys															
PWA 1484	5.0	10.0	2.0	6.0	9.0	3.0	—	5.6	—	0.10	—	—	—	—	—
Rene′ N5	7.0	7.5	1.5	5.0	6.5	3.0	—	6.2	—	0.15	0.05	0.00	0.01	—	—
CMSX-4	6.5	9.0	0.6	6.0	6.5	3.0	—	5.6	1.0	0.10	—	—	—	—	—
Third-Generation Single-Crystal Alloys															
Rene′ N6	4.2	12.5	1.4	6.0	7.2	5.4	—	5.8	—	0.15	0.05	0.00	0.01	—	—
CMSX-10	2.0	3.0	0.4	5.0	8.0	6.0	0.1	5.7	0.2	0.03	—	—	—	—	—
Wrought Superalloys															
IN 718	19.0	—	3.0	—	—	—	5.1	0.5	0.9	—	—	0.02	—	—	18.5Fe
Rene′ 41	19.0	11.0	10.0	—	—	—	—	1.5	3.1	—	0.09	0.005	—	—	—
Nimonic 80A	19.5	—	—	—	—	—	—	1.4	2.4	—	0.06	0.003	—	0.06	—
Waspaloy	19.5	13.5	4.3	—	—	—	—	1.3	3.0	—	0.08	0.006	—	—	—
Udimet 720	17.9	14.7	3.0	1.3	—	—	—	2.5	5.0	—	0.03	0.03	—	0.03	—
Powder-Processed Superalloys															
Rene′ 95	13.0	8.0	3.5	3.5	—	—	3.5	3.5	2.5	—	0.065	0.013	—	0.05	—
Rene′ 88 DT	16.0	13.0	4.0	4.0	—	—	0.7	2.1	3.7	—	0.03	0.015	—	—	—
N18	11.2	15.6	6.5	—	—	—	—	4.4	4.4	0.5	0.02	0.015	—	0.03	—
IN100	12.4	18.4	3.2	—	—	—	—	4.9	4.3	—	0.07	0.02		0.07	

Detailed information on the physical and mechanical properties of much of the newer generation super alloys remains proprietary with the inventors and developers. Hence a great deal of time was spent to search for relevant material specifications for the purpose of this project.

There are indications in the public literature from which it can be inferred that GE90 HPT stage 1 rotor blades are made of second generation, nickel-based super alloy, Rene N5, castable as single crystal [46], [6], [32]. ‘Rene N5’ is a trademark of General Electric Company. With limited information available in the public domain same material was selected and assumed to be the equivalent material for the HPT blades in the model engine. Rene N5, being a single crystal alloy possesses both satisfactory microstructural stability and excellent environmental resistance at high temperatures. It has a density of 8630 kg/m^3

[46]. In addition to addressing temperature influenced failure modes Rene N5 offers extended immunity to other failure mechanisms such as LCF and HCF [47].

Table 6-3 Rene N5 Alloy Composition[47]

Rene N5 - Alloy Compositions	
Elements	**Weight (%)**
Chromium (Cr)	7.0
Cobalt (Co)	7.5
Molybdenum (Mo)	1.5
Tungsten (W)	5.0
Tantalum (Ta)	6.5
Titanium (Ti)	0.0
Aluminum (Al)	6.2
Rhenium (Re)	3.0
Hafnium (Hf)	0.15
Carbon (C)	0.05
Boron (B)	0.004
Yttrium (Y)	0.01
Nickel (Ni)	63.086

The composition of Rene N5 is shown in Table 6-3 by weight percentage. Each of these additional elements has been chosen to serve a particular purpose in optimizing the properties for high temperature application. For instance Chromium (Cr) is present to provide oxidation and sulfidation resistance. Yttrium also has exceptional oxidation resistance. High levels of Tantalum (Ta) are found to be benelicial to high temperature strength and castability .The chemical addition of aluminium promote the creation of the γ’ phase. Creep resistance is dependent on slowing the speed of dislocation motion within a crystal structure. In modern Ni based superalloys the γ’ intermetallic phase Aluminide Ni3Al present acts as a barrier to dislocation motion and diffusion processes at elevated temperatures. For this reason, this γ’ intermetallic phase, when present in high volume fractions, drastically increases the strength of these alloys due to its ordered nature and high coherency with the γ matrix. While the elements Hafnium (Hf), Carbon (C) and Boron (B) they are beneficial to improving the tolerance for casting defects, such as low angle grain boundaries. Addition of Rhenium provides improved creep strength; however, it can potentially cause the material to become microstructurally unstable, forming undesirable TCP (topologically

close packed) phases. TCPs are potentially damaging for two reasons: they tie up Gamma and Gamma' strengthening elements in a non-useful form, thus reducing creep strength, and they can act as crack initiators because of their brittle nature.[48] Rene N6, a third generation Ni superalloy, addresses this issue where other relevant elements had to be carefully re-balanced with the addition of ruthenium to avoid this effect and provide good creep rupture strength as well as improve microstructural stability [46].

Some of the other material properties are described by the following charts and are considered as temperature dependent. Figure 6-4 shows a plot of 0.2 % Yield strength versus temperature. Figure 6-5 is a plot of ultimate tensile strength (UTS) versus temperature. All these material properties were used in the calculations ahead.

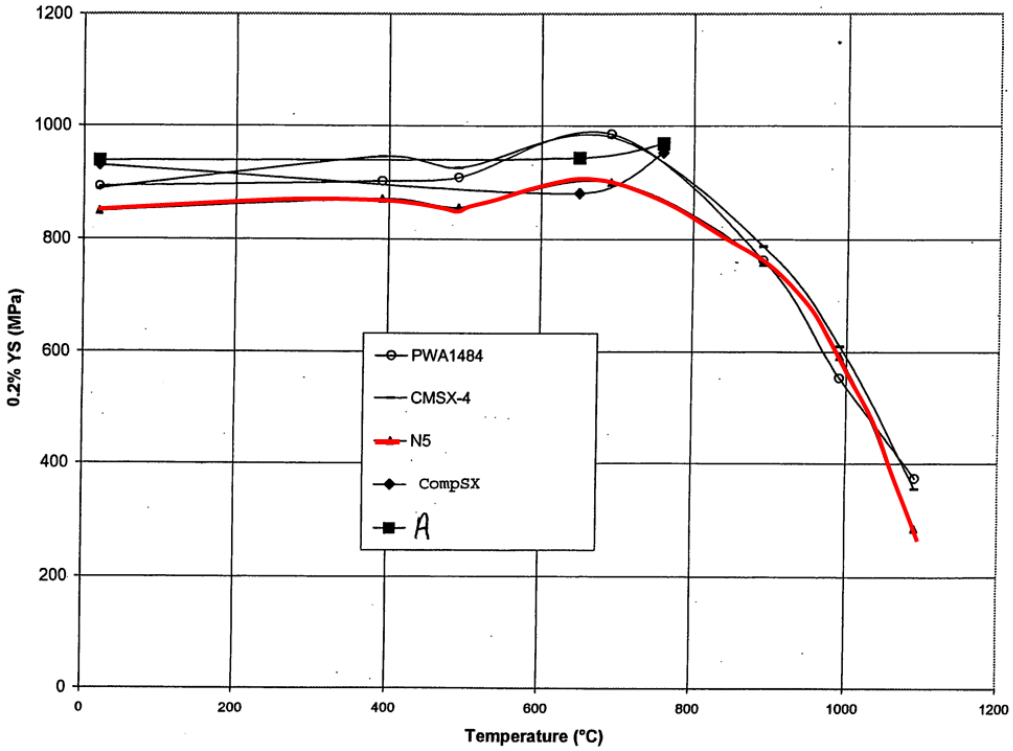

Figure 6-4 Yield Strength vs Temperature [49]

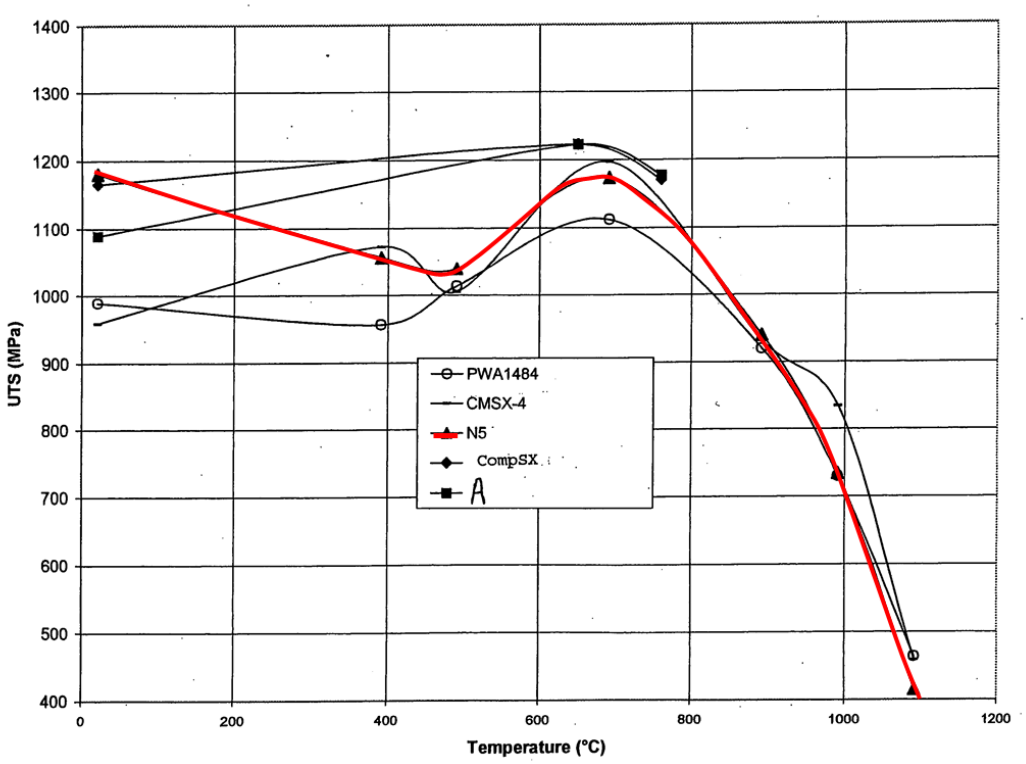

Figure 6-5 Ultimate Tensile Strength vs Temperature[49]

6.3 Stress Model

Stress model is important for evaluation of mechanical stresses acting on the turbine rotor blades during different phases of the flight mission. The stresses arise due to a variety of sources including centrifugal loads, gas bending loads, shear loads, thermal loads, and vibration loads, some being more significant than others in terms of meeting basic blade design and material strength requirements.

- Centrifugal stress act in radially outward direction and is caused due to high speed rotation of blade mass (inertia). It is steady and tensile in nature and is the main cause of blade failure due to creep under the influence of high temperature.

- Centrifugal bending moment is produced by the centrifugal load acting at a point which, due to the slight lean in the blade, is not radially in line above the centre of gravity of the blade root datum section or any other reference section.

- Gas bending moments (tangential and axial) are produced due to the change in momentum and pressure of the gas traversing through the blade. These moments result in the maximum bending stresses to occur at leading edge and trailing edge and convex surface back face. Due to the twist in the blade the stress values in each section vary from root to tip.

- Shear stresses arise from the gas pressure distribution along the blade length and from the untwisting effect of the pre-twisted blade due to centrifugal loading.

- Vibratory dynamic stresses develop when the blade is subjected to any resonant vibration, flutter or domestic object damage. Such stresses are vital for high cycle fatigue (HCF) analysis.

- Thermal stresses are caused when the turbine blade experiences 3D temperature gradients along the blade span, across the blade profile and within the metal thickness of the blade wall. It becomes even more complex when there is variation in these thermal gradients due to gas temperature fluctuations caused by changes in power settings in an engine operating cycle. This potentially results in unequal deformation in the blade fibres which gives rise to compressive and tensile stresses in different areas of the blade.

Out of all the different types of stresses, the centrifugal stress generally dominates. According to [MDOT notes] about 50% to 80% of the blade material strength is used to overcome this stress. As far as gas bending moments are concerned their effect is partially neutralized by centrifugal moment that arises from the intentional slight leaning of the turbine blade in the direction of rotation. 'Leaning' is a beneficial method of minimizing stresses in the blade and therefore it is a common design practice to lean the blade to counterbalance at least 75% of the gas bending moment at high power setting of an aero-engine [15]. Detailed calculations of gas bending stresses require considerable work and, like most design calculations, are computerized[50]. Would need advanced tools to determine the moment of inertia for aerofoil contours and the principal axis with respect to axial and tangential axes. The resulting bending stress essentially cancels the gas bending stress at the blade root, and leaves only the centrifugal stress component. Comparing to centrifugal and gas bending stress, the shear stress in turbomachine blades is considerably smaller. The stresses arising from thermal gradients are very complex and detrimental, but difficult to calculate due to lack of data, so it is not calculated in the present study. It would require sophisticated tools to do the analysis concurrently with transient and heat soakage analysis. For the purpose of engine soft life estimation, only centrifugal load was considered in the stress model, while the rest of the types of stresses were ignored due to the reasons mentioned above.

A 2-D centrifugal stress model is developed based on Cookson and Haslam notes[15] where centrifugal stress is calculated at each section along the blade span from root to tip given the HP shaft relative rotational speed PCN as an important input to the model. The cross-sectional area along the blade span was found to be quite uniform and therefore was assumed constant. Furthermore, there are gas bending moments that arise due to the velocity and pressure differences as the fluid flows over the blade. The stresses produced, in many blade designs, are offset by the geometrical leaning of the blades, thereby reducing the effect [15] [51]. Gas bending stresses, therefore, will not be considered in this project.

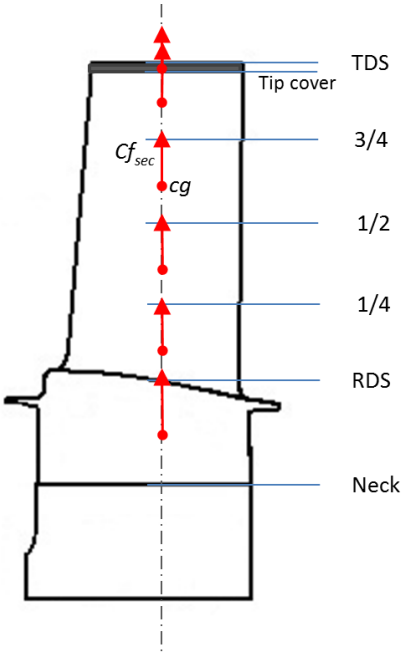

Figure 6-6 Centrifugal force acting on each blade section

HP shaft relative rotational speed PCN is an important input data to the centrifugal stress model. Actual HP shaft rotational speed denoted as 'N2' is calculated in rpm by using PCN, followed by angular velocity ω. Centrifugal forces are calculated independently on all the six blade sections using equation (6-4). Cumulative centrifugal force is then calculated at each of the six blade stations – TDS, ¾, ½, ¼, RDS, and Shank neck - by summing all the individual centrifugal forces acting on the sections above the respective station. For instance, centrifugal force acting at ½ station is the accumulation of centrifugal forces acting on blade sections (½ – ¾), (¾ - tip cover) & (tip cover – TDS). Finally, the centrifugal stress is calculated by dividing the cumulative centrifugal force at each blade station by the blade cross sectional area.

$$HP\ Spool\ Rotational\ Speed \quad N_2 = PCN \times N_{2\_100\%} \qquad \textbf{(6-1)}$$

$$Angular\ Velocity \quad \omega = \frac{2\pi N_2}{60} \qquad \textbf{(6-2)}$$

$$Centrifugal\ force \quad Cf_{sec} = m_{sec} \times r_{cg\_sec} \times \omega^2 \qquad \textbf{(6-3)}$$

$$Centrifugal\ Stress\ @\ blade\ station \quad \sigma_{bSt} = \frac{\sum all\ Cf_{sec}\ above}{A_{bst}} \qquad \textbf{(6-4)}$$

Figure 6-7 and Figure 6-8 show spanwise blade stress distribution at maximum power settings during each of the flight phases in mission 1 and mission 2 respectively. The stress at the blade shank is a bit lower due to higher cross section area at that station.

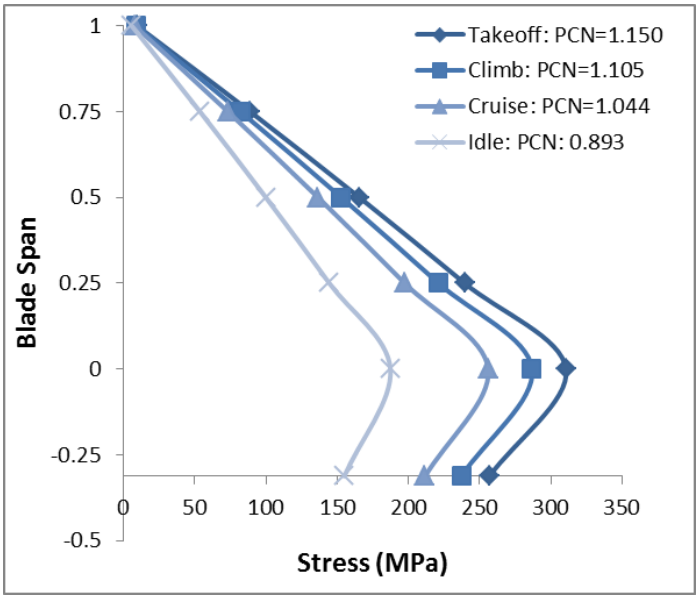

Figure 6-7 Blade Stress Distribution (Reference Mission 1)

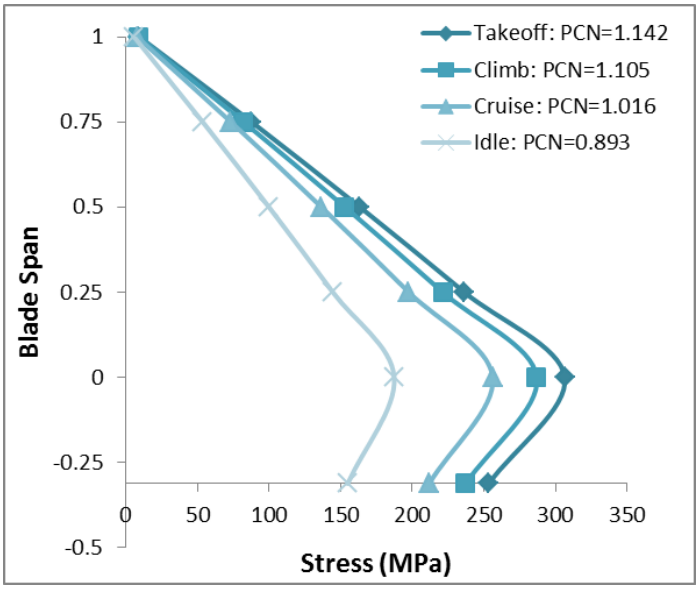

Figure 6-8 Blade Stress Distribution (Reference Mission 2)

6.4 Thermal model

Thermal model is important for evaluation of blade metal temperature. HPT blades in modern-day large civilian engines such as GE90 use convection and film cooling along with thermal barrier coating to control the blade metal temperature from exceeding its material melting point.

The blade temperature is calculated with the aid of overall cooling effectiveness ε[52], a technology factor that reflects the amount of coolant mass flow and the type of cooling used[24]. It is mathematically defined as follows:

$$\varepsilon = \frac{T_g - T_b}{T_g - T_c} \qquad \textbf{(6-5)}$$

Where,

T_g = *Free stream gas temperature*

T_b = *Blade metal temperature*

T_c = *Coolant temperature*

The cooling effectiveness ε of existing modern civil engines range between 0.5 and 0.7 [53]. GE90 engine being in the same category, ε values within the same range were chosen. A slight arbitrary linear variation of cooling effectiveness was assumed in this project, from 0.63 at the root to 0.59 at the tip considering the fact that this blade, being unshrouded, is prone to hot gas tip leakages resulting in slightly higher blade temperatures at the tip than at the root.

Another important consideration taken into account is the pattern factor or radial temperature distribution factor (RTDF), which characterizes the profile of gas temperature distribution faced by the NGVs or turbine rotor blades. Mathematically, it is expressed as follows:

$$RTDF = \frac{Tmax_{out} - Taverage_{out}}{Taverage_{out} - Taverage_{in}} \quad \textbf{(6-6)}$$

Where,

$Tmax_{out}$ = Maximum profile temperature

$Taverage_{out}$ = Temperature of the combustor/NGV exit

$Taverage_{in}$ = Temperature of the combustor inlet

The gas temperature profile formed at the annular combustor exit is not uniform, TET being lower at the walls and higher in the middle[54]. Same is the case with NGV exit traverse but with relatively lower intensity. To minimize the impact on the blade life, the radial position of the peak temperature in the profile is made to fall on the blade region experiencing less stress. Therefore, as a predominant design practice, the peak temperature is normally found in the upper half of the radial profile [53]. Generally, the RTDF values vary between 0.1 and 0.2 [8].

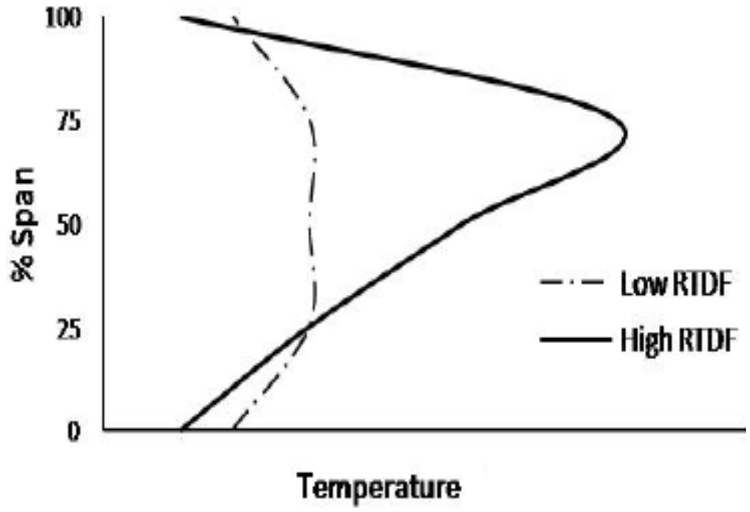

Figure 6-9 Effect of RTDF on the Gas Temperature Profile [28]

For the purpose of this project, a triangular temperature profile [28] is selected between HPT Stage 1 NGVs and blades with RTDF=0.15 and maximum rotor inlet gas temperature (RIT) occurring at approximately 75% annulus span. Following are the notations and equations used to eventually find the blade metal temperature at each of the five radial stations. See Figure 6-10.

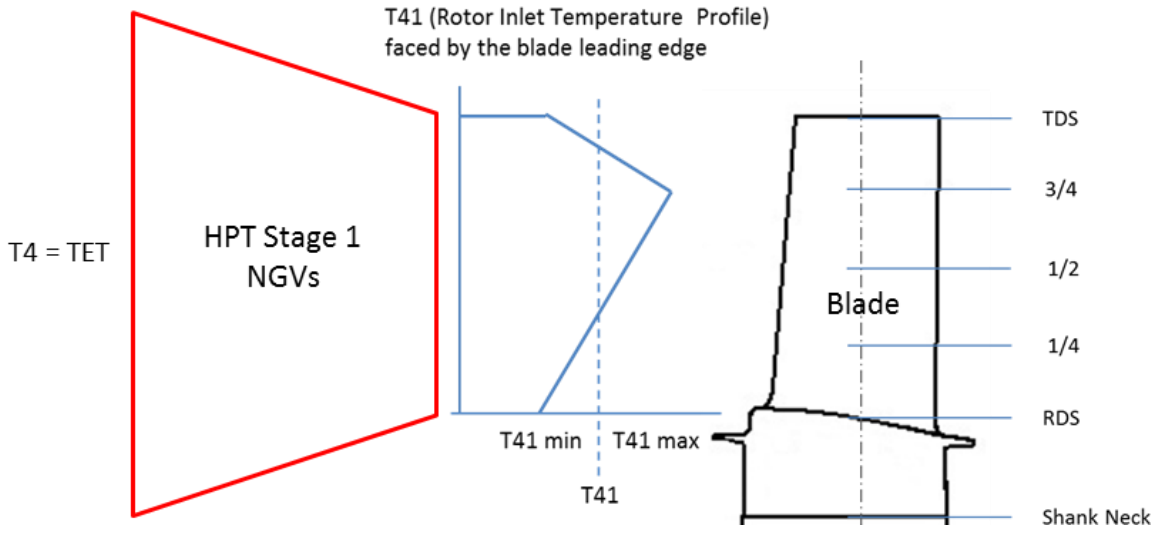

Figure 6-10 RIT Profile faced by the HPT blade

- *T_3 = HPC Discharge Temperature*

- *T_4 = Turbine Entry Temperature / Combustor Exit temperature*
- *T_{41} = Average Rotor Inlet Gas Temperature post NGV, calculated from Turbomatch simulation results. Note that out of 15% of HPC discharge air taken for cooling 9% is used for NGVs and the rest 6% is used for HPT Stage 1 blades. T41 is assumed to be T10–9/15(T10–T11), where T10 and T11 are the temperatures at stations 10 and 11 in the Turbomatch model. T10 is TET while T11 is the resultant temperature after the mixture of primary core flow and the secondary coolant flow.*

$$T_{Rise} = T_{41} - T_3 \quad \textbf{(6-7)}$$

$$T_{41\,max} = T_{41} + (T_{Rise} \times RTDF) \quad \textbf{(6-8)}$$

$$T_{41min} = \left(\frac{1}{3}\right)(5T_{41} - 2T_{41max}) \quad \textbf{(6-9)}$$

$$T_{41,25\%} = T_{41min} + \left(\frac{1}{3}\right)(T_{41\,max} - T_{41min}) \quad \textbf{(6-10)}$$

$$T_{41,50\%} = T_{41min} + \left(\frac{2}{3}\right)(T_{41\,max} - T_{41min}) \quad \textbf{(6-11)}$$

$$T_{bTDS} = T_{41min} - \varepsilon\,(T_{41min} - T_3) \quad \textbf{(6-12)}$$

$$T_{b,75\%} = T_{41max} - \varepsilon\,(T_{41max} - T_3) \quad \textbf{(6-13)}$$

$$T_{b,50\%} = T_{41,50\%} - \varepsilon\left(T_{41,50\%} - T_3\right) \quad \textbf{(6-14)}$$

$$T_{b,25\%} = T_{41,25\%} - \varepsilon\left(T_{41,25\%} - T_3\right) \quad \textbf{(6-15)}$$

$$T_{bRDS} = T_{41min} - \varepsilon\,(T_{41min} - T_3) \quad \textbf{(6-16)}$$

Figure 6-11 and Figure 6-12 show spanwise blade temperature distribution at maximum power settings during each of the flight phases in reference missions 1 and mission 2 respectively.

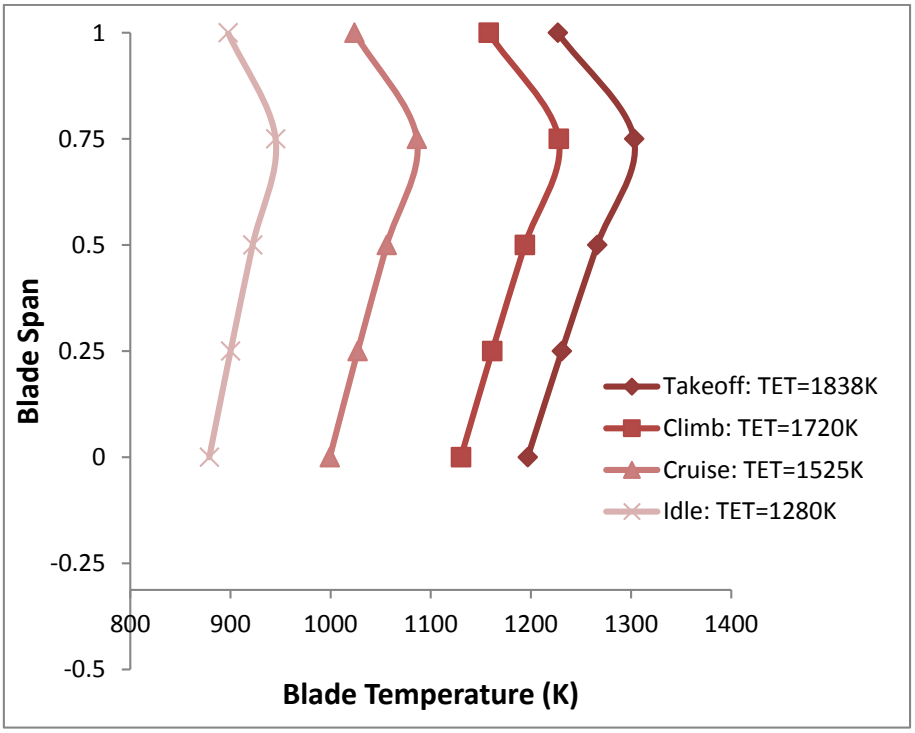

Figure 6-11 Blade Temperature Distribution (Reference Mission 1)

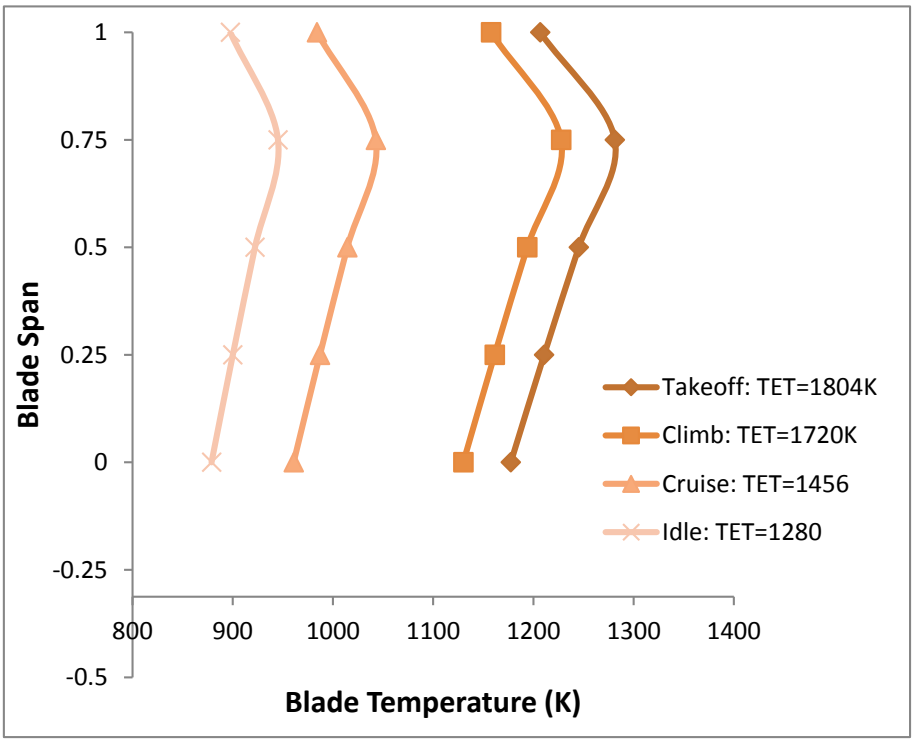

Figure 6-12 Blade Temperature Distribution (Reference Mission 2)

7 ENGINE SOFT LIFE ESTIMATION

7.1 Creep Model and Life Calculation

Creep refers to the tendency of a material to undergo progressive deformation with time under the effect of high temperature and constant mechanical stress. Creep is said to be a time-dependent deformation. Under the influence of relatively high temperature, plastic deformation of a material is bound to take place even if the stress is smaller than the yield stress. This deformation is time-dependent and is known as creep. Gas turbine engine on a civilian aircraft spends the majority of its flight time in steady state cruise conditions and therefore sets an opportunity for creep to act on the HPT blade during that time period. Creep is highly sensitive to temperature and shows its significance when metal temperature reaches about 40% to 50% of the melting temperature [15]. The cooling technology used in the HPT is always carefully and precisely designed. In the absence of appropriate cooling, the creep deformation may become large enough to cause a turbine blade to touch the casing, resulting in blade tip failure.

The creep process can be represented by the following strain versus time curve.

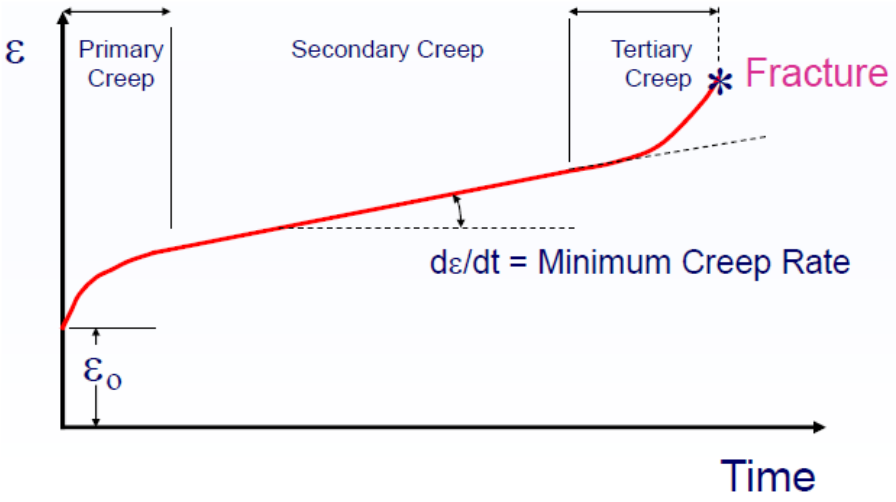

Figure 7-1 Strain vs Time Creep Curve[5]

The slope of the curve is called strain rate or creep rate. Initially, there is always some instantaneous elastic strain ε_o immediately upon application of load. Then,

in the primary stage, the high creep rate tends to drop with time as the material faces an increase in strain hardening due to the build-up of a large number of dislocations. Deformation then becomes relatively difficult as the material is strained. In the secondary stage the creep attains constancy while maintaining a balance between the two metallurgical processes of strain hardening and thermal recovery. It is this stage where the material spends most part of its creep life[15]. Lastly, in the tertiary stage, the strain rate accelerates rapidly, leading to ultimate failure known as rupture. This failure could be the result of reduction in cross sectional area often termed as necking, caused by micro structural changes such as coalescence of voids or cavities, formation of internal micro cracks, sliding of grain boundaries[8].

After determining the operating stresses and temperatures experienced by the HPT blade, it is possible to forecast the service life of the component. To estimate the cumulative creep life to failure, Larson-Miller Parameter is used followed by the application of Miner's law to account for the separate creep effects due to different operating conditions in different phases of the flight mission cycle [15]. LMP is quite sensitive, i.e. a small change in blade temperature results in large variation in predicted life [8]. It is mathematically expressed as:

$$P = \frac{T_b}{1000}(\log t_f + 20) \qquad \textbf{(7-1)}$$

Where,

P = Larson-Miller parameter (LMP)

T_b = blade temperature

t_f = time to failure in hours

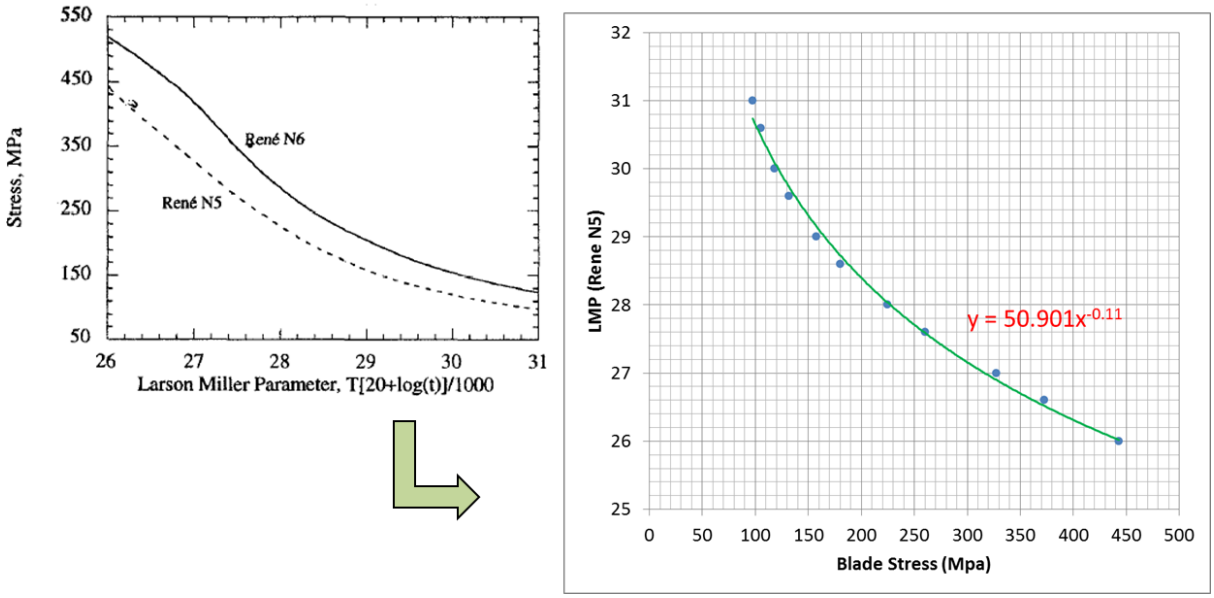

Figure 7-2 Approximate Relation between LMP and Stress for Rene N5 material [46]

Time to failure t_f is found by rearranging the above equation.

$$t_f = 10^{\left[\left(\frac{1000}{T_b}\right)P-20\right]} \quad \textbf{(7-2)}$$

Palmgren-Miner law is eventually employed to estimate the cumulative creep life of the blade taking account of all separate creep effects due to different operating conditions in different flight mission segments.

$$t_f = \frac{1}{\sum_{i=1}^{n} \frac{t_{di}}{t_{fi}}} \quad \textbf{(7-3)}$$

Where,

n = number of flight segments

t_f = cumulative creep life in hours

t_{di} = duration of the ith flight segment

t_{fi} = *time to failure for the ith segment*

Note: Creep life can also be calculated in cycles by simply dividing t_f by the entire flight duration in hours.

Following are the cumulative creep lives found for the two missions. The results are in accordance with expectations. Engine operated at higher thrust rating in flight mission 1 has a lower creep life than the engine operated at lower thrust rating in mission 2.

Table 7-1 Creep Lives for Mission 1 and 2

Mission	Aircraft Model	Engine Rating	Creep Life (Cycles)	Creep Life (Hours)
1	A773ER	TF115	7103	47945
2	A772LR	TF110	24655	166421

7.2 Low Cycle Fatigue Model & Life Calculation

Fatigue is the deterioration of an engine that comes as a result of it being exposed to varying stress loads due to change in its operating conditions.

The overall fatigue life of an engine is estimated in the following steps:

- Description of the loading history of the turbine blade
- Count of the reprisals of each type of load
- Assessment of the damage caused by each particular load, using Stress-based or Strain-based methods.
- Combine the damage caused by the load application at each level, using additive rule.

7.2.1 Rainflow Cycle Counting

Because the amplitude of loads fluctuates, it was important to introduce cycle counting methods that would compare the deterioration that results from irregular load histories with the damage caused by sets of regularly repeated load cycles.

With their respective algorithms, these methods take an irregular load history and extract individual stress cycles in a manner more suitable for lifing analysis. Often four well-known cycle counting methods are found in the literature: the Race track method, Range mean method the Range Pair method and the Rainflow method[8]. Each method has its own advantage and disadvantages and all methods can lead to different predictions of the fatigue life.

Rainflow counting, also known as ‘Pagoda Roof’ method, is considered to be the most reliable technique[55] because its fatigue life estimates are usually most conservative.Hence it was chosen to be used in the current thesis.

The rainflow algorithm contains the following list of rules that can be seen applied in this thesis in section – see Figure 7-5.

- The stress/strain time history is simplified to a sequence of peaks and valleys.
- The stress/strain time history is then turned 90° clockwise, so the starting time moves at the top.
- The peaks and valleys are considered to be a series of pagoda roofs.
- Rainflow starts at the beginning and again at the inside of every peak or valley.
- Rain flows down a pagoda roof and over the edge, where it falls vertically until it reaches a level opposite a maximum more positive (minimum more negative) than the maximum (minimum) from which it started.
- Rain also stops when it is joined by rain from a pagoda roof above
- The horizontal length of each rainflow is then counted as a half cycle at that stress/strain range.
- A pair of half cycles found to be identical in magnitude but opposite in direction can be counted as one complete cycle.

7.2.2 Damage or Life Estimation by Strain-Based Approach

The strain-based approach calculates the life at the engine’s most critical phase, namely take-off, when it experiences the maximum TET [13]. Since Low cycle fatigue involves considerable accumulation of plastic strain energy, a strain

based approach is most suitable for evaluation of fatigue life. Therefore, a combination of Coffin - Manson method, along with Neuber relationship, will be used as it has been employed by Pascovici [56] and Suria [57] in their work.

7.2.3 Damage or Life Estimation by Stress-Based Approach

Normally, the S-N curve is a plot of fully reversed loading (with mean stress equal to zero) versus life cycles to failure. But sometimes the mean stress in loaded components is not equal to zero and hence needs to be translated to equivalent reversed stress cycles in order to obtain the life by conventional S-N curve [58]. There are a few methods that facilitate this transformation based on the empirical constant damage curves illustrated in Figure 7-3 to consider the effect of inherent mean stress. For many modern materials including nickel alloys the Goodman straight line relation has been considered to most appropriate.

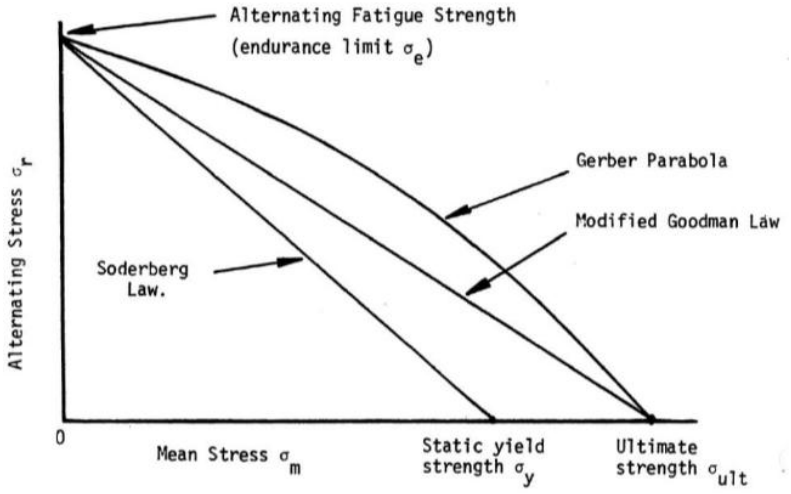

Figure 7-3 Constant Damage Curves: Soderberg, Goodman, Gerber [59]

Figure 7-4 illustrates the usage of Modified Goodman diagram to obtain fully reversed stress cycles. Point D represents the ultimate tensile strength and zero alternate stress. Point B represents fully reversed effective stress amplitude with zero mean stress. So if the stress amplitude and mean stress are known at point C, then the intended point B can be obtained by use of similar triangles with equation (7-4).

$$\frac{\sigma_a}{\sigma} + \frac{\sigma_m}{\sigma_{ULT}} = 1 \qquad \textbf{(7-4)}$$

Where

σ = Stress amplitude with zero mean stress

σ_a = Stress amplitude with non-zero mean stress σm

σ_m = Mean stress

σ_{ULT} = Ultimate tensile stress

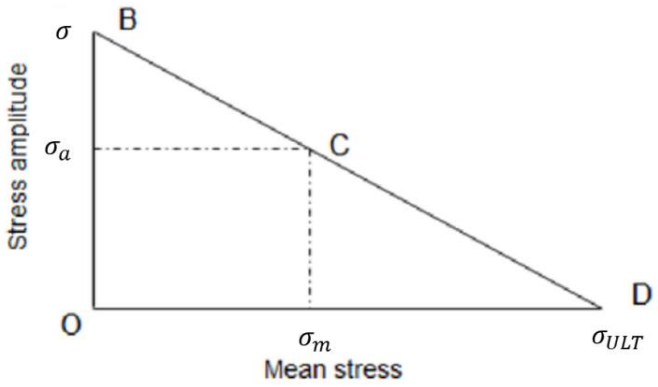

Figure 7-4 Goodman Diagram

To estimate the component's fatigue life, the individual damages calculated from each of the loading cycles are combined in a certain way to get the total damage. Several cumulative damage theories have emerged in the literature but none besides Palmgren-Miner rule is found to be universally applicable to all scenarios [60][58][55]. Palmgren-Miner rule is a simple linear cumulative damage rule according to which if the component is subjected to k number of stress amplitudes, where each stress amplitude σi for ni cycles gives an average life of Ni cycles, then the failure is expected when the linear summation of all the individual damage fractions, ni/Ni, reaches close to unity.

$$D_{fatigue} = \sum_{i=1}^{k} \frac{n_i}{N_{fi}} \approx 1 \qquad \textbf{(7-5)}$$

Where

n_i is the number of applied cycles at ith stress range

N_{fi} is the number of cycles to fatigue failure for ith stress range

k is the number of stress amplitudes/ranges/cycles.

One major limitation of the Miner's law is that it does not consider the sequence of the loading schedule, when in fact there are some cases where sequence effects are important.

7.3 Low Cycle Fatigue Life Estimation for Baseline Missions

Fatigue life calculation was performed for both flight missions 1 and 2 using the methods and algorithms discussed earlier. In this section the calculation process will be shown for mission 1 only but same was applied for mission 2 as well. Figure 7-5 shows the centrifugal stress history associated with flight mission 1, followed by identification of peaks and valleys.

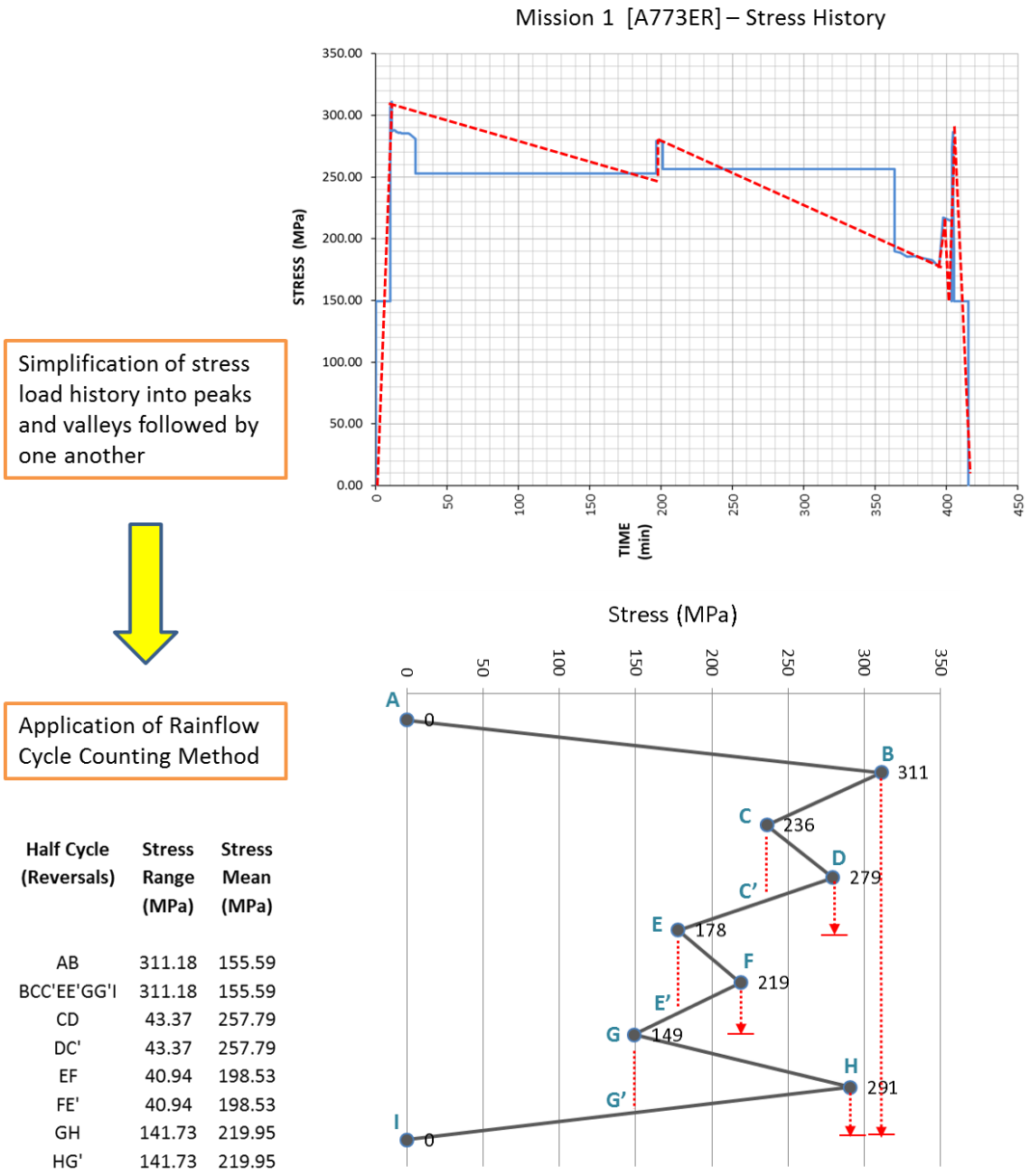

Half Cycle (Reversals)	Stress Range (MPa)	Stress Mean (MPa)
AB	311.18	155.59
BCC'EE'GG'I	311.18	155.59
CD	43.37	257.79
DC'	43.37	257.79
EF	40.94	198.53
FE'	40.94	198.53
GH	141.73	219.95
HG'	141.73	219.95

Figure 7-5 Cycle Counting by Rainflow Method

Since no finite element analysis was performed to find the stress concentration factor Kt, a reasonable value of 2.18 was assumed due to a potential stress raiser located at TDS of the blade. Together with notch sensitivity index q = 0.85, the fatigue concentration factor K_f was calculated using the equation (7-6) below.

$$K_f = q(K_t - 1) + 1 \qquad \textbf{(7-6)}$$

$$K_f = 0.85(2.18 - 1) + 1 = 2.0 \quad \textbf{(7-7)}$$

Rainflow cycle counting method was applied to extract 8 reversals (half cycles). The corresponding full 4 stress cycles are indicated in Table 7-2.

Table 7-2 Rainflow Cycle Counting applied to 4 stress cycles

Full Cycle	Qty	Stress Range (MPa)	Stress Amplitude (MPa)	Stress Mean (MPa)	Kf x σa
1 (ABI)	1	311.18	155.59	155.59	311.18
2 (CDC')	1	43.37	21.69	257.79	43.37
3 (EFE')	1	40.94	20.47	198.53	40.94
4 (GHG')	1	141.73	70.87	219.95	141.73

Strain Based Approach

LCF life of the HPT blade was first tried to be determined by strain based method using Neuber's local strain rule and Manson's 'Equal Slopes' equation. To simplify the calculation process it was assumed that the Rene N5 material behaves ideally elastic and perfectly plastic during this process. During the whole flight profile, the maximum nominal stress within the blade occurs during the takeoff phase.

Properties of Rene N5 at a temperature of 1263K during takeoff were found to be

Elastic Modulus E = 213 GPa,

Ultimate Tensile Strength σ_{Ult} = 720 MPa,

Yield Stress σ_y = 590 MPa

Using the Neuber Diagram in Figure 7-6:

Local stress at point A, $\sigma_A = K_f \times \sigma_{Nominal} = 2.0 \times 311.18 = 622.36\ MPa$

Strain at point A, $\epsilon_A = \frac{\sigma_A}{E} = 0.002926$

Application of Neuber's Rule: $(\Delta\sigma\Delta\epsilon)_{Elastic} = (\Delta\sigma\Delta\epsilon)_{Plastic} = \sigma_A\epsilon_A = \sigma_B\epsilon_B$

Stress at point B is equal to the yield strength, $\sigma_B = \sigma_y = 590\ MPa$

Strain at point B, $\epsilon_B = \frac{\sigma_A\epsilon_A}{\sigma_B} = 0.003091$

Stress at point C, $\sigma_C = \sigma_B - \sigma_A = 590 - 622.36 = -32.36\ MPa$, which is less than yield strength in compression.

It was observed that the stress cycle considered was not high enough for the yielding to take place in compression causing elastic shakedown i.e. the material would continue to oscillate along the elastic red line BC shown in Figure 7-6. A minimum stress concentration factor of 4.3 was required for the material to follow a complete hysteresis loop with elastic and plastic regions in order to estimate the low cycle fatigue. But it is not normal to have such high values for stress concentration factors. Hence the strain based method to calculate the fatigue life was discontinued at this stage. The strain based method may be applied for rather larger components such as turbine disk involving higher levels of nominal stresses.

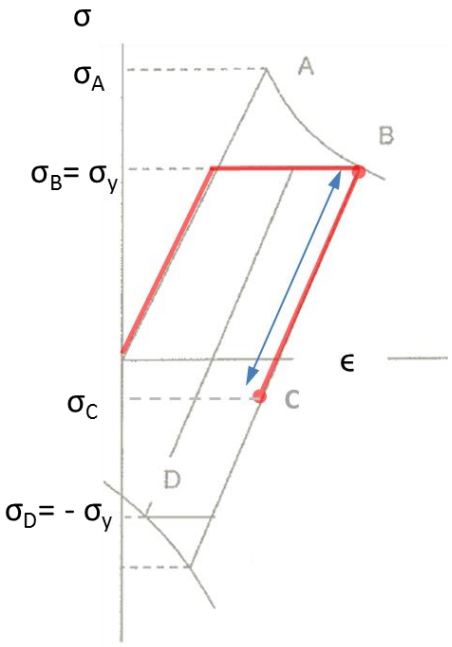

Figure 7-6 Use of Neuber's Rule to estimate total strain

Stress Based Approach

Due to the elastic shakedown the strain based calculation was no longer pursued. Alternatively, Stress based method was initiated. Due to lack of material data available for Rene N5 in public domain, the S-N relationship was derived by taking 90% UTS at 1000 cycles and endurance strength to be 30% UTS at 1,000,000 cycles and use a logarithmic relationship between these values. Such is the case for many non-ferrous materials.

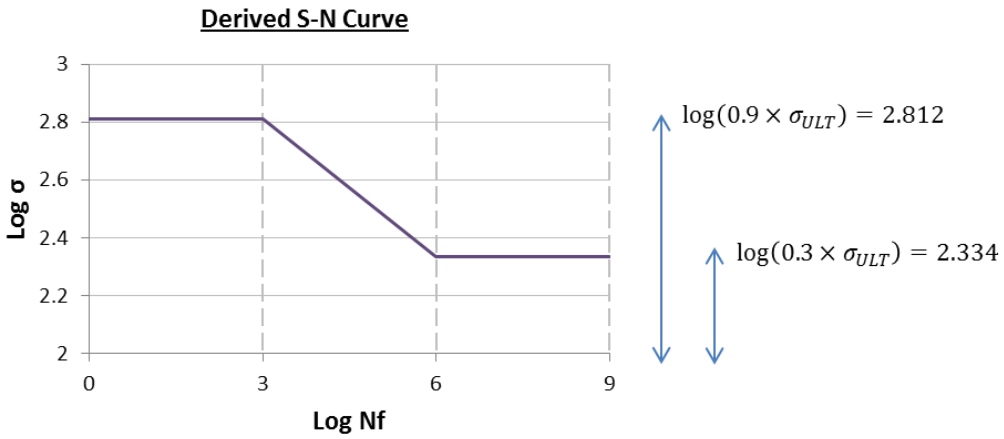

Figure 7-7 Derived SN Curve for Rene N5

Combination of Goodman diagram and derived SN curve was then used to estimate the LCF life from the damaging cycles. All the stress cycles in Table 7-2 are projected on to the y axis as fully reversed stress cycles at zero mean stress. Out of all the four only the first cycle was found to be damaging in nature, lying beyond the safe design limit represented by red line in the Goodman diagram, also known as 'line of constant damage'. See Figure 7-8.

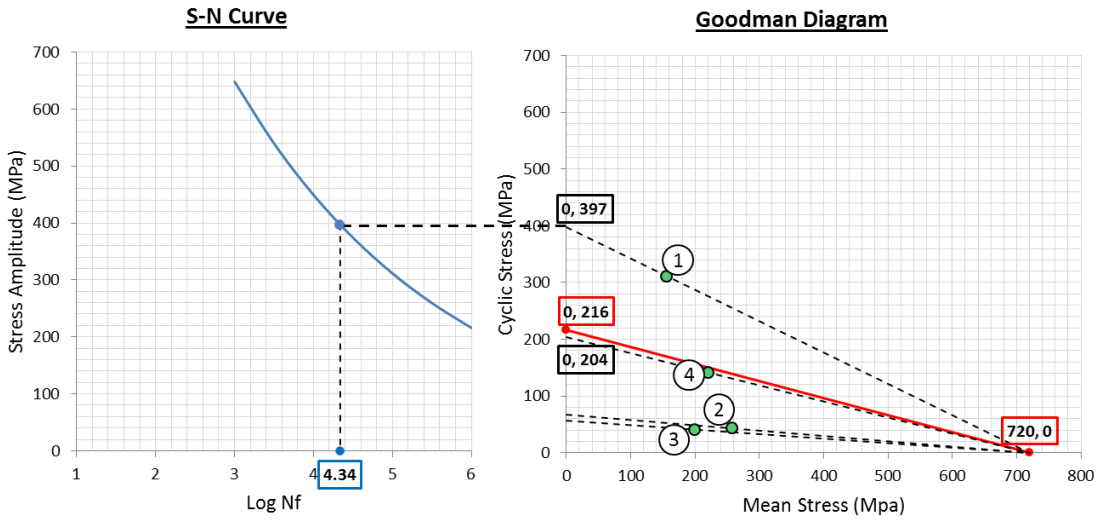

Figure 7-8 Combined S-N and Goodman Diagram

The effective stress amplitude σ at zero mean stress for the 1st cycle was calculated by means of similar triangles;

$$\frac{\sigma - 0}{\sigma_{ULT} - 0} = \frac{\sigma_{1a} - 0}{\sigma_{ULT} - \sigma_{1m}} \quad \textbf{(7-8)}$$

$$\sigma = \frac{\sigma_{ULT} \times \sigma_{1a}}{\sigma_{ULT} - \sigma_{1m}} \quad \textbf{(7-9)}$$

$$\sigma = \frac{720 \times 311.18}{720 - 155.6} = 397\ MPa \quad \textbf{(7-10)}$$

When extended on to the S-N curve in Figure 7-8, the corresponding log Nf was estimated to be 4.34 which then provided 21800 cycles. Alternatively, intermediate number of cycles between $N=10^3$ and $N=10^6$ could also be obtained by means of similar triangles using Figure 7-7.

$$\frac{\log(0.9 \times \sigma_{ULT}) - \log \sigma}{\log(N_f) - \log(10^3)} = \frac{\log(0.9 \times \sigma_{ULT}) - \log(0.3 \times \sigma_{ULT})}{\log(10^6) - \log(10^3)} \quad \textbf{(7-11)}$$

$$\frac{2.812 - 2.599}{\log(N_f) - 3.0} = \frac{2.812 - 2.334}{6.0 - 3.0} \quad \textbf{(7-12)}$$

$$\log(N_f) = 3.0 \times \frac{2.812 - 2.599}{2.812 - 2.334} + 3 \quad \textbf{(7-13)}$$

$$\log(N_f) = 4.34 \;\rightarrow\; N_f = 21{,}797\ cycles \quad \textbf{(7-14)}$$

If there were more than one damaging cycles Miner's Law would have been used for the calculation of the total life taking into account effects from all damaging cycles.

Similar process was employed to estimate the LCF life for baseline mission 2.

Nf for mission 2 equals 44,113 cycles.

7.4 Cumulative Damage for Baseline Missions

The cumulative damage due to Fatigue-creep life prediction can be dealt with in two methods. The first one is to determine the damage of creep and fatigue individually, and then by a linear damage summation rule, the damage of creep and fatigue are added together to give the total damage. This is known as the Damage Summation Method. The second one considers the damage of fatigue and creep together and uses the Strain Range Partitioning Technique or Strain Energy Partitioning Technique [61]. Among them, the linear accumulation of fatigue-creep damage is popular and simple. Hence in this study, same technique

is applied as demonstrated by Attah [17] to estimate the cumulative life of the HPT first stage blade which will be regarded as the soft life of the engine itself.

Through the linear damage accumulation method, the total damage D is equal to the summation of the fatigue damage and creep damage, which are shown in equations below.

$$D = D_{fatigue} + D_{creep} = \sum_{i=1}^{k} \frac{n_i}{N_{fi}} + \sum_{j=1}^{l} \frac{t_j}{T_{cj}} \quad \textbf{(7-15)}$$

Where

n_i is the number of applied cycles at ith stress range

N_{fi} is the number of cycles to fatigue failure for ith stress range

k is the number of stress ranges or cycles.

t_j is duration of the jth flight phase

T_{cj} is the rupture time for the jth flight phase

l is the number of different flight phases.

Table 7-3 Cumulative HPT Blade Life

Mission	Aircraft Model	Engine Rating	Creep Life (Cycles)	LCF Life (Cycles)	Cumulative Life (Cycles)
1	A773ER	TF115	7103	21797	5357
2	A772LR	TF110	24655	44113	15816

8 ENGINE TIME ON-WING ASSESSMENT

The soft lives calculated in the previous chapter were for the baseline missions without taking into account the effect of progressive engine degradation. In reality, wear occurs with engine usage which affects engine performance, for instance, compressor and turbine blades erode, tip clearances increase, etc as discussed previously in chapter 2. In order to achieve the same level of thrust as in a new or an overhauled engine, a deteriorated engine has to run hotter and/or faster to compensate for the losses. Consequently, this is accompanied by an increase in engine fuel flow and specific fuel consumption which leads to an increase in TET and EGT. Such a shift in the parameters, when compared to nominal operation, increases with usage, and ultimately reaches the maximum allowable operational limits with regards to temperature and rotational speed.

8.1 Engine Degradation Profile selection

To implant the effect of engine performance deterioration into the model, a degradation table was generated where each degradation signature or level was defined in terms of percentage deviations in efficiencies and mass flow capacities of five major engine components (LPC-Fan, LPC-Booster, HPC, HPT, and LPT), and was made to follow an increasing trend with respect to flight cycles flown in service. The table is included in Appendix C whereas the corresponding component charts are illustrated in Figure 8-1 and Figure 8-2. The table was constructed based on the following considerations:

- The relative contribution of each of the individual engine component (Fan, Booster, HPC, HPT, LPT) parameters (efficiency and flow capacity) in the degradation profile was taken from the results of the study done by NASA using the real historical data of another commercial turbofan engine JT9D used for B747, B767 and A310. References: NASA Contractor Report 135448, 1978. and NASA/TM—2003-212607[62]. The degradation

implanted is from mild to severe and signifies typical deteriorated curve encountered in large two spool turbofan engines.

- The degradation table used in this project is an extended version of that in [62] and includes many additional degradation levels at different flight cycles where the parameter values were obtained simply by linear interpolation and extrapolation.

- For each of the five components the ratio between the flow loss and efficiency loss was carefully maintained throughout the degradation levels with increasing flight cycles. The ratio of the values in every two successive degradation levels was also maintained across all the component parameters. This approach was chosen to ensure that the cumulative effect of all the degrading elements in the components matches typical shape of an overall engine performance deterioration profile reflected by continuously decreasing EGT Margin with time.

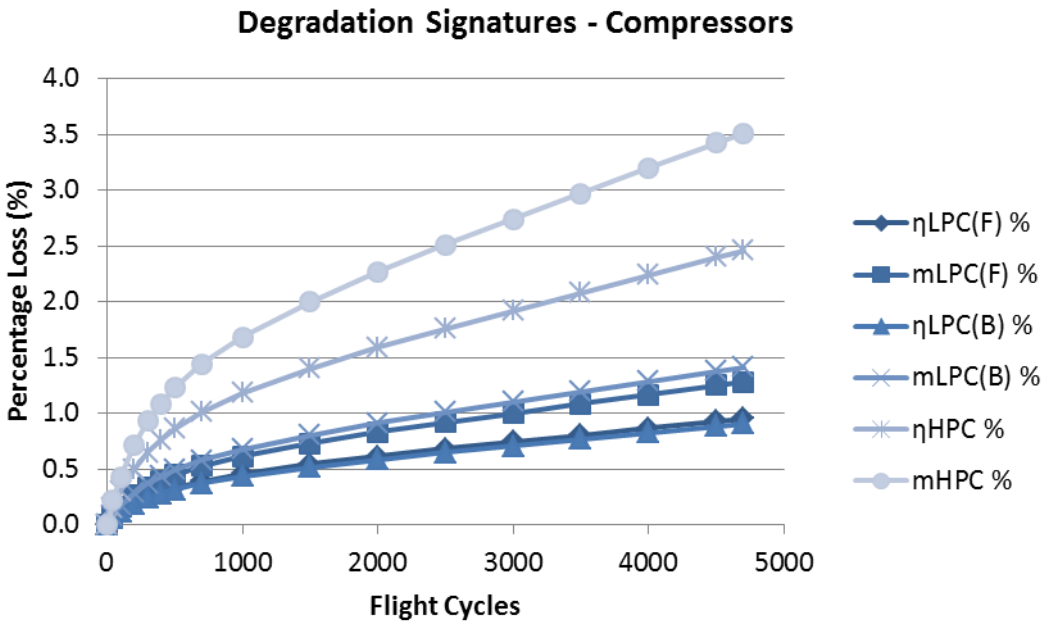

Figure 8-1: Degradation Signatures for LPC and HPC

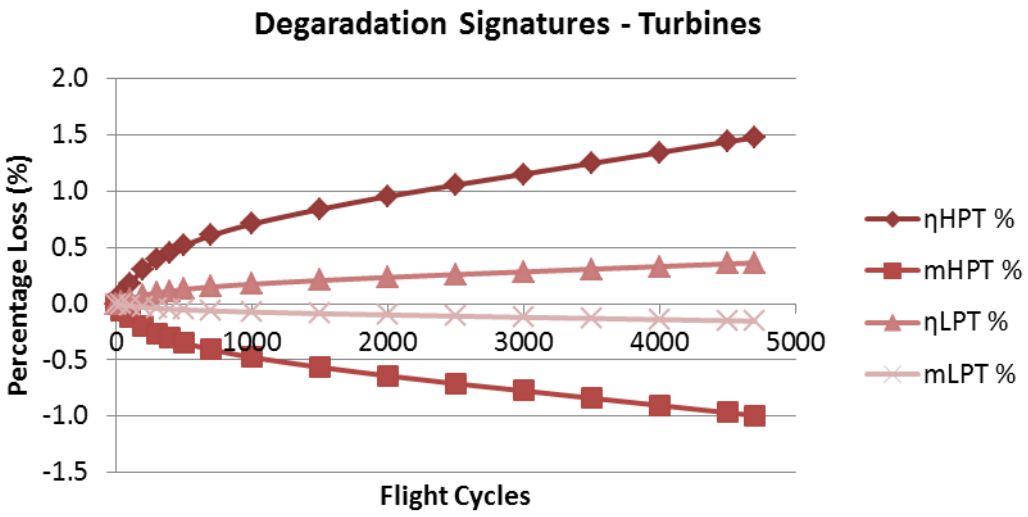

Figure 8-2 Degradation Signatures for HPT and LPT

Where,

ηLPC(F) = Fan Efficiency

mLPC(F) = Fan Flow Capacity

ηLPC(B) = Booster Efficiency

mLPC(B) = Booster Flow Capacity

ηHPC = HPC Efficiency

mHPC= HPC Flow Capacity

ηHPT = HPT Efficiency

mHPT= HPT Flow Capacity

ηLPT = LPT Efficiency

mLPT= LPT Flow Capacity

- For the sake of simplicity in the analysis, the degradation profile was assumed to be similar for both higher and lower thrust rated engines. i.e., the percentage shift in the engine parameters would be the same even though the actual values will offset depending on the thrust rating.

8.2 Effect of Engine Degradation on Performance

The EGT Margin depletion profiles in Figure 8-3 obtained for the two thrust ratings of the engine model as a result of the degradation signatures introduced earlier were compared with the description provided by Erkan , GE90 engine program manager at Turkish Technik in [63] and were found to be slightly severe but were accepted for the rest of the project analysis with the justification that such could be a typical deterioration profile expected of an engine operating in hot, harsh and sandy environment like the Middle East as compared to Europe. The TF115 engine variant at installation provides EGTM of about 42 degrees initially and then loses about 20 degrees in the first 1000 cycles of rapid erosion and then maintains a steady loss of 7 degrees per 1000 cycles thereafter.TF110 on the other hand also follows the same trend but initially starts off with a higher EGT margin of 60 degrees.

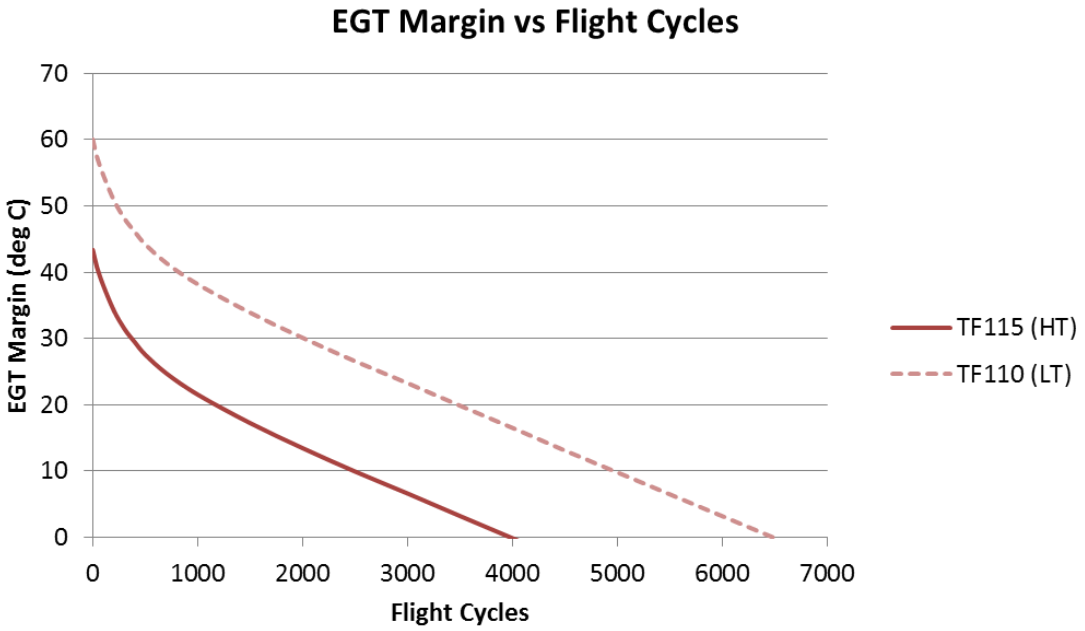

Figure 8-3 EGT Margin Deterioration

Furthermore, it was observed that EGTM becomes zero at about 4000 cycles with TF115 high thrust variant and at about 6480 cycles with TF110. This means that the engines are likely to experience EGT exceedance at those respective

intervals which would then become the reason for their immediate removal out from service. The EGTM is therefore considered as the key engine health indicator which is continuously monitored. Later in this chapter, the hardware soft lives are re-evaluated taking into account the effect of degradation and only at that stage it would be possible to determine the limiting factor for engine removal whether engine soft life due to the HPT blade deterioration or the EGTM depletion to zero.

Off design performance simulation was performed via Turbomatch with degraded components. The engine is caused to run less efficiently in generating the same level of thrust than the new or overhauled engine. Lower HPC and HPT efficiencies for instance, will demand more turbine work to compensate for the losses in compressor delivery pressure and flow capacity. This will result in an increase in engine fuel flow and SFC which in turn will give rise to TET and EGT. Following charts reflect the effect of degradation on a few of the parameters such as TET, Fuel flow and HP Shaft N2 speed.

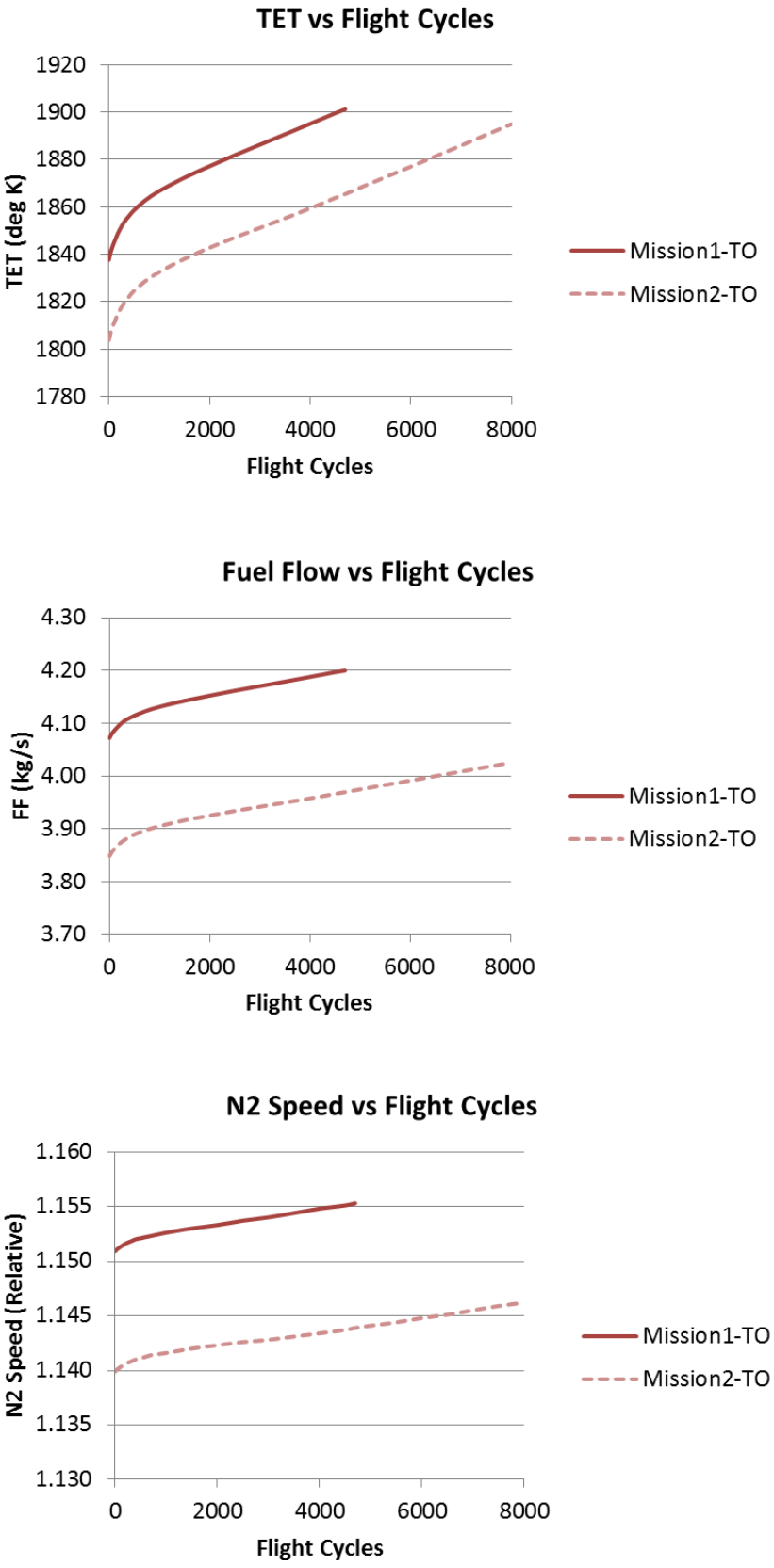

Figure 8-4 TET, FF & N2 vs Flight Cycles

8.3 Effect of Engine Degradation on Soft Life

Below is an outline of the procedure followed to estimate the soft life of the HPT blade considering progressive degradation. Flight mission 1 data is used for demonstration. Same process was used for flight mission 2.

- Let the discrete degradation levels be defined from i = 0 to k where the severity of degradation increases along with number of cycles flown.
- Let n be the number of flight cycles in service. The engine will experience ith degradation level at ni flight cycles.
- Let Ni be the predicted life the engine would achieve with ith degradation signature only.

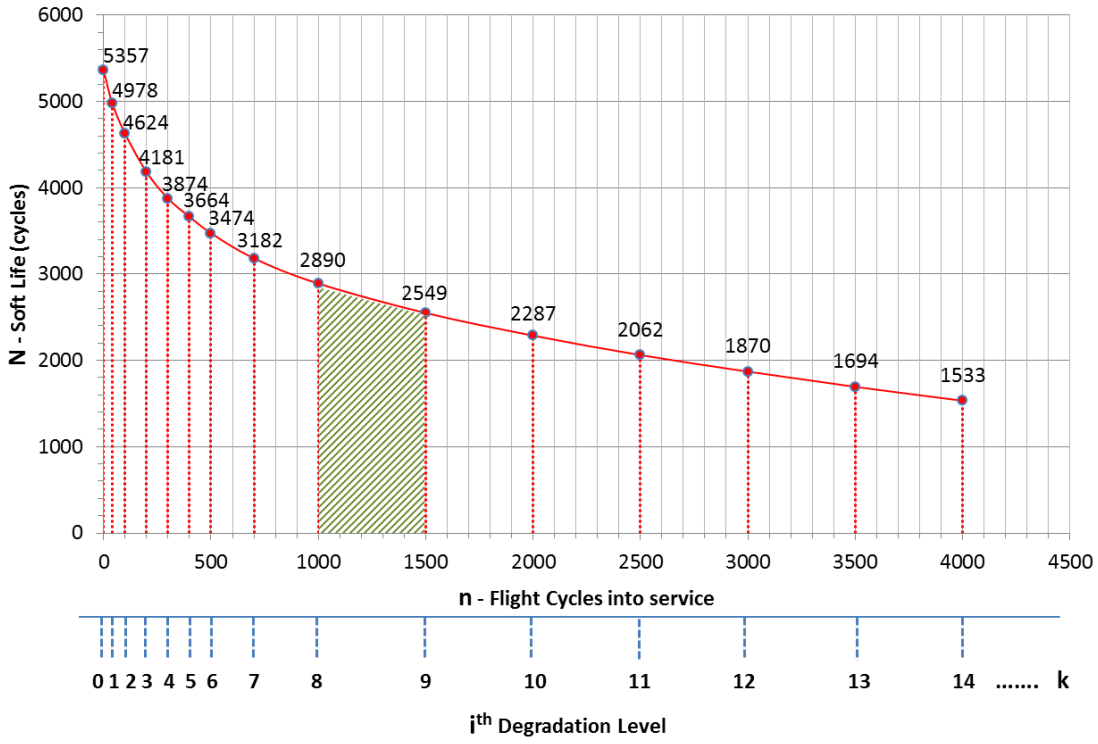

Figure 8-5 Soft Life for each Degradation Signature

Although the area under the curve in Figure 8-5 does not have a physical representation, it is rather understood as a mathematical formulation to calculate the average cumulative life CL taking into account the effect of progressive degradation the engine experiences during its operation. One method of approximating the desired area is to divide the time interval [n0, nk] the engine

remains in service into subintervals and consider the trapezoids whose bases are these subintervals and whose heights are the lives estimated at particular degradation levels. This method is known as Trapezoidal Riemann approximation [64], a well-known mathematical technique from calculus used for numerical integration.

Algebraic summation of all the trapezoidal areas is performed until the following condition is met i.e. cumulative life CL is less than or equal to actual cycles flown in service.

$$CL_k = \frac{1}{n_k} \sum_{i=1}^{k} \left[\frac{1}{2} (N_{i-1} + \mathrm{N}_i)(n_i - n_{i-1}) \right] \leq n_k \qquad \textbf{(8-1)}$$

As the engine experiences higher levels of degradation with increasing number of flight cycles the cumulative lives tend to decrease which can be viewed in

Table 8-1 Accumulative Live Calculation

Degradation level	Flight Cycles	Life due to ith degradation	Cumulative Life (Cycles)	
i / k	n_i	N_i	CL_k	
0	0	5357	5357	
1	40	4978	5168	
2	100	4624	4948	
3	200	4181	4675	
4	300	3874	4459	
5	400	3664	4287	
6	500	3474	4143	
7	700	3182	3910	
8	1000	2890	3648	
9	1500	2549	3339	
10	2000	2287	3108	
$k - 1 = 11$ → 11	2500	2062	2922	
	SL		SL	
$k = 12$ → 12	3000	1870	2762	← $CL_k \leq n_k$
13	3500	1694	2622	
14	4000	1533	2496	

. Finally, a theoretical point is reached where both of these trends intersect. It is this point of intersection which represents the estimated soft life of the engine. The engine is expected to be removed out of service after accumulating flight cycles equal to the estimated soft life SL. The accuracy could be increased by reducing the size of the intervals and defining more degradation levels in between.

Table 8-1 Accumulative Live Calculation

Degradation level	Flight Cycles	Life due to ith degradation	Cumulative Life (Cycles)	
i / k	n_i	N_i	CL_k	
0	0	5357	5357	
1	40	4978	5168	
2	100	4624	4948	
3	200	4181	4675	
4	300	3874	4459	
5	400	3664	4287	
6	500	3474	4143	
7	700	3182	3910	
8	1000	2890	3648	
9	1500	2549	3339	
10	2000	2287	3108	
$k-1=11$ → 11	2500	2062	2922	
	SL		SL	
$k=12$ → 12	3000	1870	2762	← $CL_k \leq n_k$
13	3500	1694	2622	
14	4000	1533	2496	

The soft life SL is determined using linear interpolation as follows:

$$\frac{(SL - CL_{k-1})}{(SL - n_{k-1})} = \frac{(CL_k - CL_{k-1})}{(n_k - n_{k-1})} \qquad \textbf{(8-2)}$$

$$\Rightarrow SL = \frac{n_k CL_{k-1} - n_{k-1} CL_k}{(n_k - n_{k-1}) - (CL_k - CL_{k-1})} \qquad \textbf{(8-3)}$$

$$SL_{Mission\ 1} = \frac{(3000)(2922) - (2500)(2762)}{(3000 - 2500) - (2762 - 2922)} = 2820\ cycles \qquad \textbf{(8-4)}$$

Table 8-2 Engine Soft Life for Mission 1 and 2

Mission	Aircraft Model	Engine Rating	Soft Life (With NO Degradation (Cycles)	Soft Life (With Degradation (Cycles)	% Change
1	A773ER	TF115	5357	2820	- 47%
2	A772LR	TF110	15816	6396	- 60%

So the soft life for mission 1 (high thrust) was found reduced by 48%, while the soft life for mission 2 (low thrust) was found reduced by 60% due to degradation.

Soft life for both engine thrust variants is considered to be Engine TOW since soft life calculated is less than the time it takes for EGTM to become zero which was calculated in previous section.

8.4 Effect on Engine Fuel Consumption

It can be observed that fuel consumption has a close relationship with operation costs, hence it's noticeable that commercial airlines always focus on the engine SFC. However performance degradation is inevitable with the increase in engine service life. Through research, we can see the various component parameters (flow capacity and efficiency) degradation and the way they affect the engine SFC as well as Fuel flow. Later the difference between fuel consumption of clean and degraded engine can be analyzed for both missions through conducting a simple analysis.

For each degradation signature 'i' the total fuel consumed during a single flight cycle was calculated by adding all the individual quantities consumed in each phase of the flight. Table 8-3 for example shows the total fuel consumption per flight cycle for the engine operated in reference mission 1 (with no degradation).

Table 8-3 Fuel Consumption – Reference Mission 1 (High Thrust, no degradation)

Flight Phase	Phase Interval (min)	Fuel Flow (kg/s)	Fuel Consumed (kg)
TAXI OUT	5.0	0.77	231.4
TAKEOFF	1.2	4.07	293.2
CLIMB1	16.8	3.28	3304.5
CRUISE1	168.6	1.20	12106.8
CLIMB2	4.4	1.81	477.5
CRUISE2	162.6	1.12	10960.9
DESCENT	31.3	0.91	1718.0
APPROACH	9.1	1.64	894.8
REVERSE THRUST	1.0	3.33	199.7
TAXI IN	5.0	0.77	231.4
Total	**405.0**	-	**30418.3**

Similar process was applied as in section 8.3 to estimate the average fuel consumption for the entire time period the engine stays on-wing (soft life).

- Let the discrete degradation levels be defined from i = 0 to k where the severity of degradation increases along with number of cycles flown.
- Let n be the number of flight cycles in service. The engine will experience ith degradation level at ni flight cycles.
- Let FCi be the predicted fuel (kg/cycle) the engine would consume with ith degradation signature only.
- Let AFCk be the average fuel consumption (kg/cycle) until nk cycles flown.

$$AFC_k = \frac{1}{n_k} \sum_{i=1}^{k} \left[\frac{1}{2} (FC_{i-1} + FC_i)(n_i - n_{i-1}) \right] \quad \textbf{(8-5)}$$

As the engine experiences higher levels of degradation with increasing number of flight cycles, the fuel consumption FCi tends to increase which can be viewed in Table 8-4.

Table 8-4 Fuel Consumption – High Thrust Mission 1 (with degradation)

	Degradation level	Flight Cycles	Fuel Consumption due to ith degradation level (kg/cycle)	Avg. Fuel Consumption (kg/cycle)
	i / k	n_i	FC_i	AFC_k
	0	0	30418.3	30418.3
	1	40	30473.8	30446.0
	2	100	30529.4	30479.4
	3	200	30597.7	30521.5
	4	300	30651.0	30555.8
	5	400	30688.7	30584.3
	6	500	30727.5	30609.1
	7	700	30782.7	30650.8
	8	1000	30845.0	30699.7
	9	1500	30926.7	30761.7
	10	2000	30996.5	30811.7
$k-1=11$ →	11	2500	31055.7	30854.6
		SL		AFC
$k=12$ →	12	3000	31117.3	30893.2
	13	3500	31176.8	30929.5
	14	4000	31237.3	30964.2

Average fuel consumption per cycle is determined using linear interpolation as follows:

$$\frac{(AFC - AFC_{k-1})}{(SL - n_{k-1})} = \frac{(AFC_k - AFC_{k-1})}{(n_k - n_{k-1})} \quad \textbf{(8-6)}$$

$$\Rightarrow AFC = \frac{(AFC_k - AFC_{k-1})(SL - n_{k-1})}{(n_k - n_{k-1})} + AFC_{k-1} \quad \textbf{(8-7)}$$

$$AFC_{Mission\ 1} = \frac{(30893.2 - 30854.6)(2820 - 2500)}{(3000 - 2500)} + 30854.6 = 30879.3\ kg \quad \textbf{(8-8)}$$

The values found for both missions were compared to the GE90 Fuel burn Performance analysis in [65] and were found to be in close proximity to the Block Fuel estimates for both aircraft variants B777-300ER and B777-200LR for the respective trip length.

Table 8-5 Average Fuel Consumption for Mission 1 and 2

Mission	Aircraft Model	Engine Rating	Avg Fuel Cons (With NO Degradation (kg/cycle)	Avg Fuel Cons (With Degradation (kg/cycle)	% Change
1	A773ER	TF115	30418.3	30879.3	1.51%
2	A772LR	TF110	26816.0	27456.4	2.39%

So, the average fuel consumption for mission 1 (high thrust) was found increased by 1.51%, while for mission 2 (low thrust) was found increased by 2.39% due to degradation.

The average fuel consumption was then multiplied by the life calculated earlier to give total fuel consumption for the entire period the engine stays on wing. Dividing it by number of flying hours gave the fuel burn (kg per hour). To evaluate the fuel operating cost of the engine by hour the price of Jet A-1 fuel was taken as $74 per barrel as of 26th June 2015 from reference [66]. The density of Jet A-1 fuel was taken to be 820 kg/m3 in accordance with World Jet Fuel Specifications published by ExxonMobil Aviation [67]. With the required unit conversions the average fuel cost per hour (FCPH) was finally estimated to be $3462.25 per hour for mission 1 and $3078.47 per hour for mission 2.

8.5 Effect on Engine Maintenance Cost

The engine maintenance cost structure highlighted in Figure 8-6 figure is widely known in the aviation and MRO industry. In this structure the engine MRO cost is split into DMC - direct maintenance cost and IDMC - indirect maintenance cost[68].

Engine DMC, also called shop visit DMC, generally includes expenditures related to labour, repair schemes, parts replacement and testing, required to make the engine serviceable for operation with desired performance and reliability. Often for convenience, engine DMC is further separated into two elements: one element for performance restoration by itself and the other for LLP replacement. Engine DMC or SVDMC can also be calculated in terms of dollars per flight hour by dividing total shop visit cost of an engine by its time on-wing. According to Seemann [68], unlike restoration costs, LLPs normally have hard lives which are fixed by the manufacturer and co-endorsed by regulatory authorities and therefore must be strictly respected.

Engine IDMC, on the other hand, deals with maintenance burden overheads, representing charges for indirect non-operational affairs related to maintenance; such as upgrading workshop facilities, training staff and providing administrative services etc. For the purpose of this project, only engine DMC will be considered as it represents much greater portion and more importantly, holds the characteristic of being directly affected by aircraft operation [68].

Most airlines nowadays get their engines overhauled by MRO service providers. A common type of contract is the Time and Material contract, where the airline pays according to the arranged labour rates and material costs, against a guarantee by the MRO for a certain minimum time on wing of the engine after its overhaul.

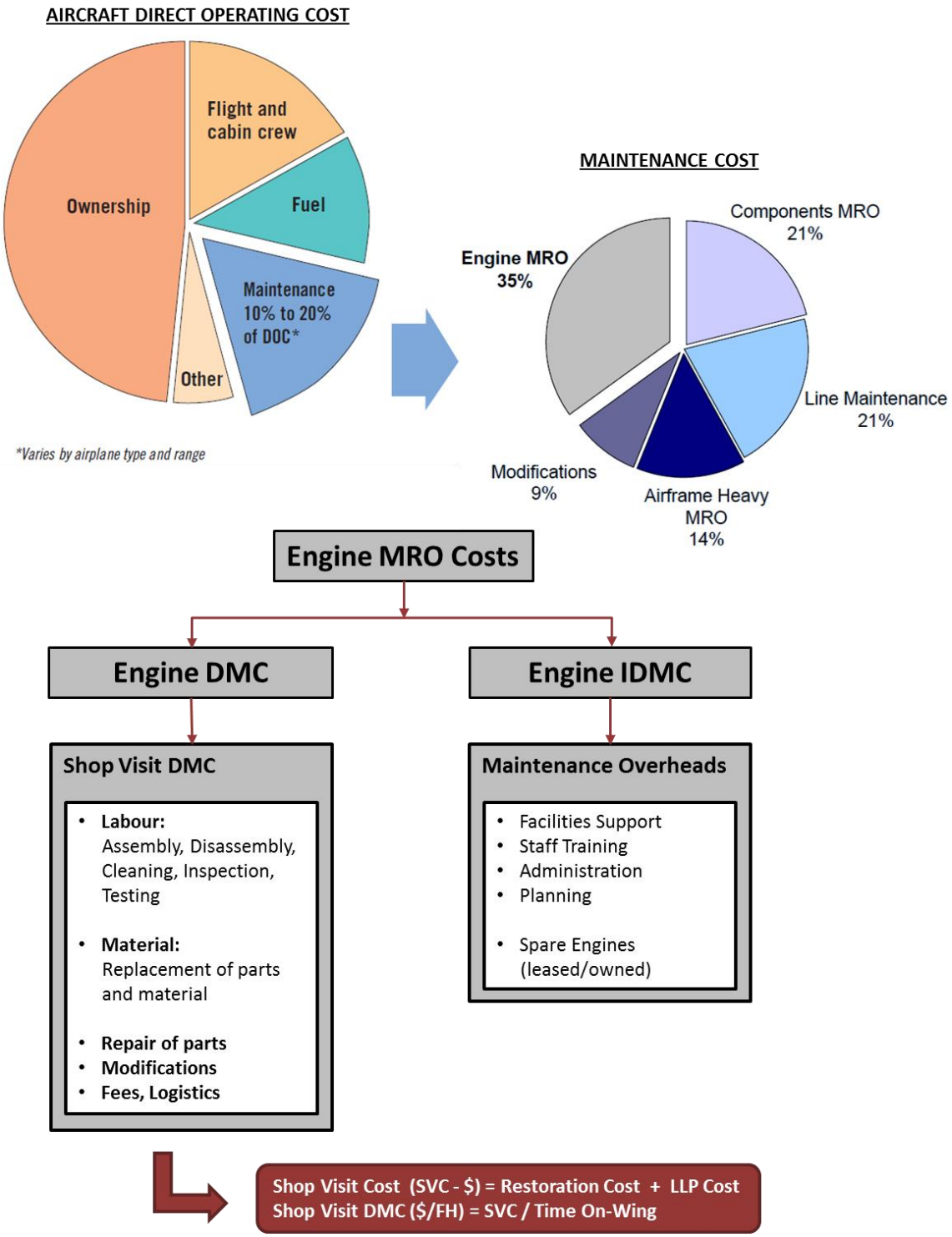

Figure 8-6 Engine Maintenance Cost breakdown [14][23][68]

For the purpose of this study following reasonable assumptions were made after reviewing the analysis of GE90 engine family maintenance costs seen in the MRO industry[63].

Average Shop Visit Restoration Cost = $7.0 million

Maintenance Reserve for the engine LLPs = 432.0 $/cycle = 432.0/6.75 (hr/cycle) = 64.15 $/hr

Normalizing any cost per flying hour helps in the visualization of cost distribution and often serves as a comparison tool to evaluate the operating economics of the engine at two different thrust ratings.

$$Shop\ Visit\ Cost\ (SVC) = Restoration\ Cost + LLP\ Cost \quad \textbf{(8-9)}$$

$$Shop\ Visit\ DMC\ (\$/hr) = \frac{SVC}{Time\ OnWing} \quad \textbf{(8-10)}$$

Since the direct maintenance cost depends on engine TOW, and the severity of operation based on parameters such as flight length, ambient conditions, TO derate and thrust rating is already inherent in the estimation model of engine soft life (or engine TOW) the DMC is in fact able to predict costs for any operational scenario.

Below are the engine maintenance costs estimated for mission 1 and mission 2 type operations.

Table 8-6 Direct Maintenance Cost for TF115 and TF110

Mission	Aircraft Model	Engine Rating	DMC (With NO Degradation) ($/hr)	DMC (With Degradation) ($/hr)	% Change
1	A773ER	TF115	257.7	431.9	67.6%
2	A772LR	TF110	129.7	226.3	74.5%

8.6 Implementation of Thrust Rating Change Option

The tools developed and utilized throughout this project allow us to conclude how thrust rating change influences an engine's life expectancy on-wing, as well as its operating and maintenance costs, as shown in Figure 8-7.

An engine operated at low thrust only has longest TOW. An engine operated at high thrust only has the shortest TOW. Between these two extremes, an engine's life expectancy on-wing can vary, when it is operated first at high thrust, then at low thrust.

The second part in Figure 8-7 shows the impact of thrust rating change on the engine's fuel consumption: at only low-thrust rating the fuel consumption per hour is minimal, at only high-thrust rating the fuel consumption per hour is maximal, while the average fuel consumption per hour gradually varies in accordance with the fraction of time it spends at each, high, then low thrust.

For the engine's maintenance cost per hour, we have a similar scenario: At only low thrust it is minimal; at only high thrust it is maximal.

However, it can be observed that the total shop visit costs slightly tend to increase as TOW increases.

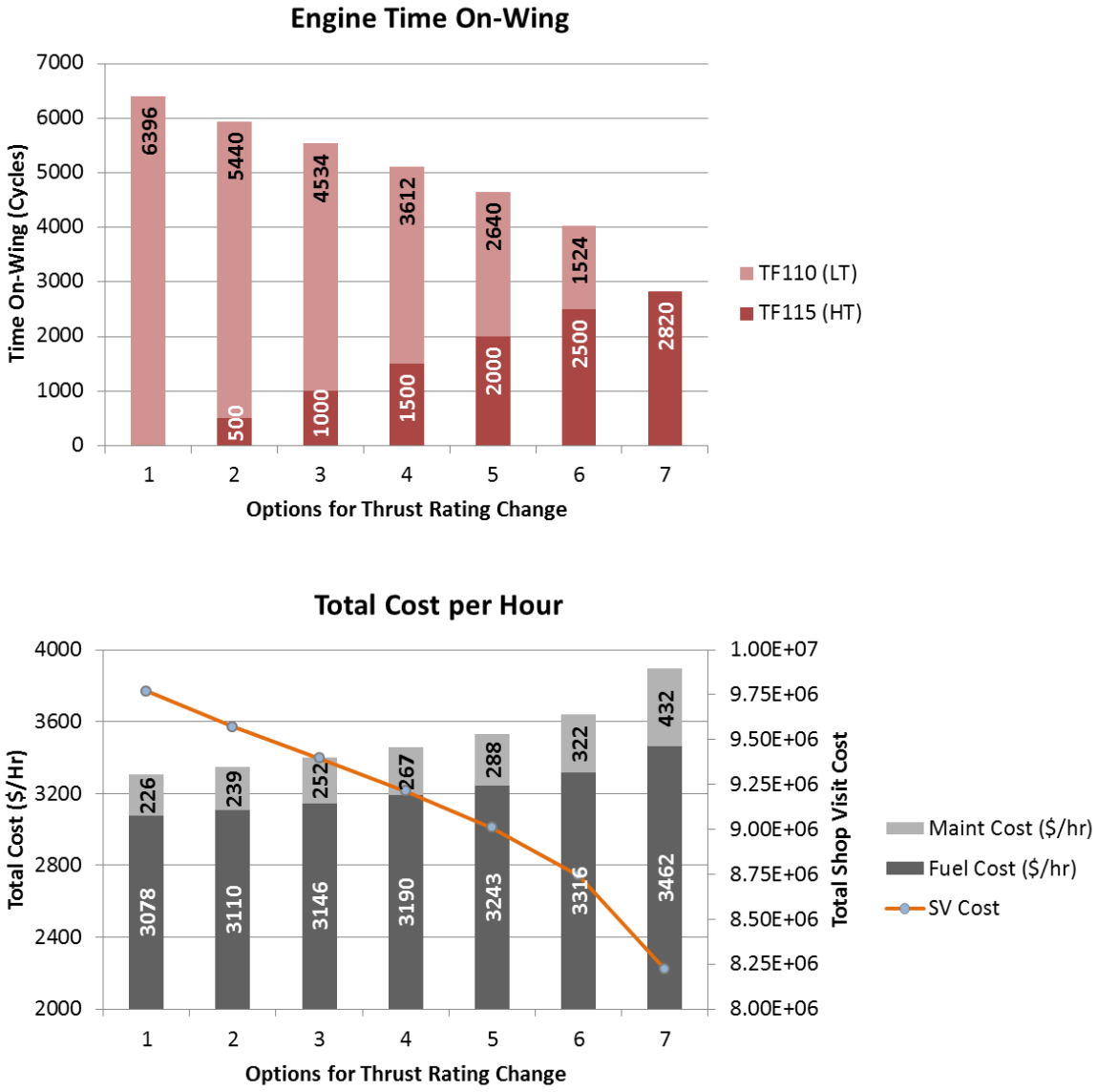

Figure 8-7 Engine Time On-Wing and Total Cost per hour considerations

The reader can observe the expected benefits of transferring the engine from a high thrust rated aircraft to a lower thrust rated aircraft at least once prior to its shop visit. However, the most interesting part of finding where the optimal shifting point lies can be done only by individual airline operators as a parametric analysis which takes into account the actual fleet. It should be noted that such a strategy can be adopted only by those operators which operate two or more aircraft models with same engine type but different thrust ratings.

9 CONCLUSIONS & FURTHER RECOMMENDATIONS

This chapter summarizes the main achievements of the research work and also highlights some of the limitations. Furthermore, it outlines few proposals for future work which would add refinements and perhaps lead to exploration of new aspects within the same research area.

9.1 Conclusions

The purpose of this project was to study the effect of the thrust rating change on the engine's life on a large civil aircraft and its repercussions on the maintenance and operating costs. Hence, this thesis is well suited to airline operators who manage a minimum of two or more aircraft variants from among the same series in their fleet. This will enable engine changeability across those aircraft variants; hence will facilitate the swap of engines from a high thrust configuration to a low thrust configuration to get benefit from extended time on-wing.

In summary the study proceeded as follows:

After obtaining adequate familiarization of Turbomatch Engine Performance Simulation tool, baseline engine model was created for a high bypass turbofan engine (similar to GE90). Design Point was chosen to be at Takeoff condition with highest thrust rating. Engine Cycle parameters were selected for best DP performance and optimum fan pressure ratio identified. Engine Off Design performance was studied. Engine behaviour with respect to change in Mach number, Altitude and OAT was found satisfactory.

After obtaining adequate familiarization of Hermes Aircraft Performance Simulation tool, two reference flight missions were established and modelled for two different versions of the same aircraft type (similar to B777-300ER and B777-200LR). Mission 1 employed aircraft certified with higher engine thrust rating and mission 2 employed aircraft with lower engine thrust rating. Both aircraft models were validated through the Range Payload Diagram.

The aircraft engine performance data generated for the two missions by the joint Turbomatch-Hermes simulation was compared. Variation in engine Thrust, Turbine Entry Temperature (TET) and HP Shaft Rotational Speed during the flight were specifically observed.

In order to evaluate the engine soft life for overhaul, high pressure turbine (HPT) blade was chosen as the component for analysis as it experiences the harshest environment inside the engine, and really determines the engine life on-wing. For this project, the HPT blade geometry was approximated using a scrapped GE90 Engine HPT Blade.

Stress model was developed to find the centrifugal stresses acting at different points along the HPT blade span. History of the HP Shaft relative rotational speed during different phases of the flight missions was used as an input to the model.

Thermal Model was developed to find the blade metal temperature along the blade span, employing technology parameters such as cooling effectiveness ε and radial temperature distribution factor RTDF. HPC discharge temperatures and turbine entry temperatures obtained from Hermes & Turbomatch simulation results are used as inputs to the model.

Creep model was created to forecast the creep life of the HPT blade. The model used the Larson Miller parameter chart for Rene N5 material. The blade stresses and temperatures computed by the stress and thermal models at different segments of the flight were inputs to the model and hence provided different times to failure for different segments. Palmgren-Miner law was eventually used to estimate the creep life of the blade taking account of all the individual fractional damages caused in each of the flight segments.

LCF analysis was performed to forecast the fatigue life of the HPT blade. First, stress range cycles were extracted through Rainflow counting method applied on simplified flight mission load history. Then Neuber notch strain based method was tried but because the stress cycles were not high enough for the yielding to take place in compression (causing elastic shakedown) this strain based method was discontinued. Alternatively, Stress based method was employed. Due to lack of material data available for Rene N5 in public domain, the S-N relationships was derived by taking 0.9xUTS at 103 cycles and 0.3xUTS at 106 cycles and use a logarithmic relationship between these values. Combination of Goodman diagram and derived SN curve was used to estimate the LCF life from the damaging cycles.

Miner's law was reused to get the cumulative fatigue-creep life of the blade. This was considered to be the soft life of the engine. Expiry of the soft life is often the reason of engine removal. Hence soft life was basically taken as Engine Time On-Wing.

The soft lives calculated so far were for the baseline missions without taking into account the effect of degradation. To incorporate engine performance deterioration, a few degradation levels were defined, gradually increasing with accumulation of more and more flight cycles to match the typical shape of a continuously increasing EGT profile. The degradation levels were defined in terms of flow and efficiency losses in major components (Fan, Booster, HPC, HPT, and LPT), values for which were carefully selected to reflect a trend that initially starts with mild degradation and gradually becomes severe with flight cycles.

The soft lives were revaluated for high and low thrust engines using the same procedure as above taking into account the progressive degradation. Different options are explored which an airline operator may exercise to influence the engine Time On-wing by sharing the engine life usage between the high thrust and the low thrust rated aircraft. The expected economic implications of such options are analyzed in terms of operational and maintenance costs.

9.2 Further Recommendations

The reference flight missions considered in this project lasted for about 7 hours per flight for both high and low thrust rated aircraft. Similar analysis could be performed for both aircraft variants on a 2 hours short haul route and a long haul 12 hours route. There are two elements that contribute to the overall hardware damage [9], the cyclic portion due to low cycle fatigue and the time dependent portion due to creep. The damage pattern i.e. the relative contribution of these two elements is expected to change based on the flight length. This perhaps would add another dimension to the study, to realize which aircraft variant is best suitable for the selected route from the perspective of engine TOW.

Although, rationally, it seems ineffective for an engine to first operate on a lower thrust rated aircraft and then further on a higher thrust rated aircraft at later stages when engine has already suffered a great deal of degradation, nevertheless it would still be worth examining such a strategy to see its impact on engine TOW; in other words an analysis on the difference if the engine first operates at high thrust for certain cycles and then at lower thrust compared to when the engine operates for the same number of cycles at a lower thrust and then at higher thrust.

The study observed that the swapping of the thrust rating could be an effective fleet management strategy to some of the operators; adding operational efficiency as well as productivity. The precise point of change needs to be analysed by weighing in many other factors of significance, and that calls for a separate study in itself. The implementation of such a strategy in a fleet of aircraft

depends on a variety of factors. Some of the most important ones include the number aircraft of a particular model in the fleet as well as the number of available spare engines for rotation. Moreover, the choice of option also depends on the no of higher thrust rated aircraft in the fleet vs lower thrust rated aircraft. Furthermore, the availability of engine spares is also a significant factor to weigh in. The study can be extended further by estimating the revenue generated per flying hour from larger models of aircraft, having more seating capacity versus smaller models, and to consider fuel burn per available seat mile. And then perhaps revisit optimization of engine utilisation to maximize profit to the airline operator.

Accuracy of the life prediction relies on the use of sophisticated physical model backed by real time flight data. Operators are hence invited to invest time and effort to make smarter use of the real flight data they have access to, through diagnostics tool and the experience with the routine bore scope inspection results, to complement, enhance and facilitate the lifing model to be able to make more accurate predictions through correlations. Real time flight data can be of significant use to these operators; the type of information that can provide analytical knowledge to be later reformed into implementation.

REFERENCES

[1] Boeing, “Boeing Next Generation 737.” [Online]. Available: http://www.boeing.com/commercial/737ng.

[2] CFM, “CFM 56-5B Turbofan Engine.” [Online]. Available: http://www.cfmaeroengines.com/engines/cfm56-5b.

[3] Boeing, “Boeing 747-8 Design Highlights (video).” [Online]. Available: http://www.boeing.com/commercial/747/#/design-highlights/technologically-advanced/engine/propulsion-ge-engine/.

[4] S. Ackert, “Engine Maintenance Concepts for financiers - Elements of Engine Shop Maintenance Costs,” *Macquarie AirFinance*, vol. 1, p. 30, 2010.

[5] A. S. Haslam, “Mechanical Integrity (Presentation Slides),” Cranfield University.

[6] E. Krimins, “Facts and Figures about the world of jet propulsion,” *GE Aviation Service Solutions*, vol. 4, GE Aviation Service Solutions, Cincinnati, OH 45215 USA, 2004.

[7] Y. G. Li, “Gas Turbine Diagnostics, (Edition 1.2), Thermal Power MSc Course Notes (Unpublished),” Cranfield University, Cranfield, UK, 2009.

[8] L. Kannan, P. Laskaridis, and R. Singh, *Lifting analysis of a turbo shaft engine.* 2011.

[9] H. Hanumanthan, A. Stitt, P. Laskaridi, and R. Singh, “Severity Estimation and Effect of Operational Parameters for Civil Aircraft Jet Engines,” 2011.

[10] CFM, “CFM56 Operational Characteristics - EGTMargin, OATL (Presentation Slides).” CFM, 2005.

[11] European Aviation Safety Agency, “Engine Type Certificate Data Sheet IM.E.002,” 2004.

[12] G. R. Halford, “Low-Cycle Thermal Fatigue,” Cleveland, Ohio, 1986.

[13] O. S. Ogunsina and A. J. B. Jackson, “Life estimation of turbofan high pressure turbine blade,” Cranfield University, Cranfield, UK, 2010.

[14] R. Heisey, “717-200: Low Maintenance Costs and High Dispatch Reliability,” *Aero*, no. 19, pp. 18–29, 2002.

[15] R. A. Cookson and A. S. Haslam, “Mechanical Design of Turbomachinery, Thermal Power MSc Course Notes (Unpublished),” Cranfield University, Cranfield, UK, 2011.

[16] C. Kjelgaard, “The GP7200 Power From Joined Forces,” 2010.

[17] P. S. Attah and T. Haslam, “Gas turbine engine component lifting studies from engine simulation software,” School of Engineering, Cranfield University., 2009.

[18] UBM Aviation Publications, “Labour Quality, not Labour Rates, drives Maintenance Cost Optimization,” *Engine Yearb.*, pp. 52–56, 2010.

[19] Boeing, “777 Family,” *Boeing*, 2013. [Online]. Available: http://www.boeing.com/commercial/777family/background.html.

[20] R. Donaldson, D. Fischer, J. Gough, and M. Rysz, “Economic Impact of Derated Climb on Large Commercial Engines, Article 8,” *Boeing Perform. Flight Oper. Eng. Conf.*, 2007.

[21] W. James and P. O'Dell, "Derated Climb Performance in Large Civil Aircraft, Article 6," in *Boeing Performance and Flight Operations Engineering Conference*, 2005.

[22] J. Marrero and P. Laskaridis, "Study into the maintenance costs of aero engines.," 2010.

[23] Jet Engine Consulting, "Engine Operating Cost, http://www.jetengineconsulting.com/pdf/JEC_Consulting_Philosophy.pdf." .

[24] H. Hanumanthan, A. Stitt, P. Laskaridis, and R. Singh, "Severity Estimation and Effect of Operational Parameters for civil Aircraft Jet Engines," in *Journal of Aerospace Engineering*, 2011.

[25] B. C. A. Department, "Gas Turbine Engine Parts Subject To Retirement Or Ultimate (Scrap) Lives," vol. Airworthin. AAC-014, Barbados, 2007.

[26] J. Liu and P. Pilidis, "High bypass ratio civil engine variable rating control," School of Engineering, Cranfield University, 2011.

[27] I. Bosdas and P. Pilidis, "Payload and runway length effect on variable rating control for a civil turbofan," School of Engineering, Cranfield University., 2009.

[28] M. F. Bin Abdul Ghafir and Y. Li, "Performance based creep life estimation for gas turbines application," School of Engineering, Cranfield University., 2011.

[29] B. Morey, "Aerospace leads in additive manufacturing," *SAE International*, 2012. [Online]. Available: http://www.sae.org/mags/aem/manuf/11207.

[30] M. Naeem, "Implications of Aero-Engine Deterioration for a Military

Aircraft's Performance," Cranfield University, 1999.

[31] G. E. Aviation, "Model GE90-115B," *G.E*. [Online]. Available: http://www.geaviation.com/engines/commercial/ge90/ge90-115b.html. [Accessed: 01-Apr-2015].

[32] M. Daly, "General Electrics," *Jane's Aero Engines*, no. 27, pp. 535–543, 2010.

[33] A. Jackson, "Optimisation of Aero and Industrial Gas Turbine Design for the Environment," Cranfield University.

[34] P. Pilidis and J. Palmer, "Gas Turbine Theory And Performance (Unpublished)." Cranfield University, 2010.

[35] P. Walsh and P. Fletcher, *Gas Turbine Performance*, 2nd ed. Blackwell Schience, 2004.

[36] Rolls Royce, *The Jet Engine*. 2005.

[37] Wikipedia, "US standard atmosphere 1962." [Online]. Available: https://en.wikipedia.org/wiki/File:Comparison_US_standard_atmosphere_1962.svg.

[38] J. Anderson, *Aircraft Performance and Design*, 1st ed. The McGraw Hill Companies, 1999.

[39] kokpit.com, "AEROPLANE PERFORMANCE." [Online]. Available: http://www.kokpit.com/steady_flight.html.

[40] J. Anderson, *Introduction to Flight*, 4th ed. The McGraw Hill Companies, 2000.

[41] S. Ackert, “Aircraft Payload-Range Analysis for Financiers,” *Aircr. Monit.*, 2013.

[42] Boeing, “777-200LR / -300ER / -Freighter Airplane Characteristics for Airport Planning,” 2015. [Online]. Available: http://www.boeing.com/assets/pdf/commercial/airports/acaps/777_2lr3er.pdf.

[43] B. VENEDIGER, “CIVIL AIRCRAFT TRAJECTORY ANALYSES - IMPACT OF ENGINE DEGRADATION ON FUEL BURN AND EMISSIONS,” Cranfield University.

[44] Emirates Airline, “GE90 Line Maintenance Training - chapter 72.” 2010.

[45] S. Tin and T. Pollock, “Nickel-Based Superalloys for Advanced Turbine Engines: Chemistry, Microstructure, and Properties,” *J. Propuls. Power*, vol. 22, no. 2, 2006.

[46] W. S. Walston, K. S. O’Hara, E. W. Ross, T. M. Pollock, and W. H. Murphy, “Rene N6: Third Generation Single Crystal Superalloy,” GE Aircraft Engines, Cincinnati, OH 45215, 1996.

[47] Wuckusic et al, “Property-balanced Nickel-base Superalloys for Producing Single Crystal Articles,” 6074602, 2000.

[48] R. Bowman, “Superalloys: A Primer and History.” [Online]. Available: http://www.ewp.rpi.edu/hartford/~ernesto/F2008/EP/Materials4Students/Greer/Superalloys.pdf.

[49] J. et al Corrigan, “NICKEL BASE SUPERALLOY AND SINGLE CRYSTAL CASTINGS,” US 2005/0000603 A1, 2005.

[50] H. I. H. Saravanamutoo, G. F. C. Rogers, and H. and Cohen, *Gas Turbine*

Theory, vol. 5. Pearson Education Limited, England, 2001.

[51] T. Tinga, W. B. De Wolf, P. J. Wisser, and S. Woldendorp, “Integrated Lifing Analysis of a Film-Cooled Turbine Blade,” in *Ageing Mechanisms and Control: Part B - Monitoring and Management of Gas Turbine Fleets for Extended Life and Reduced Costs*.

[52] P. Rubini, “Blade Cooling Notes.” University of Hull, UK.

[53] H. Hanumanthan, R. Singh, and C. U. S. of Engineering, “Severity estimation and shop visit prediction of civil aircraft engines,” 2011.

[54] E. Rodriguez and P. Laskaridis, “Impact of climb segment on life and fuel consumption for a large turbofan engine,” School of Engineering, Cranfield University., 2009.

[55] A. Haslam and P. Laskaridis, “Fatigue & Fracture (Unpublished).” Cranfield University, 2013.

[56] D. S. Pascovici, R. Singh, and S. Ogaji, *Thermo economic and risk analysis for advanced long-range aero engines*. School of Engineering, Cranfield University., 2008.

[57] O. Vigna Suria and S. Ogaji, “Flexible lifing model for gas turbines: creep and low cycle fatigue approach,” CRANFIELD UNIVERSITY, 2006.

[58] GUODONG CHEN, “THE PRELIMINARY DESIGN OF A HP TURBINE DISK AND BLADE AND THE ANALYSIS OF THE LIFING PROCEDURE FOR THE DISK,” Cranfield University, 2010.

[59] N. Singh and A. S. Haslam, “Estimation of fatigue and creep life on HP turbine rotor blade.,” CRANFIELD UNIVERSITY, 2011.

[60] A. O. Abu and P. Pilidis, “An Integrated Approach for Physics based Lifing of Gas Turbines (PHD Thesis),” Cranfield University, 2011.

[61] S. Manson and G. Halford, “Chapter 6: Total Strain-Based Strain-Range Partitioning - Isothermal and Thermomechanical Fatigue,” in *Fatigue and Durability of Metals at High temperature*, ASM International, 2009.

[62] J. Litt and E. M. Aylward, “Adaptive Detuning of a Multivariable Controller in Response to Turbofan Engine Degradation NASA/TM-2003-212723, ARL-TR-3091, E-14247, NAS 1.15:212723,” 2003.

[63] GE90, “GE90 Family Maintenance Cost,” *Aircr. Commer.*, no. 84, 2012.

[64] J. Stewart, *Calculus Single Variable*, 3rd ed. 1995.

[65] General Electric, “GE90 Growth Fuel Burn Performance,” *Aircr. Commer.*, no. 84, 2012.

[66] IATA, “Jet Fuel Price Monitor.” [Online]. Available: http://www.iata.org/publications/economics/fuel-monitor/Pages/index.aspx.

[67] E. M. Aviation, “World Jet Fuel Specifications,” 2005.

[68] R. Seemann, “Modeling the Life Cycle Cost of Jet Engine Maintenance,” Technische Universitaet Hamburg-Harburg, Institut fuer Lufttransportsysteme, Hamburg, 2010.

BIBLIOGRAPHY

- A. Haslam and P. Laskaridis, “Fatigue & Fracture (Unpublished).” Cranfield University, 2013.

- A. Jackson, “OPTIMISATION OF AERO AND INDUSTRIAL GAS TURBINE DESIGN FOR THE ENVIRONMENT,” Cranfield University.

- B. VENEDIGER, “CIVIL AIRCRAFT TRAJECTORY ANALYSES - IMPACT OF ENGINE DEGRADATION ON FUEL BURN AND EMISSIONS,” Cranfield University.

- E. Rodriguez and P. Laskaridis, “Impact of climb segment on life and fuel consumption for a large turbofan engine,” School of Engineering, Cranfield University., 2009.

- H. Hanumanthan, A. Stitt, P. Laskaridi, and R. Singh, “Severity Estimation and Effect of Operational Parameters for Civil Aircraft Jet Engines,” 2011.

- I. Bosdas and P. Pilidis, “Payload and runway length effect on variable rating control for a civil turbofan,” School of Engineering, Cranfield University., 2009.

- J. Anderson, *Aircraft Performance and Design*, 1st ed. The McGraw Hill Companies, 1999.

- J. Anderson, *Introduction to Flight*, 4th ed. The McGraw Hill Companies, 2000.

- J. Liu and P. Pilidis, “High bypass ratio civil engine variable rating control,” School of Engineering, Cranfield University, 2011.

- L. Kannan, P. Laskaridis, and R. Singh, *Lifting analysis of a turbo shaft engine.* 2011.

- M. F. Bin Abdul Ghafir and Y. Li, “Performance based creep life estimation for gas turbines application,” School of Engineering, Cranfield University., 2011.

- M. Naeem, “Implications of Aero-Engine Deterioration for a Military Aircraft’s Performance,” Cranfield University, 1999.

- P. S. Attah and T. Haslam, “Gas turbine engine component lifting studies from engine simulation software,” School of Engineering, Cranfield University., 2009.

- P. Walsh and P. Fletcher, *Gas Turbine Performance*, 2nd ed. Blackwell Schience, 2004.

- P. Pilidis and J. Palmer, “Gas Turbine Theory And Performance (Unpublished).” Cranfield University, 2010.

- P. Rubini, “Blade Cooling Notes.” University of Hull, UK.

- R. A. Cookson and A. S. Haslam, “Mechanical Design of Turbomachinery, Thermal Power MSc Course Notes (Unpublished),” Cranfield University, Cranfield, UK, 2011.

- R. Seemann, “Modeling the Life Cycle Cost of Jet Engine Maintenance,” Technische Universitaet Hamburg-Harburg, Institut fuer Lufttransportsysteme, Hamburg, 2010.

- S. Ackert, “Engine Maintenance Concepts for financiers - Elements of Engine Shop Maintenance Costs,” *Macquarie AirFinance*, vol. 1, p. 30, 2010.

- S. Haslam, “Mechanical Integrity (Presentation Slides),” Cranfield University.

- Y. G. Li, “Gas Turbine Diagnostics, (Edition 1.2), Thermal Power MSc Course Notes (Unpublished),” Cranfield University, Cranfield, UK, 2009.

APPENDICES

Appendix A Engine Model (Turbomatch)

```
 TURBOMATCH SCHEME - Windows XP version (July 2009)

LIMITS:100 Codewords, 800 Brick Data Items, 50 Station Vector
15 BD Items printable by any call of:-
OUTPUT, OUTPBD, OUTPSV, PLOTIT, PLOTBD or PLOTSV

 Input "Program" follows

!TURBOMATCH SCHEME - Windows XP version (July 2009)


!LIMITS:100 Codewords, 800 Brick Data Items, 50 Station Vector

!15 BD Items printable by any call of:-

!OUTPUT, OUTPBD, OUTPSV, PLOTIT, PLOTBD or PLOTSV


!Input "Program" follows


!High Bypass Turbofan Engine (2-spool, Seperate Exhaust)

!Configuration Similar to Engine Type: GE90-115B/110B

!Model Name: GE90code.dat


!Modeled by: Syed Atif Shafi

!Date: 01-09-2013


!Design point:

!Certified Maximum Takeoff Thrust Rating

!Thrust: 115,540 lbf (514 kN) @ Sea Level Static , ISA + 15 deg C

!FPR=1.657, BPR=7.1, OPR=42.2, TET=1925K, Mass Flow 1640 kg/s


!Other data

!Fan RPM 100%: 2,355
```

```
!Core RPM 100%: 9,332

_____________________________________________________________


////
OD SI KE VA FP
 -1
 -1
INTAKE   S1,2          D1-6               R300
COMPRE   S2,3          D7-18              R305      V7    V8
PREMAS   S3,15,4       D19-22                       V19
DUCTER   S15,16        D23-27             R310
NOZCON   S16,17,1      D143,144           R351
COMPRE   S4,5          D33-44             R320      V33
PREMAS   S5,19,6       D77-80
COMPRE   S6,7          D53-64             R335      V53   V54
PREMAS   S7,20,8       D97-100
PREMAS   S8,18,9       D101-104
BURNER   S9,10         D105-112           R350
MIXEES   S10,18,11
TURBIN   S11,12        D113-127                     V114
TURBIN   S12,13        D128-142                     V129
NOZCON   S13,14,1      D145,146           R355
PERFOR   S1,0,0        D147-150,355,300,350,351,0,0,0,0,0
CODEND



BRICK DATA////

!INTAKE ============================================================
1 0                ! Altitude
2 15               ! Deviation from ISA temperature
3 0                ! Mach number
4 -1               ! Pressure recovery
5 0                ! Deviation from ISA pressure [atm]
6 0                ! Relative humidity [%]

!FAN ================================================================
7 0.85             ! Surge Margin
8 1.035            ! DP Relative rotational speed PCN (N1)
9 1.65             ! DP Fan Pressure ratio
10 0.9             ! DP Isentropic efficiency
11 0               ! Error selection
12 1               ! Compressor Map Number
13 1               ! Shaft number
14 1               ! Scaling Factor of Pressure Ratio - Degradation
factor
15 1               ! Scaling Factor of Non-D Mass Flow - Degradation
factor
16 1               ! Scaling Factor of Isentropic Efficiency -
Degradation fact
17 -1              ! Effective component volume [m^3]
18 0               ! Stator angle (VSV) relative to DP

!BYPASS (PREMAS) ====================================================
19 0.877           ! LAMDA W BYPASS (Wout/Win) BPR = 7.1:1
```

```
 20 0                ! DELTA W
 21 1                ! LAMBDA P
 22 0                ! DELTA P

 !FAN DUCT (DUCTER) ========================================
 23 0                ! No Reheat
 24 0.015            ! Total pressure loss = 1.5%
 25 0                ! Combustion efficiency
 26 100000           ! Limiting value of Fuel Flow (=100000 if not
needed)
 27 -1               ! Effective component volume [m^3]

 !BOOSTER (LP COMPRESSOR) ==================================
 33 0.85             ! Surge Margin
 34 1.0              ! DP Relative rotational speed PCN (N1)
 35 1.5407           ! DP Pressure ratio
 36 0.88             ! DP isentropic efficiency
 37 1                ! Error selection
 38 1                ! Compressor Map Number
 39 1                ! Shaft number
 40 1                ! Scaling Factor of Pressure Ratio - Degradation
factor
 41 1                ! Scaling Factor of Non-D Mass Flow - Degradation
factor
 42 1                ! Scaling Factor of Isentropic Efficiency -
Degradation fact
 43 -1               ! Effective component volume [m^3]
 44 0                ! Stator angle (VSV) relative to DP

 !BOOSTER DISCHARGE BLEED (PREMAS) ==========================
 77 0.012            ! LAMDA W
 78 0                ! DELTA W
 79 1                ! LAMBDA P
 80 0                ! DELTA P

 !HP COMPRESSOR ============================================
 53 0.85             ! Surge Margin
 54 1.175            ! DP Relative rotational speed PCN (N2)
 55 16.6             ! DP Pressure ratio
 56 0.88             ! DP isentropic efficiency
 57 1                ! Error selection
 58 3                ! Compressor Map Number
 59 2                ! Shaft number
 60 1                ! Scaling Factor of Pressure Ratio - Degradation
factor
 61 1                ! Scaling Factor of Non-D Mass Flow - Degradation
factor
 62 1                ! Scaling Factor of Isentropic Efficiency -
Degradation fact
 63 -1               ! Effective component volume [m^3]
 64 0                ! Stator angle (VSV) relative to DP

 !HPC CUSTOMER BLEED (PREMAS) ===============================
 97 0.070            ! LAMDA W
 98 0                ! DELTA W
 99 1                ! LAMBDA P
 100 0               ! DELTA P

 !HPC BLEED FOR COOLING ====================================
```

```
 101 0.15            ! LAMDA W (9% for NGV, 6% for HPT Stage 1 Rotor)
 102 0               ! DELTA W
 103 1               ! LAMBDA P
 104 0               ! DELTA P

 !BURNER ============================================
 105 0.05            ! Total pressure loss = 5%
 106 0.999           ! Combustion efficiency
 107 -1              ! Fuel flow (If -1, FF depends on the stated
output TET)
 108 0               ! (>0) Water flow [kg s-1 or lb s-1] or (<0)
Water to air ra
 109 288             ! Temperature of water stream [K]
 110 0               ! Phase of water (0=liquid, 1=vapour)
 111 1               ! Scaling factor of combustion efficiency -
Degradation fact
 112 -1              ! Effective component volume [m^3]

 !HP TURBINE ========================================
 113 0               ! Auxiliary Work
 114 0.9             ! DP Relative ND massflow
 115 0.8             ! DP Relative ND speed
 116 0.90            ! DP isentropic efficiency
 117 -1              ! DP Relative speed PCN (-1 for compressor
turbine)
 118 2               ! Shaft Number (Spool #2)
 119 5               ! Turbine map number
 120 -1              ! Power law index "n" (POWER = PCN^n) If n=-1,
auxilary work
 121 1               ! Scaling factor of TF (ND inlet mass flow) -
Degradation fa
 122 1               ! Scaling factor of DH (enthalpy change) -
Degradation facto
 123 1               ! Scaling factor of isentropic efficiency -
Degradation fact
 124 155.53          ! DP Rotor rotational speed [RPS]
 125 30              ! Rotor moment of inertia [kg.m^2]
 126 -1              ! Effective component volume [m^3]
 127 0               ! NGV angle, relative to DP

 !LP TURBINE ========================================
 128 0               ! Auxiliary Work
 129 0.9             ! DP Relative ND massflow
 130 0.8             ! DP Relative ND speed
 131 0.90            ! DP isentropic efficiency
 132 -1              ! DP Relative speed PCN (-1 for compressor
turbine)
 133 1               ! Shaft Number (Spool #1)
 134 5               ! Turbine map number
 135 -1              ! Power law index "n" (POWER = PCN^n) If n=-1,
auxilary work
 136 1               ! Scaling factor of TF (ND inlet mass flow) -
Degradation fa
 137 1               ! Scaling factor of DH (enthalpy change) -
Degradation facto
 138 1               ! Scaling factor of isentropic efficiency -
Degradation fact
 139 39.25           ! DP Rotor rotational speed [RPS]
 140 150             ! Rotor moment of inertia [kg.m^2]
```

```
 141 -1              ! Effective component volume [m^3]
 142 0               ! NGV angle, relative to D.P.

 !BYPASS NOZZLE ============================================
 143 -1              ! Swich set (= "1" if exit area "floats", "-1" if
exit area
 144 -1              ! Scaling factor

 !CONVERGENT NOZZLE ========================================
 145 -1              ! Swich set (= "1" if exit area "floats", "-1" if
exit area
 146 -1              ! Scaling factor

 !ENGINE SIMULATION RESULT (PERFOR) ========================
 147 -1              ! Power output - Power or Power turbin
 148 -1              ! Propeller efficiency (= -1 for
turbojet/turbofan)
 149 0               ! Scaling index ("1" = scaling needed, "0" = no
scaling)
 150 0               ! Required DP net thrust (Turbofan)


 -1
 1 2 1640            ! DP Mass flow (kg/s)
 10 6 1925           ! DP TET (K)
 -1

 Number of Variables calculated by Appendix 4 Procedure
 (excluding any Splitters and/or Compressors on same Shaft)     =  8
 Number of obligatory Errors calculated by Appendix 4 Procedure =  6

                                                    Processor time
23:10:08

 ********************************************


                 The Units for this Run are as follows:-

 Temperature = K   Pressure = Atmospheres   Length = metres

 Area = sq metres  Mass Flow = kg/sec       Velocity = metres/sec

 Force = Newtons   s.f.c.(Thrust) =  mg/N sec   s.f.c.(Power) = mg/J

 Sp. Thrust =    N/kg/sec     Power =   Watts
1

      ***** DESIGN POINT ENGINE CALCULATIONS *****


 ***** AMBIENT AND INLET parameters *****
 Alt. =      0.0      I.S.A. Dev. =   15.000       PDev. =    0.000
 Mach No. =  0.00     Etar = 1.0000        Momentum Drag =      0.00
 Rel.Humidity =  0.00

 ***** COMPRESSOR  1 parameters *****
```

```
 PRSF =  0.14833E+01     ETASF =  0.10527E+01     WASF =  0.26679E+01
 DGPRSF =  0.10000E+01   DGETASF =  0.10000E+01   DGWASF =
0.10000E+01
 Z = 0.85000             PR =   1.650             ETA = 0.90000
 PCN =   1.0350          CN = 1.03500             COMWK =  0.86392E+08
 STATOR ANGLE =   0.00

 ***** CONVERGENT NOZZLE  1 parameters *****
 NCOSF =  0.10000E+01  DGNCOSF =  0.10000E+01
 Area =  4.1649          Exit Velocity =  305.82  Gross Thrust =
439849.27
 Nozzle Coeff. =  0.10000E+01

 ***** COMPRESSOR  2 parameters *****
 PRSF =  0.12339E+01     ETASF =  0.10293E+01     WASF =  0.21527E+00
 DGPRSF =  0.10000E+01   DGETASF =  0.10000E+01   DGWASF =
0.10000E+01
 Z = 0.85000             PR =   1.541             ETA = 0.88000
 PCN =   1.0350          CN = 1.03500             COMWK =  0.10877E+08
 STATOR ANGLE =   0.00

 ***** COMPRESSOR  3 parameters *****
 PRSF =  0.15635E+01     ETASF =  0.10808E+01     WASF =  0.71192E+00
 DGPRSF =  0.10000E+01   DGETASF =  0.10000E+01   DGWASF =
0.10000E+01
 Z = 0.85000             PR =  16.600             ETA = 0.88000
 PCN =   1.1750          CN = 1.17500             COMWK =  0.11420E+09
 STATOR ANGLE =   0.00

 ***** COMBUSTION CHAMBER parameters *****
 ETASF =  0.99900E+00  DGETASF =  0.10000E+01
 ETA = 0.99900           DLP = 2.1100       WFB =   4.5853       WWB =
0.00000

 ***** TURBINE  1 parameters *****
 CNSF =  0.93697E+02     ETASF =  0.10579E+01     TFSF =  0.81870E+00
 DHSF =  0.30967E+05
 DGETASF =  0.10000E+01   DGTFSF =  0.10000E+01   DGDHSF =
0.10000E+01
 TF =  245.041            ETA = 0.90000            CN =  2.600
 AUXWK =  0.00000E+00     NGV ANGLE = 0.00

 ***** TURBINE  2 parameters *****
 CNSF =  0.91209E+02     ETASF =  0.10577E+01     TFSF =  0.32508E+01
 DHSF =  0.35861E+05
 DGETASF =  0.10000E+01   DGTFSF =  0.10000E+01   DGDHSF =
0.10000E+01
 TF =  244.954            ETA = 0.90000            CN =  2.600
 AUXWK =  0.00000E+00     NGV ANGLE = 0.00

 ***** CONVERGENT NOZZLE  2 parameters *****
 NCOSF =  0.10000E+01  DGNCOSF =  0.10000E+01
 Area =  1.1520          Exit Velocity =  386.79  Gross Thrust =
73463.95
 Nozzle Coeff. =  0.10000E+01


 Scale Factor on above Mass Flows, Areas, Thrusts & Powers =
1.0000
```

Station	F.A.R.	Mass Flow	Pstatic	Ptotal	Tstatic	Ttotal	Vel
Area	W.A.R.	X					
1	0.00000	1640.000	1.00000	1.00000	303.15	303.15	0.0
******	0.00000	0.000					
2	0.00000	1640.000	******	1.00000	******	303.15	******
******	0.00000	0.000					
3	0.00000	1640.000	******	1.65000	******	355.19	******
******	0.00000	0.000					
4	0.00000	201.720	******	1.65000	******	355.19	******
******	0.00000	0.000					
5	0.00000	201.720	******	2.54216	******	408.21	******
******	0.00000	0.000					
6	0.00000	199.299	******	2.54216	******	408.21	******
******	0.00000	0.000					
7	0.00000	199.299	******	42.19977	******	940.78	******
******	0.00000	0.000					
8	0.00000	185.348	******	42.19977	******	940.78	******
******	0.00000	0.000					
9	0.00000	157.546	******	42.19977	******	940.78	******
******	0.00000	0.000					
10	0.02910	162.131	******	40.08978	******	1925.00	******
******	0.00000	0.000					
11	0.02474	189.934	******	40.08978	******	1793.02	******
******	0.00000	0.000					
12	0.02474	189.934	******	8.66032	******	1318.27	******
******	0.00000	0.000					
13	0.02474	189.934	******	1.35327	******	891.43	******
******	0.00000	0.000					
14	0.02474	189.934	1.00000	1.35327	826.24	891.43	386.8
1.1520	0.00000	0.000					
15	0.00000	1438.280	******	1.65000	******	355.19	******
******	0.00000	0.000					
16	0.00000	1438.280	******	1.62525	******	355.19	******
******	0.00000	0.000					
17	0.00000	1438.280	1.00000	1.62525	309.00	355.19	305.8
4.1649	0.00000	0.000					
18	0.00000	27.802	******	42.19977	******	940.78	******
******	0.00000	0.000					
19	0.00000	2.421	******	2.54216	******	408.21	******
******	0.00000	0.000					
20	0.00000	13.951	******	42.19977	******	940.78	******
******	0.00000	0.000					

```
  Gross Thrust = 513313.23
 Momentum Drag =      0.00
    Net Thrust = 513313.23
     Fuel Flow =    4.5853
        s.f.c. =   8.93276
    Sp. Thrust =   312.996
     Sim. time =   0.0000
           Time Now 23:10:08

 ***********************************************
```

Appendix B Flight Mission Specifications (Hermes)

B.1 Flight Mission 1 – A773ER

```
!Input file for the geometric, mission and engine specifications of the
aircraft Boeing777-300ER; Engine:GE90-115B
ENGINE_SPEC:GE90code.dat!programmed in Turbomatch
!GEOMETRIC DETAILS
! Wing Geometry
436.8          ! AcWingAInit - Wing area
9.69           ! AcWingAspr - Aspect ratio
0.155          ! AcWingCThir - Thickness chord ratio
31.64          ! AcWingSwpa - Sweep angle (in degrees)
0.205          ! AcWingTpr - Taper ratio
0.165          ! AcWingRtThir - Root thinkness ratio
0.145            ! AcWingOtThir - Outer thikness ratio
! Tailplane Geometry =horizontal plane
84.40          ! AcTailAInit - Tailplane area
4.50           ! AcTailAspr - Aspect ratio
0.105          ! AcTailCThir - Thickness chord ratio
35.00          ! AcTailSwpa - Sweep angle (in degrees)
0.350          ! AcTailTpr - Taper ratio
0.12           ! AcTailRtThir - Root thinkness ratio
0.1            ! AcTailOtThir - Outer thikness ratio
! Fin Geometry= vertical tail
44.40          ! AcFinA - Fin area
9.80           ! AcFinSpan - Span
0.120          ! AcFinCThir - Thickness chord ratio
40.0           ! AcFinSwpa - Sweep angle (in degrees)
0.300          ! AcFinTpr - Taper ratio
0.145          ! AcFinRtThir - Root thinkness ratio
0.120          ! AcFinOtThir - Outer thikness ratio
! Fuselage Geometry
6.20           ! AcFusDia - Diameter
72.87          ! AcFusLen - Length
! Landing Gear Characteristics
2                 ! AcLGTyp1 - Landing gear type ***0=default, 1=Bogie,
2=Small twin wheel***
1                   ! AcLgTyp2= 0,1,2
1                   ! AcLgTyp3= 0,1,2
-1                  ! AcLgTyp4= 0,1,2,-1 *** -1=if the aircraft only has
3 LG -1 has to be declared
-1                  ! AcLgTyp5= 0,1,2,-1 *** for the last 2 values
2                   ! AcLGDepl - Number of segments with LG down for
descent
! High lift systems
1                   ! AcFlapSegTo -Number of Segments with flaps
deployed during TO
3                   ! AcFlapSegApp - Number of Segments with flaps
deployed for approach
2                   ! ACFlapSegLand - Number of Segments with flaps
deployed during Landing
1.10         ! AcExtSrTo - Wing area extension ratio TO
1.15         ! AcExtSrApp - Wing area extension ratio approach
1.20         ! AcExtSrLand - Wing area extension ratio Landing
5.0          ! AcFlapAngleTo - Flap Angle TO IN DEGREES
20.0         ! AcFlapAngleApp - Flap Angle Approach
30.0         ! AcFlapAngleLand - Flap Angle Land
```

```
2           ! AcFlapSlots - Number of Flap Slots (1-3)
! Engine Geometry
4.10          ! EngNacDiaInit - Diameter
6.3           ! EngNacLenInit - Length
!XXXXXXXXXXXXXXXXXXXXXXXXXXXXXXXXXXXXXXXXXXXXXXX
!MISSION/WEIGHT SPECIFICATION DATA
149957        ! AcAfrWtInit - Airframe weight (OEW = 167829 kg (Source:
Boeing Company) minus Engine Wt)
2             ! AcEngNb - Number of Engines
8936          ! EngWtInit - Engine weight,  (kg/engine)
65000          ! AcPldWt - Payload weight, (kg) [(360 seats x (75+35)
kg/pax) + 25400 kg Cargo]
60000         ! AcFuelWtInit - Fuel weight,  (kg)
69853         ! AcPldWtmax  - Maximum payload weight, kg
145538        ! AcFuelWtmax - Maximum fuel weight,  kg
251290        ! AcLandWtmax - Maximum landing weight, kg
351535        ! AcToWtmax - Maximum take-off weight, kg (Source: Boeing
Company)
0.0          ! DVFuelRatio - Diversion fuel weight to total fuel weight
(%)
0.15          ! AcFuelContpc - Relative contigency fuel to remain after
landing (%)
5750          ! AcRng - Range to be flown (km)       ! Mission (2)
200.          ! AcRngdv - Diversion Range to be flown (km)
2            ! AcMisType - Mission to be flown (1-fixed fuel get range)
or (2-fixed range for given Pload get fuel)
1              ! DvMission - specify if diversion mission is to be run
(1- NO diversion mission) or (2- YES to diversion mission)
!XXXXXXXXXXXXXXXXXXXXXXXXXXXXXXXXXXXXXXXXXXXXXXX
!CRUISE MAIN/DIVERSION AND HOLDING DATA
2             ! number of cruise altitudes and Mach numbers
1           ! number of cruise Temperature Deviations from ISA day (the
trip is splitted equally into this number of parts. Every part has the
respective DTisa)
1             ! number of diversion cruise altitudes
200.           ! Cruise small segment time Interval in (min). This value
affects the accuracy of the calculations, so keep it small.
10058, 11583. ! Cruise altitudes in [m] (WARNING: THE ALTITUDES CANNOT
BE THE SAME!!!!!!!!!!)
0.83,0.85    ! Cruise Mach numbers, the same number with cruise altitudes
5.          ! Cruise ambient temperature deviation from ISA, in [K]
6096.         ! Diversion cruise altitudes (m)
0.45          ! Diversion cruise Mach numbers,
7.           ! Diversion cruise ambient temperature deviation from ISA,
in [K]
762.0         ! Holding altitude (m)
15.           ! Hold Time in (min)
!XXXXXXXXXXXXXXXXXXXXXXXXXXXXXXXXXXXXXXXXXXXXXXX
!CLIMB DATA
20          ! Climb segments Number
! Altitudes(m)    | DTisa(K) | EAS(knots) | Power(0.-1.)
557.20 15. 230. 1.
900.00 14. 230. 0.995
1500.00 13. 240. 0.99
1981.20 12. 240. 0.985
2438.40 11. 250. 0.98
2743.20 10. 250. 0.975
3048.00 9. 250. 0.97
3657.60 9. 260. 0.97
```

```
4267.20 8. 270. 0.965
4876.80 8. 280. 0.965
5486.40 7. 290. 0.96
6096.00 6. 300. 0.96
7620.00 5. 310. 0.96
8077.20 5. 320. 0.95
9144.00 5. 320. 0.95
10058.00 5. 320. 0.95
10668.00 5. 320. 0.95
10972.00 5. 320. 0.94
11227.00 5. 320. 0.94
11887.00 5. 320. 0.94
!XXXXXXXXXXXXXXXXXXXXXXXXXXXXXXXXXXXXXXXXXXXXXXXXXX
!DESCENT DATA
11          ! Descent segments Number
! The altitudes are dependant on the final cruise altitude. So they are
calculated inside the code.
! DTisa(K)  |  TAS(knots)  |  Power(0.-1.)  ****Note: the last 3 power
settings use the Approach rating
5. 245.0 0.8                          ! Flight Idle Rating
6. 240.0 0.8                          ! Flight Idle Rating
7. 230.0 0.8                              ! Flight Idle Rating
7. 220.0 0.8                          ! Flight Idle Rating
9. 210.0 0.8                          ! Flight Idle Rating
9. 200.0 0.8                          ! Flight Idle Rating
11. 185.0 0.8                         ! Flight Idle Rating
13. 140.0 0.8                         ! Flight Idle Rating
13. 105.0 1                     ! Approach Rating
15. 85.0 1                     ! Approach Rating
15. 80.0 0.8                          ! Approach Rating
!XXXXXXXXXXXXXXXXXXXXXXXXXXXXXXXXXXXXXXXXXXXXXXXXXX
!LANDING DATA
0.01       ! Note: Do not put final landing altitude = 0.0, use a very
small value instead.
80    ! Approach speed (TAS), in [m/s]
15.00      ! Deviation from standard atmosphere for Landing in [K]
1.5      ! Duration of Landing phase in [min]
!XXXXXXXXXXXXXXXXXXXXXXXXXXXXXXXXXXXXXXXXXXXXXXXXXX
!TAXI and TAKE-OFF DATA
0.02      ! AcTaxiCf1 - Runway Friction Coefficient
0.3       ! AcTaxiCf2 - Runway Friction Coefficient,BREAKES-OFF
10.0       ! AcTaxiTime - Taxi time in [min] (12mins for LR, 9mins for
SR)
1.2       ! AcToTime - Take-off time in [min]
0.00      ! AcToALT - Take-off altitude in [m]
15.00   ! Take-off temperature deviation from ISA in [K]
0.1     ! TakeOff Derate (Real Values from 0 to 1, 0.0->100% of Maximum
Thrust, 1.0->0% of Maximum Thrust)
!XXXXXXXXXXXXXXXXXXXXXXXXXXXXXXXXXXXXXXXXXXXXXXXXXX
!NUMERICAL TOLERANCES AND INITIAL GUESSES
1.D-11                        !  Climb  and  Descent  internal  loops
relative accuracy
1.D-09                        ! Main mission range relative accuracy
1.D-09                        !  Diversion  mission  range  relative
accuracy
1.D-07                        !  Fuel  weight  outer  iteration  loop
relative accuracy
480.D00                       ! Main mission duration guess 1 (for
secant method, modify it only if there is a convergence problem)
```

```
260.D00                        ! Main mission duration guess 2 (for
secant method, modify it only if there is a convergence problem)
!XXXXXXXXXXXXXXXXXXXXXXXXXXXXXXXXXXXXXXXXXXXXXXX
!TMATCHCALLS SPECIFICATIONS (*****HERMES DOES NOT READ THIS PART*****)
!-------------------------------------------------------------------
-----
!Number of points in the Engine Design Point input file to be skipped
!before the mission profile starts (including the design point)
1
!-------------------------------------------------------------------
-----
!Burner exit station number
10
!-------------------------------------------------------------------
-----
!ENGINE TET RANGE FOR EACH PHASE
20                      ! TET number for Take Off
20                      ! TET number for Climb
2                       ! TET number for Main and Diversion Cruise
10                      ! TET number for Flight Idle(Descent) and Ground
Idle
10                      ! TET number for Approach
5.                      ! TET step change in [K] for Take Off
5.                      ! TET step change in [K] for Climb
5.                      ! TET step change in [K] for Main and Diversion
Cruise
5.                      !  TET  step  change  in  [K]  for  Flight
Idle(Descent) and Ground Idle
5.                      ! TET step change in [K] for Approach
1925.             ! Max TET in [K] for Take Off
1720.             ! Max TET in [K] for Climb
1580.             ! Max TET in [K] for Main Mission Cruise
1280.             ! Max TET in [K] for Flight Idle(Descent) and Ground
Idle
1410.             ! Max TET in [K] for Approach
!-------------------------------------------------------------------
-----
!ADDITIONAL ENGINE PERFORMANCE STATION VECTOR DATA (STATION, ITEM)
4                       !  Number  of  additional  engine  performance
station vector data
!Station | Item
9 6
10 6
11 6
12 6
!-------------------------------------------------------------------
-----
!ADDITIONAL ENGINE PERFORMANCE BRICK DATA (DESCRIPTION, BRICK NO, ITEM)
3                       ! Number of additional engine performance brick
data
!Description | BrickNo | Item (WARNING: The BrickNo is defined according
to the tabular output file of turbomatch )
LPC_PCN 2 2
HPC_PCN 7 2
FF 14 7
!-------------------------------------------------------------------
-----
!ADDITIONAL OFF DESIGN ENGINE CONFIGURATIONS (LIKE BLEEDS etc.)
```

```
!Specify additional off design specification for each flight phase (e.g.
for brick data 26 "26 0.95")
1                       ! Number of additional off design specifications
for each flight phase
!You have to specify the same number of additional specs for all the
phases, i.e. if you specify something you have to do it for every flight
phase
!-------------------------------------------------------------------------
-----
!TAKE OFF SPECIFICATIONS
!-------------------------------------------------------------------------
-----
142 1200. 0. 0. ! BDnum TET ValueBelowTET ValueAboveTET
!-------------------------------------------------------------------------
-----
!CLIMB SPECIFICATIONS
!-------------------------------------------------------------------------
-----
142 1200. 0. 0. ! BDnum TET ValueBelowTET ValueAboveTET
!-------------------------------------------------------------------------
-----
!CRUISE SPECIFICATIONS
!-------------------------------------------------------------------------
-----
142 1200. 0. 0. ! BDnum TET ValueBelowTET ValueAboveTET
!-------------------------------------------------------------------------
-----
!FLIGHT/GROUND IDLE SPECIFICATIONS
!-------------------------------------------------------------------------
-----
142 1200. 0. 0. ! BDnum TET ValueBelowTET ValueAboveTET
!-------------------------------------------------------------------------
-----
!APPROACH SPECIFICATIONS
!-------------------------------------------------------------------------
-----
142 1200. 0. 0. ! BDnum TET ValueBelowTET ValueAboveTET
!-------------------------------------------------------------------------
-----
!INPUT AND OUTPUT FILE PATHS
!Engine Design Point Specification file (input to Hermes)
GE90code.dat
```

B.2 Flight Mission 2 – A772LR

```
!Input file for the geometric, mission and engine specifications of
the aircraft Boeing777-200LR; Engine:GE90-110B
ENGINE_SPEC:GE90code.dat!programmed in Turbomatch
!GEOMETRIC DETAILS
! Wing Geometry
436.8          ! AcWingAInit - Wing area
9.69           ! AcWingAspr - Aspect ratio
0.155          ! AcWingCThir - Thickness chord ratio
31.64          ! AcWingSwpa - Sweep angle (in degrees)
0.205          ! AcWingTpr - Taper ratio
0.165          ! AcWingRtThir - Root thinkness ratio
0.145          ! AcWingOtThir - Outer thikness ratio
! Tailplane Geometry =horizontal plane
84.40          ! AcTailAInit - Tailplane area
4.50           ! AcTailAspr - Aspect ratio
0.105          ! AcTailCThir - Thickness chord ratio
35.00          ! AcTailSwpa - Sweep angle (in degrees)
0.350          ! AcTailTpr - Taper ratio
0.12           ! AcTailRtThir - Root thinkness ratio
0.1            ! AcTailOtThir - Outer thikness ratio
! Fin Geometry= vertical tail
44.40          ! AcFinA - Fin area
9.80           ! AcFinSpan - Span
0.120          ! AcFinCThir - Thickness chord ratio
40.0           ! AcFinSwpa - Sweep angle (in degrees)
0.300          ! AcFinTpr - Taper ratio
0.145          ! AcFinRtThir - Root thinkness ratio
0.120          ! AcFinOtThir - Outer thikness ratio
! Fuselage Geometry
6.20           ! AcFusDia - Diameter
62.94          ! AcFusLen - Length
! Landing Gear Characteristics
2                  ! AcLGTyp1 - Landing gear type ***0=default,
1=Bogie, 2=Small twin wheel***
1                    ! AcLgTyp2= 0,1,2
1                    ! AcLgTyp3= 0,1,2
-1                   ! AcLgTyp4= 0,1,2,-1 *** -1=if the aircraft only
has 3 LG -1 has to be declared
-1                   ! AcLgTyp5= 0,1,2,-1 *** for the last 2 values
2                    ! AcLGDepl - Number of segments with LG down for
descent
! High lift systems
1                    ! AcFlapSegTo -Number of Segments with flaps
deployed during TO
3                    ! AcFlapSegApp - Number of Segments with flaps
deployed for approach
2                    ! ACFlapSegLand - Number of Segments with flaps
deployed during Landing
1.10         ! AcExtSrTo - Wing area extension ratio TO
1.15         ! AcExtSrApp - Wing area extension ratio approach
1.20         ! AcExtSrLand - Wing area extension ratio Landing
5.0          ! AcFlapAngleTo - Flap Angle TO IN DEGREES
20.0         ! AcFlapAngleApp - Flap Angle Approach
30.0         ! AcFlapAngleLand - Flap Angle Land
2            ! AcFlapSlots - Number of Flap Slots (1-3)
! Engine Geometry
4.10           ! EngNacDiaInit - Diameter
```

```
6.3           ! EngNacLenInit - Length
!XXXXXXXXXXXXXXXXXXXXXXXXXXXXXXXXXXXXXXXXXXXXXXX
!MISSION/WEIGHT SPECIFICATION DATA
127278        ! AcAfrWtInit - Airframe weight (OEW = 145150 kg
(Source: Boeing Company) minus Engine Wt)
2             ! AcEngNb - Number of Engines
8936          ! EngWtInit - Engine weight,  (kg/engine)
59100         ! AcPldWt - Payload weight, (kg) [(270 seats x (75+35)
kg/pax) + 29400 kg Cargo]
54000         ! AcFuelWtInit - Fuel weight,  (kg)
63957         ! AcPldWtmax  - Maximum payload weight, kg
145538        ! AcFuelWtmax - Maximum fuel weight,  kg
223168        ! AcLandWtmax - Maximum landing weight, kg
347452        ! AcToWtmax - Maximum take-off weight, kg (Source:
Boeing Company)
0.0           ! DVFuelRatio - Diversion fuel weight to total fuel
weight (%)
0.15          ! AcFuelContpc - Relative contigency fuel to remain
after landing (%)
5760          ! AcRng - Range to be flown (km)       ! Mission (2)
200.          ! AcRngdv - Diversion Range to be flown (km)
2             ! AcMisType - Mission to be flown (1-fixed fuel get
range) or (2-fixed range for given Pload get fuel)
1             ! DvMission - specify if diversion mission is to be run
(1- NO diversion mission) or (2- YES to diversion mission)
!XXXXXXXXXXXXXXXXXXXXXXXXXXXXXXXXXXXXXXXXXXXXXXX
!CRUISE MAIN/DIVERSION AND HOLDING DATA
2             ! number of cruise altitudes and Mach numbers
1           ! number of cruise Temperature Deviations from ISA day
(the trip is splitted equally into this number of parts. Every part
has the respective DTisa)
1             ! number of diversion cruise altitudes
200.           ! Cruise small segment time Interval in (min). This
value affects the accuracy of the calculations, so keep it small.
10058.,11583. ! Cruise altitudes in [m] (WARNING: THE ALTITUDES CANNOT
BE THE SAME!!!!!!!!!!)
0.83,0.85     ! Cruise Mach numbers, the same number with cruise
altitudes
5.          ! Cruise ambient temperature deviation from ISA, in [K]
6096.         ! Diversion cruise altitudes (m)
0.45          ! Diversion cruise Mach numbers,
7.            ! Diversion cruise ambient temperature deviation from
ISA, in [K]
762.0         ! Holding altitude (m)
15.           ! Hold Time in (min)
!XXXXXXXXXXXXXXXXXXXXXXXXXXXXXXXXXXXXXXXXXXXXXXX
!CLIMB DATA
20          ! Climb segments Number
! Altitudes(m)    | DTisa(K) | EAS(knots) | Power(0.-1.)
557.20 15. 230. 1
900.00 14. 230. 0.995
1500.00 13. 240. 0.99
1981.20 12. 240. 0.985
2438.40 11. 250. 0.98
2743.20 10. 250. 0.975
3048.00 9. 250. 0.97
3657.60 9. 260. 0.97
4267.20 8. 270. 0.965
4876.80 8. 280. 0.965
```

```
5486.40 7. 290. 0.96
6096.00 6. 300. 0.96
7620.00 5. 310. 0.96
8077.20 5. 320. 0.95
9144.00 5. 320. 0.95
10058.00 5. 320. 0.95
10668.00 5. 320. 0.95
10972.00 5. 320. 0.94
11227.00 5. 320. 0.94
11887.00 5. 320. 0.94
!XXXXXXXXXXXXXXXXXXXXXXXXXXXXXXXXXXXXXXXXXXXXXXXXXX
!DESCENT DATA
11          ! Descent segments Number
! The altitudes are dependant on the final cruise altitude. So they
are calculated inside the code.
! DTisa(K)  | TAS(knots) | Power(0.-1.) ****Note: the last 3 power
settings use the Approach rating
5. 245.0 0.75                        ! Flight Idle Rating
6. 240.0 0.75                        ! Flight Idle Rating
7. 230.0 0.75                            ! Flight Idle Rating
7. 220.0 0.75                        ! Flight Idle Rating
9. 210.0 0.75                        ! Flight Idle Rating
9. 200.0 0.75                        ! Flight Idle Rating
11. 185.0 0.75                       ! Flight Idle Rating
13. 140.0 0.75                       ! Flight Idle Rating
13. 105.0 1                    ! Approach Rating
15. 85.0 1                    ! Approach Rating
15. 80.0 0.75                        ! Approach Rating
!XXXXXXXXXXXXXXXXXXXXXXXXXXXXXXXXXXXXXXXXXXXXXXXXXX
!LANDING DATA
0.01      ! Note: Do not put final landing altitude = 0.0, use a very
small value instead.
77.5      ! Approach speed (TAS), in [m/s]
15.00     ! Deviation from standard atmosphere for Landing in [K]
1.5       ! Duration of Landing phase in [min]
!XXXXXXXXXXXXXXXXXXXXXXXXXXXXXXXXXXXXXXXXXXXXXXXXXX
!TAXI and TAKE-OFF DATA
0.02      ! AcTaxiCf1 - Runway Friction Coefficient
0.3       ! AcTaxiCf2 - Runway Friction Coefficient,BREAKES-OFF
10.0      ! AcTaxiTime - Taxi time in [min] (12mins for LR, 9mins for
SR)
1.2       ! AcToTime - Take-off time in [min]
0.00      ! AcToALT - Take-off altitude in [m]
15.00   ! Take-off temperature deviation from ISA in [K]
0.1418        ! TakeOff Derate (Real Values from 0 to 1, 0.0->100% of
Maximum Thrust, 1.0->0% of Maximum Thrust)
!XXXXXXXXXXXXXXXXXXXXXXXXXXXXXXXXXXXXXXXXXXXXXXXXXX
!NUMERICAL TOLERANCES AND INITIAL GUESSES
1.D-11                        ! Climb and Descent internal loops
relative accuracy
1.D-09                        ! Main mission range relative accuracy
1.D-09                        ! Diversion mission range relative
accuracy
1.D-07                        ! Fuel weight outer iteration loop
relative accuracy
480.D00                       ! Main mission duration guess 1 (for
secant method, modify it only if there is a convergence problem)
260.D00                       ! Main mission duration guess 2 (for
secant method, modify it only if there is a convergence problem)
```

```
!XXXXXXXXXXXXXXXXXXXXXXXXXXXXXXXXXXXXXXXXXXXXXXXX
!TMATCHCALLS SPECIFICATIONS (*****HERMES DOES NOT READ THIS PART*****)
!-------------------------------------------------------------------
-----
!Number of points in the Engine Design Point input file to be skipped
!before the mission profile starts (including the design point)
1
!-------------------------------------------------------------------
-----
!Burner exit station number
10
!-------------------------------------------------------------------
-----
!ENGINE TET RANGE FOR EACH PHASE
20                      ! TET number for Take Off
20                      ! TET number for Climb
2                       ! TET number for Main and Diversion Cruise
10                      ! TET number for Flight Idle(Descent) and
Ground Idle
10                      ! TET number for Approach
5.                      ! TET step change in [K] for Take Off
5.                      ! TET step change in [K] for Climb
5.                      ! TET step change in [K] for Main and
Diversion Cruise
5.                      ! TET step change in [K] for Flight
Idle(Descent) and Ground Idle
5.                      ! TET step change in [K] for Approach
1925.             ! Max TET in [K] for Take Off
1640.             ! Max TET in [K] for Climb
1580.             ! Max TET in [K] for Main Mission Cruise
1280.             ! Max TET in [K] for Flight Idle(Descent) and Ground
Idle
1380.             ! Max TET in [K] for Approach
!-------------------------------------------------------------------
-----
!ADDITIONAL ENGINE PERFORMANCE STATION VECTOR DATA (STATION, ITEM)
4                       ! Number of additional engine performance
station vector data
!Station | Item
9 6
10 6
11 6
12 6
!-------------------------------------------------------------------
-----
!ADDITIONAL ENGINE PERFORMANCE BRICK DATA (DESCRIPTION, BRICK NO,
ITEM)
3                       ! Number of additional engine performance
brick data
!Description | BrickNo | Item (WARNING: The BrickNo is defined
according to the tabular output file of turbomatch )
LPC_PCN 2 2
HPC_PCN 7 2
FF 14 7
!-------------------------------------------------------------------
-----
!ADDITIONAL OFF DESIGN ENGINE CONFIGURATIONS (LIKE BLEEDS etc.)
!Specify additional off design specification for each flight phase
(e.g. for brick data 26 "26 0.95")
```

```
1                       ! Number of additional off design
specifications for each flight phase
!You have to specify the same number of additional specs for all the
phases, i.e. if you specify something you have to do it for every
flight phase
!-------------------------------------------------------------------
-----
!TAKE OFF SPECIFICATIONS
!-------------------------------------------------------------------
-----
142 1200. 0. 0. ! BDnum TET ValueBelowTET ValueAboveTET
!-------------------------------------------------------------------
-----
!CLIMB SPECIFICATIONS
!-------------------------------------------------------------------
-----
142 1200. 0. 0. ! BDnum TET ValueBelowTET ValueAboveTET
!-------------------------------------------------------------------
-----
!CRUISE SPECIFICATIONS
!-------------------------------------------------------------------
-----
142 1200. 0. 0. ! BDnum TET ValueBelowTET ValueAboveTET
!-------------------------------------------------------------------
-----
!FLIGHT/GROUND IDLE SPECIFICATIONS
!-------------------------------------------------------------------
-----
142 1200. 0. 0. ! BDnum TET ValueBelowTET ValueAboveTET
!-------------------------------------------------------------------
-----
!APPROACH SPECIFICATIONS
!-------------------------------------------------------------------
-----
142 1200. 0. 0. ! BDnum TET ValueBelowTET ValueAboveTET
!-------------------------------------------------------------------
-----
!INPUT AND OUTPUT FILE PATHS
!Engine Design Point Specification file (input to Hermes)
GE90code.dat
```

		LPC(Fan)		LPC (Booster)		HPC		HPT		LPT	
Degrade level	Flight Cycles	$\eta_{LPC(F)}$ %	$m_{LPC(F)}$ %	$\eta_{LPC(B)}$ %	$m_{LPC(B)}$ %	η_{HPC} %	m_{HPC} %	η_{HPT} %	m_{HPT} %	η_{LPT} %	m_{LPT} %
0	0	0.000	0.000	0.000	0.000	0.000	0.000	0.000	0.000	0.000	0.000
1	40	0.058	0.078	0.055	0.086	0.150	0.214	0.090	-0.061	0.022	-0.009
2	100	0.116	0.156	0.110	0.172	0.300	0.428	0.180	-0.121	0.044	-0.019
3	200	0.194	0.261	0.184	0.287	0.500	0.714	0.300	-0.202	0.074	-0.031
4	300	0.252	0.339	0.239	0.373	0.650	0.928	0.390	-0.262	0.096	-0.041
5	400	0.294	0.396	0.280	0.436	0.760	1.085	0.456	-0.307	0.112	-0.048
6	500	0.333	0.448	0.316	0.494	0.860	1.228	0.516	-0.347	0.127	-0.054
7	700	0.391	0.526	0.372	0.580	1.010	1.442	0.606	-0.408	0.149	-0.064
8	1000	0.457	0.615	0.434	0.677	1.180	1.685	0.708	-0.476	0.174	-0.074
9	1500	0.542	0.730	0.515	0.804	1.400	1.999	0.840	-0.565	0.207	-0.088
10	2000	0.615	0.829	0.585	0.913	1.590	2.271	0.954	-0.642	0.235	-0.100
11	2500	0.681	0.917	0.648	1.010	1.760	2.513	1.056	-0.711	0.260	-0.111
12	3000	0.743	1.001	0.707	1.102	1.920	2.742	1.152	-0.775	0.283	-0.121
13	3500	0.805	1.084	0.765	1.194	2.080	2.970	1.248	-0.840	0.307	-0.131
14	4000	0.867	1.168	0.824	1.286	2.240	3.199	1.344	-0.905	0.331	-0.141
15	4500	0.929	1.251	0.883	1.378	2.400	3.427	1.440	-0.969	0.354	-0.151
16	4700	0.952	1.282	0.905	1.412	2.460	3.513	1.476	-0.993	0.363	-0.155

nLPC(F) = Fan Efficiency

mLPC(F) = Fan Flow Capacity

nLPC(B) = Booster Efficiency

mLPC(B) = Booster Flow Capacity

nHPC = HPC Efficiency

mHPC= HPC Flow Capacity

nHPT = HPT Efficiency

mHPT= HPT Flow Capacity

nLPT = LPT Efficiency

mLPT= LPT Flow Capacity